Antimalarial Evaluation of Quinoline-triazole Mn(I) and Re(I) PhotoCORMs

Fatima-Zahra Ishmail

University of Cape Town

December 2019

Antimalarial Evaluation of Quinoline-triazole Mn(I) and Re(I) PhotoCORMs

By

Fatima-Zahra Ishmail

Dissertation presented for the degree

MSc of Science

Supervisor: **Associate Professor Gregory S. Smith (UCT)**

Department of Chemistry
University of Cape Town
Rondebosch, 7701
Cape Town

December 2019

Plagiarism Declaration

I know the meaning of plagiarism and declare that all of the work in the document, **"Antimalarial Evaluation of Quinoline-triazole Mn(I) and Re(I) PhotoCORMs",** is my own work and to the best of my knowledge has never been submitted for examination for any degree at any university. All sources of information are cited and fully referenced.

Signature: Signed by candidate

Date: 09/12/2019

Acknowledgments

First and foremost, I would like to express my deepest gratitude to my supervisor Assoc. Professor Gregory Smith for his indispensable guidance and constructive criticism. I thank him for always motivating me to think outside of the box and pushing me to do better. I would like to thank Siyabonga Ngubane for his invaluable advice throughout my Msc and for initiating constructive discussions that pushed me to think beyond what is in front of me.

I extend my gratitude to the PhD students in the GS research group, for their knowledge they have willingly shared with me and the helping hand they always extended forward. To Sheperd Siangwata, who has been a mentor, I thank you for always encouraging me and constantly reminding me that regardless of the struggle I am faced with “agh, it will be fine man”. For his guidance and support I am truly grateful and indebted.

I thank Marwaan Rylands for taking the time to read through my chapters and provide critical suggestions that helped me better word and understand the chemistry of my work.

To my fellow MSc colleagues, Athi, Diana, Simone and Stephen I am grateful for the laughs and the memes we have shared. To my partner in crime Diana Melis, I am grateful for our shared love of food and cake.

To those establishments that have provided me with financial support, NRF, UCT postgraduate funding office and to York university for their travel grant I say thank you.

I extend my gratitude to my parents, brothers, sister-in-law’s and mother-in-law for their unmatched support and faith in my ability to succeed. Lastly, to my husband, Jawad Abrahams you have been a pillar of strength, my biggest motivator and supporter. I thank you for encouraging me every step of the way and having faith in me when I had none.

Abstract

Malaria remains a disease of global health concern, as thousands of people fall victim to it annually. Despite the continuous development of new malaria chemotherapies, the parasite has adapted and mutated, conferring multi-drug resistant strains. The constant emergence of drug-resistant strains of malaria and the decrease in efficacy of most front-line treatments calls for the urgent development of new antimalarial chemotherapeutic drugs. It is of great importance to develop compounds that target resistant strains of malaria. Chloroquine is one of the most significantly studied antimalarials to date and its derivatives have been mainstays in malaria treatment. It has also been established that carbon monoxide (CO) is able to prevent Experimental Cerebral Malaria (ECM) (a severe form of malaria) through the prevention of haemoglobin oxidation. This study investigated the synthesis, characterization and biological evaluation as antiplasmodial agents of two new quinoline-1,2,4-triazole ligands and their respective Mn(I) and Re(I) tricarbonyl complexes. The two ligands differ in the presence of an extended amino-propyl chain conjugated to the quinoline scaffold, which has proven to confer greater antimalarial activity. Furthermore, the complexes were evaluated for their potential as photoCORMs (photo-induced Carbon Monoxide Releasing Molecules) and the CO-releasing effects on the antiplasmodial activity were evaluated.

Two manganese tricarbonyl complexes (**Mn-1** and **Mn-2**: contains amino-propyl chain) were evaluated for their CO-releasing properties upon photoexcitation with UV light at 365 nm. Both complexes release CO upon photoexcitation in DCM, DMSO/PBS and DMSO/growth medium solutions. The rate of CO-release is medium-dependent and the **Mn-1** complex releases CO faster than the **Mn-2** complex.

The ligands and metal complexes were evaluated for their *in vitro* antiplasmodial activity against the NF54-chloroquine-sensitive and the K1-chloroquine-resistant strains of *Plasmodium falciparum* (*P. falciparum)*. All tested compounds show good antiplasmodial activity with IC_{50} values in the low micromolar range. The manganese and rhenium analogues

exhibit similar antiplasmodial activities, with IC_{50} values of 3.81 μM and 4.61 μM in the CQ-sensitive strain respectively. Both complexes retain their activity in the CQ-resistant strain with resistance indices of 1. The ligand containing the amino-propyl chain (**L2**) exhibits the greatest antiplasmodial activity with IC_{50} values of 0.33 μM and 0.69 μM in the CQ-sensitive and -resistant strains respectively. The manganese complex thereof (**Mn-2**) has IC_{50} values of 0.54 μM and 1.16 μM in the CQ-sensitive and -resistant strains respectively.

The antiplasmodial activity of the manganese complexes **Mn-1** and **Mn-2** increases 7- and 3-fold respectively upon photoexcitation at 365 nm in the K1-CQ-resistant strain. The increase in antimalarial activity exhibited upon light-induced CO-release presents a promising mechanism of combating drug-resistant *P. falciparum*. Mechanistic studies of these compounds indicate that they potentially work *via* β-hematin inhibition, with the metal complexes being greater inhibitors than CQ. Upon photo-induced CO-release, the β-hematin inhibition of complex **Mn-1** increases drastically.

Conference/Symposium Contributions

1. **Presentation:** Fatima-Zahra Ishmail and Gregory Smith, *The Synthesis and Antimalarial Evaluation of Aminoquinoline-triazole containing Mn and Re Tricarbonyl Complexes*, presented at the Cape Organometallic Symposium (COS), Cape Town, South Africa **2019.**
2. **Poster Presentation:** Fatima-Zahra Ishmail and Gregory Smith, *Antimalarial Evaluation of Quinoline-triazole Mn(I) and Re(I) PhotoCORMs,* presented at the 9th International Symposium on Bioorganometallic Chemistry (ISBOMC), York, United Kingdom **2019.**

Awards

1. Best poster prize at ISBOMC 2019

Abbreviations

ACT	Artemisinin Combination Therapy
ATR	Attenuated total reflectance
BCN	Bicyclo-[6.1.0]nonyne
br	Broad
CNR	Click and release
COMb	Carboxy-myoglobin
CORMs	Carbon Monoxide-Releasing Molecules
CQ	Chloroquine
CQDP	Chloroquine diphosphate
CuAAC	Copper-catalyzed azide/alkyne cycloaddition
d	doublet (NMR)
DCM	Dichloromethane
dd	doublet of doublets (NMR)
Deoxy-Mb	Deoxy myoglobin
DHFR	Dihydrofolate reductase
DHPS	Dihydropteroate synthase
DIPEA	*N,N*-Diisopropylethylamine
DMF	Dimethyl formamide
DMSO	Dimethylsulfoxide

ECM	Experimental cerebral malaria
EI	Electron Impact
eq.	Equivalent(s)
EtOAc	Ethyl acetate
fac	Facial
FAQ	Fluoroamodiaquine
FQ	Ferroquine
FT-IR	Fourier transform infrared spectroscopy
FV	Food vacuole
HO	Heme oxygenase
HPPK	Hydroxymethylpterin Pyrophosphokinase
HSQC	Heteronuclear single quantum correlation
Hz	Hertz
ILCT	Intraligand charge transfer
IR	Infrared
J	Coupling constant
Lit.	Literature
m	Multiplet (NMR)
m/z	Mass to charge ratio
Mb	Myoglobin
MB	Methylene Blue
MDR	Multi drug resistant
MeCN	Acetonitrile

MeOH	Methanol
mer	Meridional
MLCT	Metal-to-ligand charge tranfer
MsCl	Methanesulfonyl chloride
NADH	Nicotinamide adenine dinucleotide
NMR	Nuclear magnetic resonan
p	Pentet (NMR)
PBS	Phosphate buffer saline
pfCRT	*Plasmodium falciparum* Chloroquine Resistance Transporter
photoCORMs	Photo-activated Carbon Monoxide-Releasing Molecules
pLDH	Plasmodium lactate dehydrogenase
q	quartet (NMR)
RBC	Red blood cell
ROS	Reactive Oxygen Species
s	Singlet (NMR)
S_NAR	Nucleophilic Aromatic Substitution
$SOCl_2$	Thionyl chloride
SP	Sulfadoxine-pyrimethamine
t	triplet (NMR)
THF	Tetrahydrofuran
TPCPD	Tetraphenylcyclopentadienone
UV	Ultra-violet

Table of Contents

Chapter 1

Introduction: Malaria

1.1. History and prevalence of malaria

Malaria is a mosquito-borne infectious disease caused by a protozoan of the *Plasmodium* genus.[1] The disease is proposed to date back to as early as 2700 BC,[2] where there are several references made to its symptoms in ancient Mesopotamia clay tablets, Egyptian papyri, Indian writings and Greek texts.[1] Malaria is thought to have arrived in Rome in the first century AD *via* the Nile River to the Mediterranean after which it reached Greece, England and Denmark. For the 2 000 years that followed, malaria flourished in Europe, as many fell victims to it.[2]

The malaria parasite was first discovered in the blood of infected patients by Alphonse Laveran in 1880.[3] The Italian neurophysiologist, Camillo Golgi later discovered in 1886 that there were at least two forms of the disease, the "tertian" and the "quartan" forms.[4] The tertian form occurs in patients who have a fever every other day and the quartan form occurs when patients have a fever every third day. Golgi noticed that these two forms were accompanied by different numbers of new parasites.[5] Ronald Ross was the first to discover that avian and human malaria uses mosquitoes as its vector.[6] The sexual stage of the parasites' life cycle was discovered by William MacCallum in 1897 whereas the transmission process was discovered in infected birds by Ronald Ross in 1898.[1] Finally, the dormant stage of the parasites life cycle was discovered to take place in the liver by Wojciech Krotoski in 1982.[1]

Malaria has plagued the United States for decades but nowhere past or present has it taken a bigger toll than it has on Africa.[2] Approximately 50% of the world's population is at risk of contracting the disease.[7] According to the latest World Malaria Report, there were 219 million malaria cases and 435 000 related deaths in 2017.[8] Most of these deaths occur in pregnant woman and children under the age of 5, majority of who die within 72 hours of their symptoms.[9,10] There are several species of malaria parasites, but only five cause infection in

humans, these are: *P. falciparum, P. vivax, P. ovale, P. malariae, and P. knowlesi*, with *P. falciparum* being responsible for the majority of the deaths.[11]

1.2. Biology of the *Plasmodium* parasite

The life cycle of the *Plasmodium* parasite shown in **Figure 1.1** illustrates that the parasite requires two hosts: a mosquito (the vector) and a human host.[12] Sexual reproduction occurs in the mosquito and asexual reproduction takes place in the human.

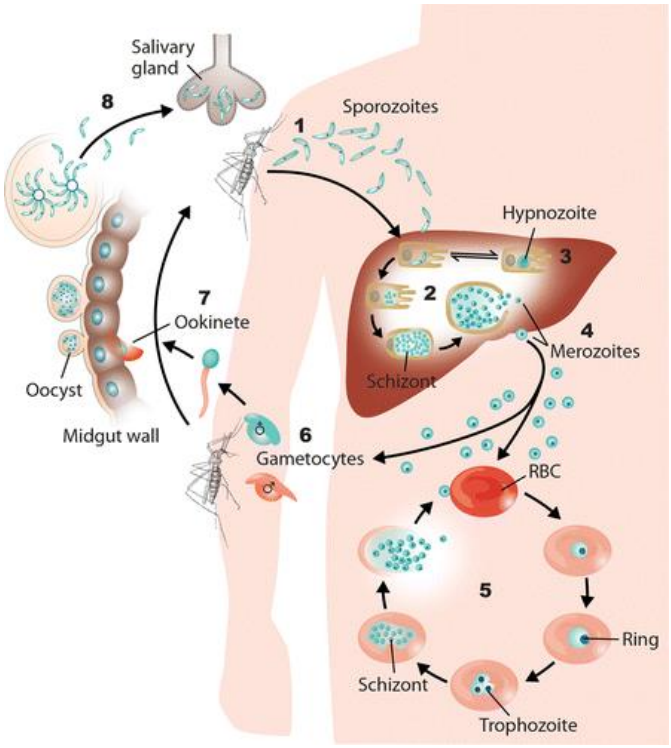

Figure 1.1. Life cycle of the *Plasmodium* parasite.[12]

The parasitic life cycle begins when an infected female *Anopheles* mosquito takes a blood meal from the human host.[13] The sporozoites from the parasite are injected into the humans' bloodstream *via* the mosquitos' saliva. These sporozoites enter the liver, where they mature and multiply, eventually causing the cells to rupture releasing merozoites back into the

bloodstream.[14] These merozoites invade the red blood cells (RBCs) where they undergo asexual reproduction, forming either schizonts or trophozoites. Each schizont then divides, once again forming merozoites that are released to invade erythrocytes.[12] Several merozoites mature into gametocytes (both male and female) at which point a mosquito can once again take a blood meal, taking up the *Plasmodium* gametes, initiating the sexual reproductive cycle in the mosquito.[15] The female and male gametes fuse and are taken up into the midgut where they mature and the life cycle repeats itself.[12]

Parasitic pathogenesis only occurs during the asexual blood stage of the life cycle.[11] During this stage, the parasite consumes and degrades the haemoglobin found in the RBCs.[11,16] Degradation occurs in an acidic food vacuole (FV) with pH range of 5.2-5.6.[16] In the FV, the iron centre of haemoglobin undergoes oxidation to form Heme.[17] At high enough concentrations, this heme is toxic to *Plasmodium* as it produces reactive oxygen species (ROS), as illustrated in **Figure 1.2**.[18] ROS causes "lipid peroxidation", a toxic process whereby the lipids in the membrane of the parasite degrade, resulting in parasitic death.[16]

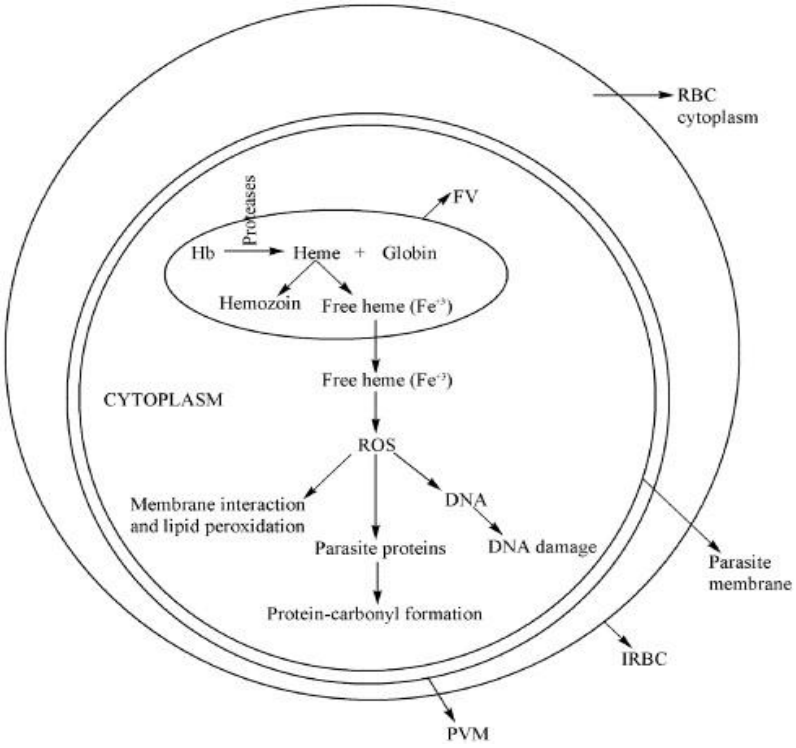

Figure 1.2. Proposed mechanisms of free heme toxicity in the malaria parasite. Haemoglobin (Hb), food vacuole (FV), infected red blood cell (IRBC), Parasitophorous vacuolar membrane (PMV), reactive oxygen species (ROS).

To avoid susceptibility to lipid peroxidation and subsequent death, the parasite has evolved a detoxification method, during which free heme is polymerized into a form of β-haematin known as hemozoin.[19] Hemozoin is a highly insoluble crystalline molecule that forms in the digestive vacuole of the parasite.[20] There is evidence indicating that hemozoin (**Figure 1.3**) is a polymeric dimer of heme.[21] The mechanism of hemozoin formation is unclear but has been thoroughly debated over the years.[11,16] Some of these proposed mechanisms include protein-mediated hemozoin formation,[22,23] lipid-mediated hemozoin formation,[24] biomineralization,[25] or biocrystallization.[26] Hemozoin can also spontaneously be synthesized by incubating monomeric hematin (at 37 ℃ and pH 4.8) in the absence of parasitic material to form the synthetic form of hemozoin known as β-hematin.[18] Hemozoin resembles β-haematin chemically, spectroscopically and crystallographically which serves as great importance when considering designs for new antimalarial drugs.[16]

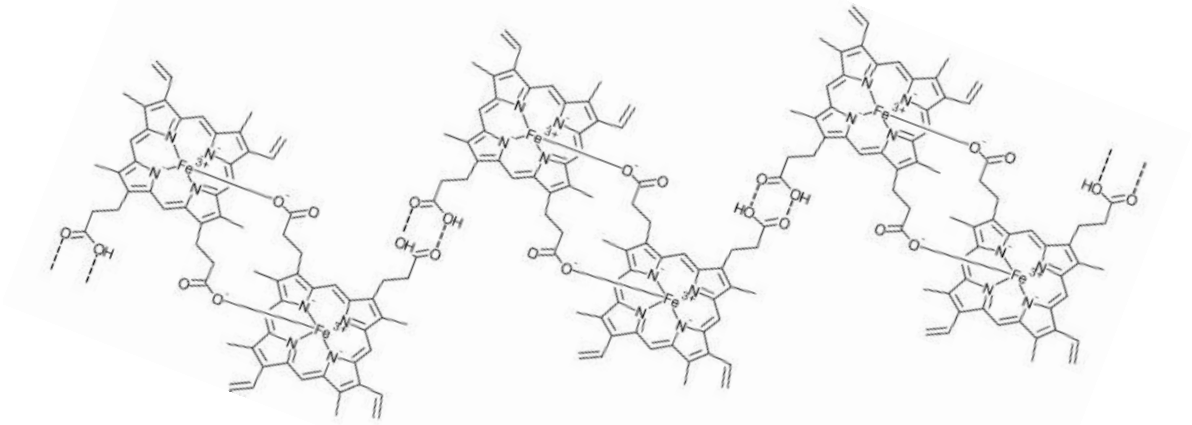

Figure 1.3. Structure of hemozoin.

1.3. Treatment

Quinine (**Figure 1.4**) was one of the first drugs used to treat malaria, going down in history as one of the first chemical compounds to successfully treat an infectious disease.[27] Quinine naturally occurs in the bark of Cinchona trees and was isolated in 1820.[28] Studies carried out in the years 1866-1868 resulted in the discovery of other cinchona alkaloids such as quinidine,

cinchonine and cinchonidine which are also effective antimalarials. Quinine was primarily used until the 1920s when more effective antimalarials were synthesized.[27]

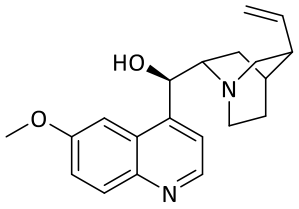

Figure 1.4. Structure of Quinine.

Guttmann *et al.* reported the antimalarial properties of a synthetic thiazine dye, methylene blue (MB) in 1891,[29] and it was the first synthetic drug used to treat malaria.[30] Its identification as an antimalarial led to the discovery of 8-aminoquinolines.[31] Subsequently, methylene blue analogues were synthesized in which the methyl group was replaced with a simple side chain.[32] These analogues exhibit increased antimalarial activity, leading to the belief that these side chains elicit favourable activities. From here, pamaquine (**Figure 1.5**) was discovered in the 1920s and was first used in 1926, but was later found to exhibit high toxicity.[32] Primaquine (**Figure 1.5**) was then synthesized as a less toxic derivative and is used to eradicate *P.vivax* and *P.ovale* strains in the liver stage.[32,33]

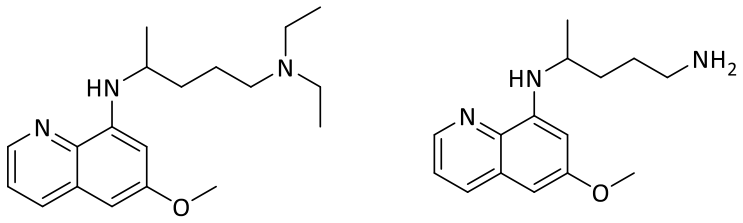

Figure 1.5. Structure of two methylene blue analogues (pamaquine and primaquine) used as antimalarial agents

The antimalarial activity and reduced toxicity of the primaquine led to the application of side chains in several other heterocycles, leading to the discovery of chloroquine (CQ) (**Figure 1.6**).[32] Chloroquine was largely used until the beginning of the 1940's when resistance emerged.[27]

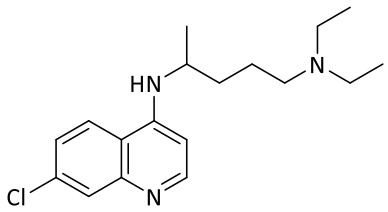

Figure 1.6. Structure of the antimalarial chloroquine.

Before the emergence of resistance, chloroquine was the ideal antimalarial drug, displaying high therapeutic activity, low toxicity and low cost.[34] As previously mentioned in **Section 1.2**, the malaria parasite detoxifies free heme *via* polymerization into hemozoin. In CQ-susceptible strains of malaria, CQ can prevent the detoxification process. Drugs like quinine and chloroquine inhibit hematin polymerization and the accumulation of free heme, rendering these drugs toxic to the parasite.[35] Chloroquine also inhibits β-haematin synthesis at physiological temperatures.[36,37]

1.3.1. Quinoline and non-quinoline drugs

Over the many years that malaria has been a global health problem, many antimalarial chemotherapeutics have been synthesized. These include compounds based on the well-known quinoline scaffold of chloroquine as well as compounds based on different scaffolds. Among the non-quinoline containing antimalarials are the artemisinin's which are used in the current antimalarial regime. Currently, the frontline treatment for malaria is artemisinin combination therapy (ACT).[38] ACT combines artemisinin or an artemisinin derivative and a drug from a different class such as mefloquine, piperaquine and lumefantrine.[39,40] Professor Youyou Tu won the 2015 Nobel Prize in Physiology or Medicine for her vital role in the

discovery of artemisinin.[41]

1.3.1.1. Quinoline-based antimalarials

The quinoline scaffold has prevailed over the years in pharmacologically synthesized compounds as well as in nature.[37] This scaffold is historically considered to be one of the most vital in antimalarial drug discovery, with CQ dominating these groups of compounds. Other quinoline derivatives include amodiaquine, piperaquine, primaquine, quinine and mefloquine, some of which are shown in **Figure 1.7**.[42] None of these alternate drugs have shown any pharmacological superiority over chloroquine and therefore the search for a more or as effective drug continues.[43] CQ gains its antimalarial properties through π-π stacking, allowing the drug to prevent hemozoin formation.[44] This π-π stacking occurs through interaction of the 4-aminoquinoline scaffold with the heme group or by the drug docking into the grooves of hemozoin, preventing crystal growth.[42] The toxic hematins are able to leave the digestive vacuole and enter into the parasite cytosol where oxidative stress is induced.

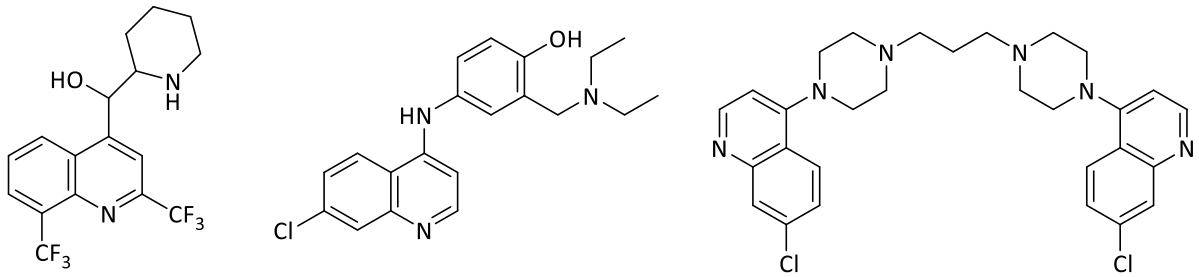

Figure 1.7. Structures of quinoline derivatives.

CQ is administered orally to patients in the form of CQ-phosphate tablets and is a blood schizonticidal drug. Blood schizonticidal drugs only act efficiently during the RBC stage of the parasite's life cycle,[45] losing its efficacy once the parasite progresses into the liver stage. CQ can be divided into three parts as labelled in **Figure 1.8**.[43] The tertiary amine found on ring **B**

is essential for the uptake and accumulation of the drug in the parasitic food vacuole.[43, 46] The aromatic and quinine rings **A** and **B** are essential for π-π stacking of the molecule in the heme and any alteration to the Cl at position 7 has shown to render the compound less potent.[43] The π-π stacking allows the drug to intercalate between the polymeric crystal packing in the acidic food vacuole of the parasite, forming a dimeric hematin complex and therefore inhibiting the heme crystallization process.[47]

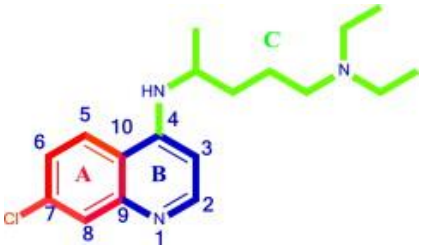

Figure 1.8. Labelled structure of CQ.[43]

CQ is a weak base with pKa of 8.1 (quinoline nitrogen) and 10.2 (diethylamine side-chain nitrogen), it enters into the acidic parasitic FV (pH of 5-5.2) in its unprotonated form.[45] Uncharged CQ is membrane permeable and can, therefore, easily diffuse into the FV.[48] When entering into the FV, chloroquine becomes protonated, a form which is not membrane permeable resulting in the accumulation of the drug in the FV.[49] CQ inhibits the polymerization of free heme into hemozoin, increasing intracellular heme.[50]

The development of new 4-aminoquinoline derivatives is a valid strategy for malaria treatment, due to the promising antimalarial properties exhibited by chloroquine and its derivatives.[43,51] Amodiaquine (**Figure 1.7**) is one such derivative, but due to side effects like hepatoxicity and agranulocytosis, its clinical use was restricted.[52] This led to the synthesis of fluoroamodiaquine (**Figure 1.9**). O'Neill *et al*. demonstrated that fluoroamodiaquine (FAQ) retains the antimalarial activity observed for amodiaquine but does not exhibit the toxic side effects.[53]

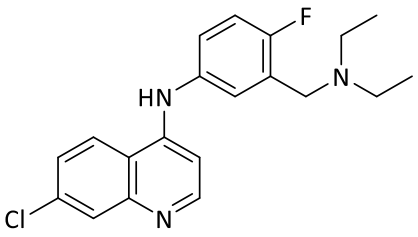

Figure 1.9. Structure of fluoroamodiaquine.

Stocks *et al*. generated a series of short-chain CQ derivatives, shown in **Figure 1.10.**[54] The derivative containing the tert-butyl terminal amino group in the side-chain (d) was the most active. This derivative showed a 4- and 20-fold increase in antimalarial activity against the C2Bu-CQ-sensitive and K1-CQ-resistant strains.

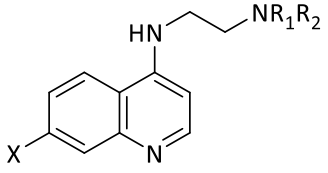

a. X=Cl, R_1=H, R_2=t-Bu
b. X=Cl, R_1, R_2=alkyl
c. X=Cf_3, R_1, R_2=alkyl
d. X=CF_3, R_1=H, R_2=t-bu

Figure 1.10. CQ derivatives synthesised by Stock *et al.*[54]

Madrid *et al.* synthesized a library of chloroquine derivatives in which the diethylamino side-chain was replaced with bulkier groups as shown in **Figure 1.11**.[55] The IC_{50} values of the synthesized compounds show superior antimalarial activity in two CQ-resistant strains (W2 and Dd2) compared to CQ. The derivative containing the bromobenzaldehyde moiety in the R_2 position and a propyl chain in the R_1 position exhibited the greatest antimalarial activity with an IC_{50} value of 11 nm compared to 23 nm for CQ.

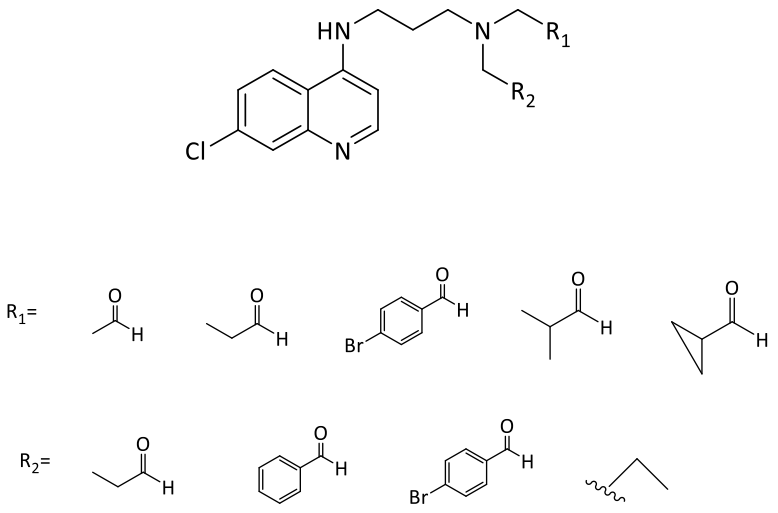

Figure 1.11. CQ derivatives synthesised by Madrid *et al*.[55]

Sunduru *et al*. synthesized a series of thiourea, thiazolidinedione and thioparabanic acid derivatives of 4-aminoquinolines.[56] These compounds were evaluated for their *in vitro* antiplasmodial activity and the thiourea derivative shown in **Figure 1.12** exhibited the highest antiplasmodial activity. The thiourea derivative has an IC_{50} value of 6.07 ng/mL against the 3D7-CQ-sensitive strain of *P. falciparum*.

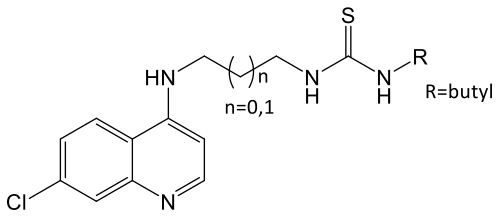

Figure 1.12. Thiourea derivative which exhibits the highest antiplasmodial activity against CQ-sensitive strain of *P. falciparum*.[56]

1.3.1.2. Non-quinoline based drugs

Among the well-known non-quinoline antimalarials is artemisinin (**Figure 1.13**). Artemisinin was discovered by Chinese researches and exhibits high potency against CQ-sensitive strains of *P.falciparum*.[57] The biological activity and complicated structure of artemisinin led to the investigation and synthesis of artemisinin analogues that exhibit higher potency than artemisinin itself.[58]

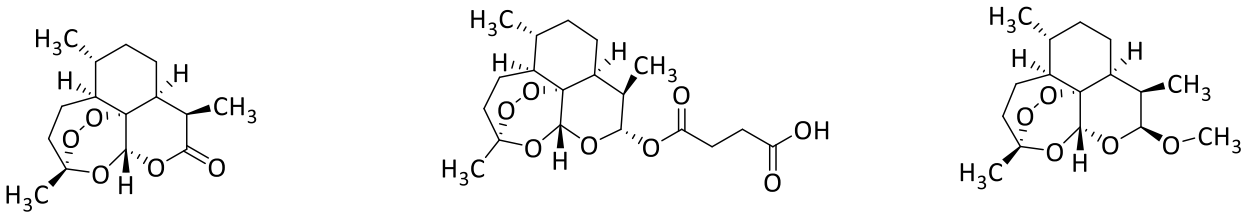

Figure 1.13. Structure of artemisinin and two of its derivatives

The mechanism of action of artemisinin and its derivatives are different from quinoline-based drugs, as their structures differ vastly. Artemisinin contains an endoperoxide bridge and peroxides are known to produce reactive oxygen species.[59] Inside the patristic FV, artemisinin interacts with free heme and the peroxide bridge is cleaved, producing ROS.[60] Their exact mechanism of action is debated but it is proposed to occur through both a parasite-specific and non-specific mechanism.[61]

Currently, the front-line treatment for malaria is artemisinin combination therapy (ACT). ACT increases the efficacy of the treatment by targeting more than one stage in the parasites life-cycle, decreasing the probability of resistance.[12] The artemisinin derivatives are the fastest acting compared to all other antimalarials.[62] This class of drug also displays a wider range of antimalarial activity, acting at more than one stage of the parasite life cycle.[63] Initially, it exerts its activity at the young ring stage and then prevents the maturation of the parasite into the more pathogenic stages.[62,64]

Another class of non-quinoline antimalarial drugs is the antifolates and is comprised of sulfa drugs that can be subdivided into two classes: class I and class II antifolates. Antifolates target the folate metabolism in the malaria parasite (**Figure 1.14**), which is an important metabolic pathway in the parasite's survival.[65] Class I antifolates inhibit dihydropteroate synthase (DHPS). Class II antifolates inhibit dihydrofolate reductase (DHFR).[66] DHFR and DHPS inhibitors are used in combination in order to produce a synergistic outcome.[67] Drugs belonging to class I include: sulfadoxine, sulfalene and dapsone. Those belonging to class II include: proguanil, chlorproguanil, clociguanil and pyrimethamine.[66]

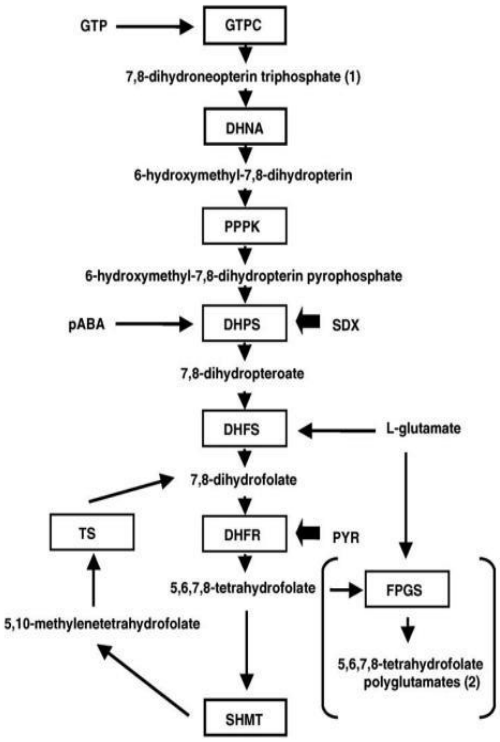

Figure 1.14. Parasitic folate pathway, showing the principle enzymes and subtrates.[62]

The folate derivatives synthesized *via* the folate pathway are essential cellular cofactors and provide single carbon (C1) units that are used in the following metabolic pathways: methionine, purines and pyrimidine's biosynthesis.[68] These single carbon units are essential for DNA replication and the initiation of protein synthesis in mitochondria.[68] Thus, any drug that inhibits the various enzymes involved in this pathway can be exploited in the development of antimalarials.[68] Pyrimethamine and cycloguanil (the active form of proguanil)

targets the DHFR activity of the parasites bifunctional DHFR-thymidylate synthetase (TS) protein.[69] The sulfa drugs affect the dihydropteroate synthetase (DHPS) activity of the bifunctional hydroxymethylpterin pyrophosphokinase (HPPK)-DHPS protein. Each of these antifolate drugs acts to competitively inhibit the parasites natural substrates.[69]

1.4. Drug resistance

Despite the extensive resources and research that goes into the investigation of effective antimalarials, drug-resistant strains of malaria continue to triumph. The geographical map shown in **Figure 1.15** illustrates that malaria is endemic in areas of America, Africa, Asia and Sub-Saharan Africa. Most of these regions are dominated by CQ or multi-drug resistant strains of malaria.

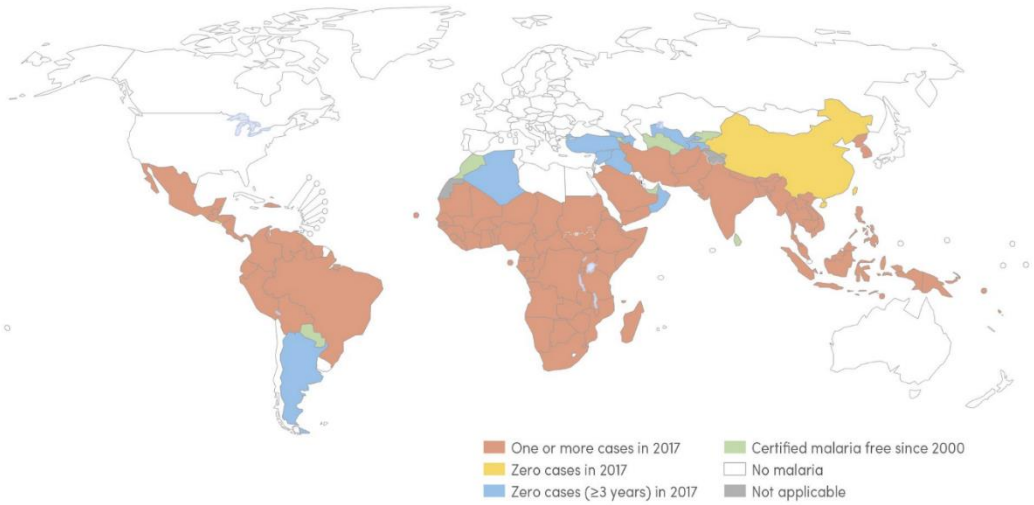

Figure 1.15. Geographical distribution of malaria obtained from the 2018 World Malaria Report.[8]

As previously mentioned in **Section 1.3.1.1**, CQ was widely used as the mainstay drug until the emergence of CQ-resistant strains of *P. falciparum*. This led to the use of antifolate combination *SP* (sulfadoxine-pyrimethamine) chemotherapy.[70] Resistance to antifolate combination therapy subsequently led to the use of the current ACT frontline treatment.[70] In 2008 Dondorp *et al*. documented resistance to artesunate monotherapy in the *P.falciparum* species.[71] The development of ACT resistance threatens the population as scientists fear that malaria may soon become untreatable.[72] The progressive emergence of resistance to all synthesized antimalarials has resulted in the development of multi-drug resistant (MDR) strains of the parasite.[73]

The mechanism by which the malaria parasite becomes resistant to antimalarials usually involves chromosomal mutations.[74] CQ-resistance in *P.falciparum* is conferred by the mutation in the *pfCRT (Plasmodium falciparum* Chloroquine Resistance Transporter) gene.[75] Parasites with the mutated *PfCRT gene* has the ability to transport protonated CQ out of the cell, preventing the accumulation of the drug and resulting in CQ-resistance.[76] Pyrimethamine and sulfa drug (PS, antifolates) resistance are attributed to mutations in the genes coding for the DHFR and DHPS enzymes.[77] Resistance to antifolates can result from various mechanisms such as the overproduction of DHFR or the reduced ability of the antifolate to diffuse across the cell membrane.[78] Artemisinin resistance differs from other antimalarials, as it is based on the enhanced entry of a larger number of young ring forms of the parasite into quiescence.[79] Upon treatment with artemisinin, a large number of parasites become dormant and growth is resumed once artemisinin is no longer present.[80] This enhanced ability to enter into quiescence is conferred by mutations in the *Pfk13 gene.*[80]

1.5. Hybrid molecules

Combination therapy is often used as an attempt to overcome resistance in diseases like malaria. Combination therapy involves the administration of two or more drugs at the same time to target more than one stage of a disease. The challenge with combination therapy is deciding the appropriate combinations of drugs and the correct doses of each drug. Instead of using two drugs in combination, molecular hybridization is a compelling alternative.

Molecular hybridization combines two pharmacologically active scaffolds into a single compound to increase the overall efficacy of the compound.[81] The synthesis of hybrid molecules has become a promising method in the development of anti-cancer,[82] anti-tuberculosis,[83] and antimalarial drugs.[84] Due to the constant emergence of drug-resistant strains of malaria, it is essential to develop treatments that may eventually put an end to the prevalence of the deadly disease. The notion of hybrid molecules presents an opportunity to generate dual activity in antimalarials whereby two pharmacophores are introduced into a single molecule.[85] This is done in hopes of synthesizing a compound with higher antiplasmodial activity than each of the individual drugs. [85]

1.5.1. Structure of hybrid molecules

Hybrid molecules can be synthesized either *via* direct conjugation through a linker or by combining different haptophoric moieties of two or more drugs.[81] Therefore, hybrid molecules can either be classified as 1) cleavable hybrids: two molecules directly linked or *via* spacers, which are hybrids that produce dual modes of action. 2) non-cleavable hybrids: two molecules connected *via* a linker that is enzymatically non-cleavable, these hybrids retain the pharmacological properties of both pharmacophores in a single compound. 3) Overlapping/ merged hybrids: obtained *via* the overlap of related structural moieties of two pharmacophores, these hybrids may or may not exhibit the biological properties of the parent molecules (**Figure 1.16**).[81]

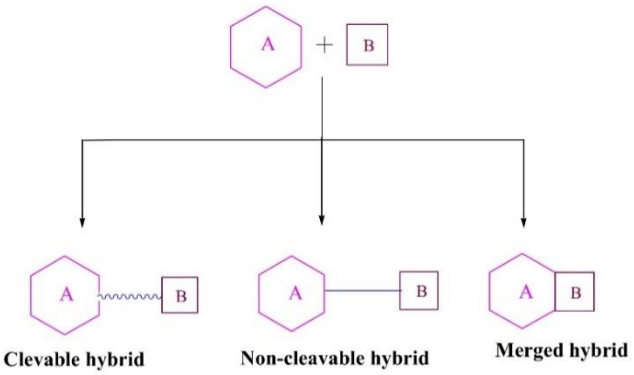

Figure 1.16. Representation of Cleavable, Non-cleavable and merged hybrids.[82]

1.5.2. Quinoline-triazole hybrids

Many studies report various antimalarial hybrids such as the artemisinin-based hybrids,[86] trioxaquines,[84] and quinoline-triazoles.[87] Triazoles have been reported to exhibit a range of biological activity such as antifungal, antibacterial, antitubercular and antimalarial.[88,89] The quinoline-triazole hybrids have therefore been studied extensively and display high antiplasmodial activity against several strains of *P.falciparum*. [88, 90, 91]

Manohar *et al.* report a series of 4-aminoquinoline-1,2,3-triazole and 4-aminoquinoline-1,2,3 triazole-1,3,5-triazine hybrid compounds.[88] The two most active compounds are shown in **Figure 1.17**.

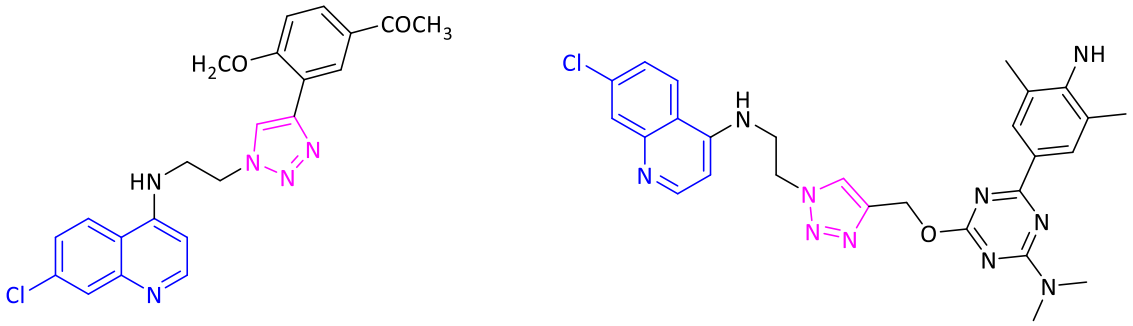

Figure 1.17. Structures of most active 4- aminoquinoline-triazole and 4-aminoquinoline-triazole-triazine hybrid molecules that were synthesised by Manohar *et al.*[89]

The *in vitro* antimalarial activity of these hybrid molecules was determined against the D6-CQ-sensitive and W2-CQ-resistant strains of *P. falciparum*. The 4-aminoquinoline-triazole hybrid containing the aryl scaffold (**Figure 1.17, left**) has an IC_{50} value of 0.65 μM. The 4-aminoquinoline-triazole-triazine hybrid on the right in **Figure 1.17** has an IC_{50} value of 0.58 μM. This study also showed that 4-aminoquinoline –triazoles and –triazole-triazines displayed higher potency as the carbon spacer between the secondary amine and triazole ring increased from 1 to 3. This trend was attributed to the increase in lipophilicity as the carbon

spacer was changed from 1 to 3.[88]

Boechat *et al*. reports on a series of quinoline-1,2,3-triazole hybrid compounds with the general structure shown in **Figure 1.18**.[90] The molecule shown on the right represents the hybrid that exhibits the highest activity with an IC_{50} value of 1.4 μM. All 11 synthesized compounds displayed moderate to good activity and none showed toxicity to healthy monkey kidney cells.[90]

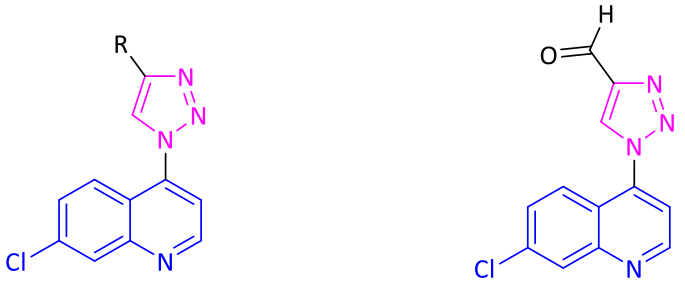

Figure 1.18. General structures of 4- aminoquinoline-triazole hybrid molecules synthesised by Boechat *et al.* (left) and most active hybrid (right).[91]

Pereira *et al*. synthesized a series of 4-aminoquinoline-1,2,3-triazole hybrids in which there were varying substituents on the 4-position of the triazole ring.[90]

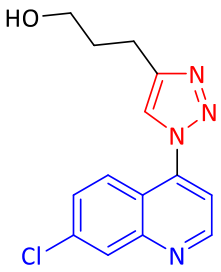

Figure 19. Structure of most active 4-aminoquinoline-triazole hybrid synthesized by Pereira *et al*.[91]

The 4-aminoquinoline-triazole hybrids were evaluated for their in vitro antiplasmodial activity against the W2-CQ-resistant strain of *P. falciparum*. The compounds displayed moderate antiplasmodial activity and low cytotoxicity when tested in Hep G2A16 cells. The hybrid shown in **Figure 1.19** exhibited the highest antimalarial activity with an IC_{50} value of 9.6 µM.[92]

1.6. Metals in Medicine

The use of metals in medicine serves as a very important bridge between inorganic chemistry and the medical industry. Metallodrugs are used to detect and treat several diseases due to their biological applications on cellular living systems.[93] Ancient history indicates that metal-based drugs have been used as early as ancient Greece where silver was used to treat wounds and ulcers.[94] The ancient Egyptians used copper to sterilize water and the medicinal use of gold in China dates all the way to 2500 BC.[95]

In modern medicine, cisplatin (**Figure 1.20**) was one of the first completely inorganic compounds used. Cisplatin is a platinum-based drug that was first discovered by Rosenberg for its ability to inhibit cellular division in *Escherichia coli*.[96] This led to the discovery of its antitumor properties in mice.[97] The successful use of Cisplatin and other platinum-based anticancer drugs has prompted the investigation of metal-based compounds that could potentially be used to combat other diseases.[98]

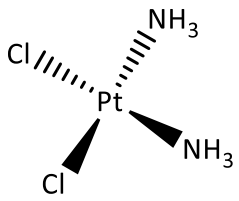

Figure 1.20. Structure of Cisplatin.

Metal complexes have been reported to treat insulin resistance,[99] inflammation,[100] microbial infections,[101] and parasitic diseases.[102] The medicinal properties of metal compounds are

appealing as they provide a unique approach to drug synthesis. The addition of metal centers to organic drugs can also be used as a method of improving the efficacy of that organic drug.[16] The reactivity of the metal complex can be specified through metal and ligand choice. Metal-based compounds are suitable for tropical parasitic disease treatment due to their excellent selectivity towards parasitic biomolecules as opposed to the host's biomolecules.[103]

1.6.1. Metalloantimalarials

Sanchez-Delgado *et al*. were one of the first groups to synthesize transition metal (Rh and Ru) complexes with a CQ scaffold that exhibited comparable antimalarial activity to CQ.[104] Initially a rhodium chloroquine derived complex **[Rh(COD)(CQ)Cl]** (**Figure 1.21,** left) was synthesized and tested for its antimalarial properties.[104] The complex exhibited similar *in vivo* antimalarial activity to CQ. To increase the biological activity of the complex, ruthenium was used, and the ancillary ligand varied (**Figure 1.21,** middle and right). These $Ru^{II}(\eta^6$-arene) chloroquine derivatives showed good antimalarial activity in both CQ-susceptible and -resistant strains of *P. falciparum*.[11]

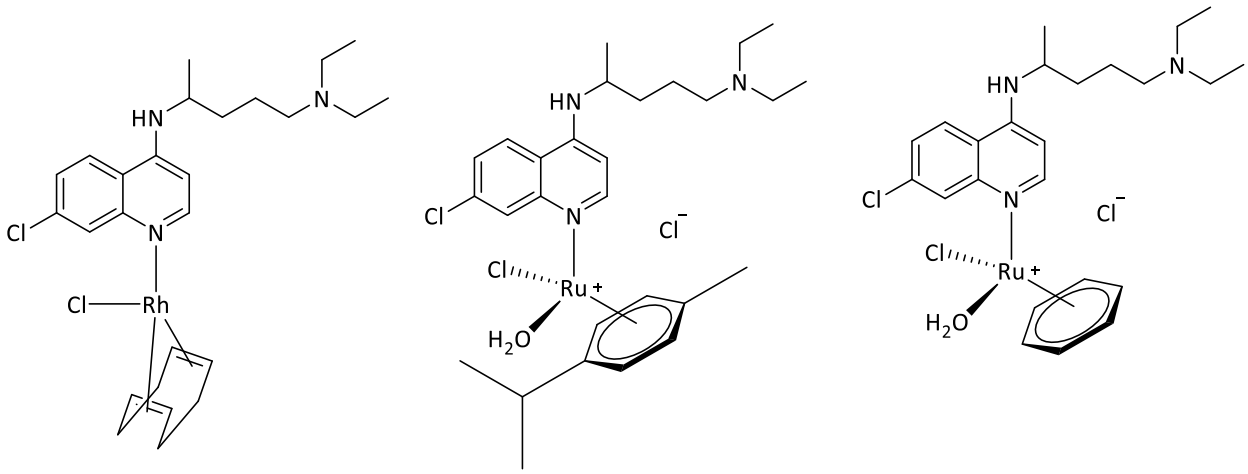

[Rh(COD)(CQ)Cl] [(p-Cymene)Ru(II)$Cl_2(H_2O)$(CQ)] [(benzene)Ru(II)(Cl)(H_2O)(CQ)]Cl

Figure 1.21. CQ derived metal complexes synthesized by Sanchez-Delgado *et al*.[105]

Scientists were encouraged by the enhanced activity of metal complexes leading to the development of other CQ-metal complexes. This includes the complexation of gold,[105] iridium,[106] and platinum,[107] to the organic CQ antimalarial. Due to the proven medical application of ferrocene complexes,[108] ferroquine (FQ) was synthesized.[16] FQ is a ferrocenyl derivative of CQ (**Figure 1.22**). FQ is active against both CQ-sensitive and -resistant strains of *P. falciparum*. A more active derivative of FQ is yet to be found, despite the many studies done on FQ and 120 of its derivatives.[109] The ferrocene derivative is currently undergoing phase IIb clinical trials and is being tested in combination with artefenomel (an antiparasitic agent).[110] It is quite evident that the modification of CQ with a metallic component such as the ferrocenyl moiety has rendered some advantageous antimalarial properties.

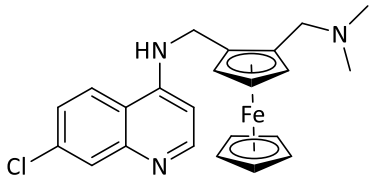

Figure 1.22. Structure of ferroquine.

The biological activity of FQ does not arise directly from the interaction of the organometallic moiety with parasitic proteins but can be afforded to two major aspects.[40] The first is that, like CQ, FQ contains the 4-aminoquinoline moiety that allows the compound to accumulate in the parasite's digestive vacuole.[111] This prevents important metabolic processes and ultimately leads to parasitic death.[111] The second mode of action involves the ferrocenyl substituent which generates hydroxyl (OH) radical species.[112] The production of these radical species prevents the formation of merozoites (a form of the parasite that enters red blood cells during the parasite's life-cycle).[112]

Literature reports on many more metal-based antimalarials that makes use of various other transition metal centres like osmium, palladium, copper, nickel, cobalt, iridium and zinc.[113] Many of these complexes also exhibit higher antimalarial activity than the free uncomplexed ligand, like the palladium complexes reported by Chellan *et al*.[114]

1.7. Metal carbonyls

Metal carbonyls play a crucial role in organometallic chemistry and have become popular in medicinal chemistry as carbon monoxide releasing molecules (CORMs) (see **Section 1.8**).[115,116] The carbonyl group bonds to the metal centre *via* σ bonding.[117] Overlap of CO σ-orbitals with that of an empty d-orbital of the metal results in a strong σ-bond formation and delocalization of π-d electrons from the metal ion into an empty π*-orbital (anti-bonding) of the CO.[117] This is called π-back-donation and results in a stronger M-C bond, but a weaker C-O bond.[117] Carbon monoxide (CO) is capable of forming complexes with both main group elements and transition metals, making it a versatile ligand. Some metal carbonyl complexes are also photoreactive, allowing them to undergo photo-induced reversible and non-reversible ligand exchanges and substitutions.[117] For this reason, metal carbonyls can also function as benign transporters for CO, the basis of CORMs that will be discussed later.[118]

1.7.1. Group 7 transition metal carbonyls

1.7.1.1. Rhenium carbonyls

Re(I) *fac*-tricarbonyl complexes that bear a low energy π* orbital have been found to be luminescent and biocompatible.[119] Similar to the luminescent d^6 Ir(III) and Ru(II) complexes, Re(I) tricarbonyl complexes are kinetically inert reducing the toxicity associated with heavy metal ion release.[120] Re(I) carbonyl complexes have been used in photodynamic therapy in which non-toxic photosensitizers generate toxic species like ROS.[121] This oxidative stress results in cell damage and can be applied in the treatment of cancer or infectious diseases like malaria.[119] The rhenium tricarbonyl complex shown in **Figure 1.23** contains a chloroquine-derived ancillary ligand and was evaluated for its antiparasitic activity against the *Trypanosoma brucei* strain of malaria. The complex exhibited an IC_{50} value of 0.9 μM and low toxicity against normal human cells.[122]

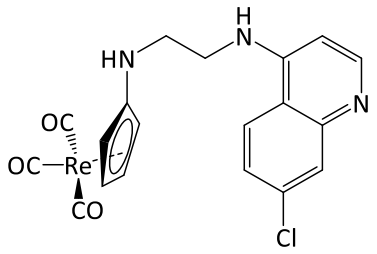

Figure 1.23. Chloroquine-containing rhenium tricarbonyl.

Toro *et al.* synthesized a series of ferrocenyl and cyrhetrenyl benzimidazoles which were evaluated for their antimalarial activity against the 3D7-CQ-susceptible and W2-CQ-resistant strains of *P.falciparum*.[123] The cyrhetrenyl complexes shown in **Figure 1.24** exhibited higher activity than the ferrocenyl analogs with IC_{50} values ranging from 10.4-26.5 µM.

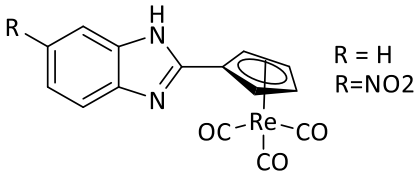

Figure 1.24. Cyrhetrenyl benzimidazoles synthesized by Toro *et al.*[123]

1.7.1.2. Manganese Carbonyls

One of the well-known manganese carbonyls is manganese decacarbonyl, which has been extensively studied for its photo-dissociative properties,[118] and was one of the first Mn carbonyls identified for its photo-dissociative properties.

Simpson *et al.* Synthesized a series of five Mn(I) tricarbonyl complexes containing three azole ligands.[124] The antiparasitic activity of the complexes were evaluated against *Leishmania major* and *Trypanosoma brucei*. Upon metalation, the Mn(I) tricarbonyl complexes exhibited low IC_{50} values but high toxicity towards the mammalian cell lines 293T and J774. The metal

complex shown in **Figure 1.25** showed the highest potency against *Trypanosoma brucei* with an IC_{50} value of 0.7 µM and exhibited selectivity towards the parasite as opposed to the mammalian cells.[124]

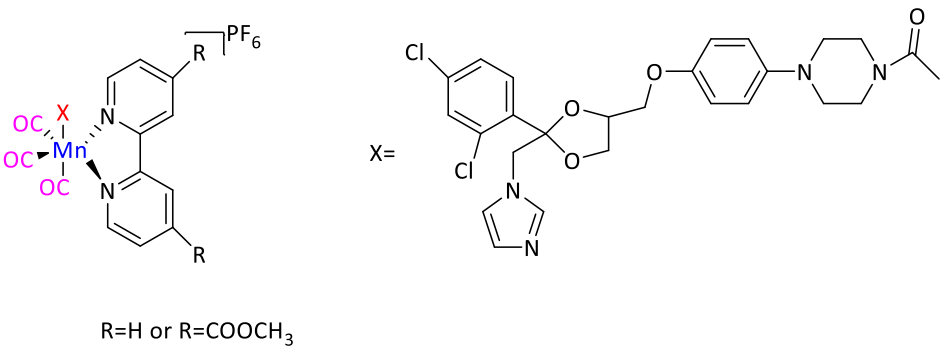

R=H or R=$COOCH_3$

Figure 1.25. Mn(I) tricarbonyl complex that exhibits good antiparasitic activity.

Minimum research has gone into the biological properties of manganese carbonyls as complexes. These complexes have more widely been studied as Carbon Monoxide-Releasing Molecules (CORMs) due to their dissociative properties.

1.7.2. Carbon monoxide-Releasing molecules (CORMs)

The use of metal carbonyls as biological agents has become popular in medicinal chemistry in the form of carbon monoxide releasing molecules (CORMs). CO-release from CORMs is initiated by external stimuli such as hydrolysis or solvolysis,[125] enzymes,[126] pH changes,[127] temperature,[128] and light.[129] CORMs mainly consist of transition metal carbonyls but non-metallic CORMs have been reported in the literature.[130,131] The CO-release rates and toxicological profiles of many organic CORMs were unfavourable and thus further studies were not performed.[132]

1.7.2.1. Carbon monoxide as a therapeutic agent

CO is largely associated with carbon monoxide poisoning due to its high affinity for hemoglobin,[133] and thus has a toxic effect on the oxygen metabolism.[134] Although toxic at high concentrations, CO is also endogenously produced in minuscule amounts in mammalian cells under stress conditions and serves as a molecular messenger.[135] Mammalian cells produce CO *via* the heme degradation process shown in **Figure 1.26**. During this process, heme oxygenase (HO) degrades heme into biliverdin, carbon monoxide and of Fe^{2+}.[136] Heme oxygenase's consist of HO-1, HO-2 and HO-3. HO-1 is induced during stress, HO-2 is a constitutive form and HO-3 is largely inactive.[136]

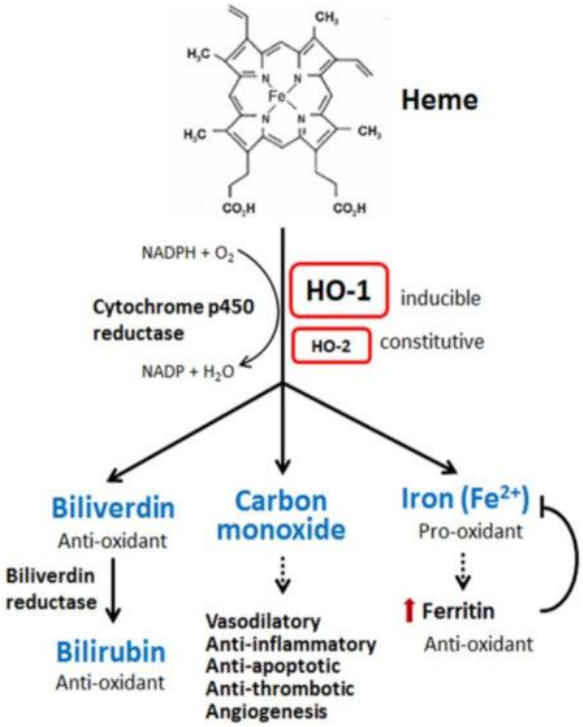

Figure 1.26. Heme (left) and the degradation process of heme to bilirubin (right).[138]

CO plays an essential role in metabolic processes such as inflammation,[137] apoptosis,[138] vasodilation,[139]and in the inhibition of platelet accumulation.[140] In addition to the therapeutic effects displayed by the gasotransmitter (a gaseous compound with a biochemical function), the application of CO extends much further. CO has received significant acknowledgment in

the medical field for its application as an anticancer agent,[116] antimicrobial properties,[141] antimalarial,[142] and its successful use in organ transplants.[143-144] CO also exhibits cytoprotective properties against certain reactive oxygen species that cause oxidative stress in cells.[134] For these reasons, the use of CO as a therapeutic agent has gained momentum for its potential applications at non-toxic concentrations.[125] The mechanism of action by which CO works to treat the aforementioned illnesses varies but is not fully understood for either of them. The mechanism of CO as an antimicrobial agent is hypothesized to be through the inhibition of DNA replication and cellular respiration.[145] Other evidence indicates that CO causes global changes in gene expression of microorganisms as well as in cell function.[145] In cancer treatment CO can prevent the expression of proteins that promote cancer, inhibit proliferation and induce ROS production.[146] The gaseous molecule provides protection against malaria by inhibiting the degradation of haemoglobin into free heme.[142] This subsequently prevents the polymerization of heme into hemozoin.

CO has played a vital role as a therapeutic agent and as a form of treatment for several diseases but the administration of CO as gas is not suggested. This is due to its toxicity and inability to control the localization or selectivity of gaseous CO.[9] CORMs present a safer alternative method of CO-administration. CORMs allow for CO-release to be site-specific, dose-controlled and intensified presenting a viable approach for antiparasitic treatments that use new modes of action.[145]

1.7.2.2. Non-metallic CORMs

Several purely organic CORMs have been synthesized and reported in the literature. This includes methylene chloride which releases CO post degradation. CO-release from methylene chloride was used to effectively inhibit allogeneic chronic rejection in rats.[147] Motterlini *et al.* identified a boranocarbonate ($Na_2[H_3BCO_2]$) titled CORM-A1 (**Figure 1.27**) as an organic CORM which releases CO in aqueous solutions.[128]

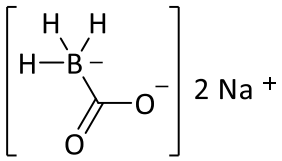

Figure 1.27. CORM-A1 identified by Motterlini *et al.* as an organic CO-releasing molecule in aqueous solution.128

Ayudhya *et al*. synthesized the first example of an amine carboxyboranes that releases CO under physiological conditions.[148] Wang *et al.* report on molecules that release CO via a "click-and-release" (CNR) mechanism.[149] In this method, the compounds are stable on their own but can react with each other to release CO. An example is tetraphenylcyclopentadienone (**6a in Figure 1.28**, TPCPD) and bicyclo-[6.1.0]nonyne (**7a**, BCN) which react *via* an inverse electron demand Dield-Alder reaction to release CO. Although these examples release CO *via* hydrolysis, organic PhotoCORMs have also been reported in the literature.

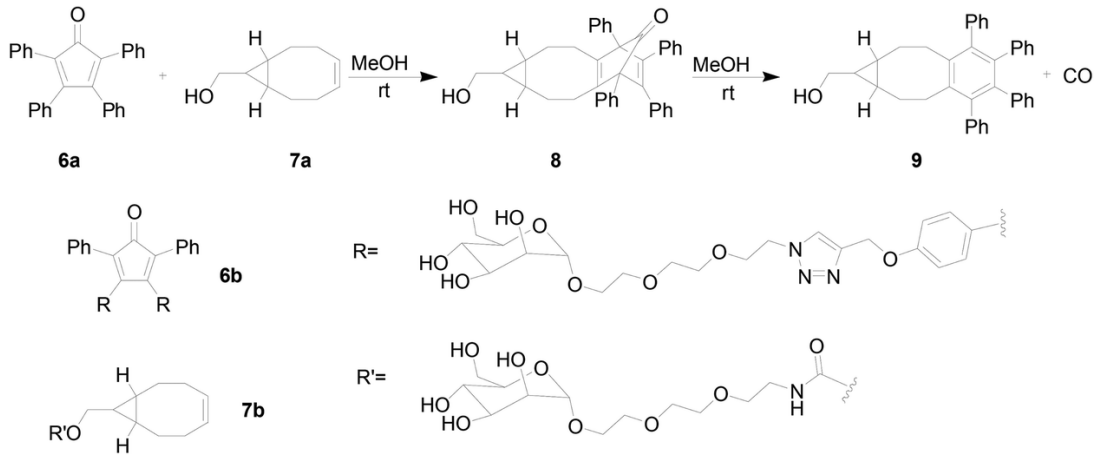

Figure 1.28. Inverse electron demand Dield-Alder reaction between tetraphenylcyclopentadienone (TPCPD, **6a**) and bicyclo-[6.1.0]nonyne (BCN, **7a**) to release CO

Examples of unsaturated cyclic α-diketones,[150] xanthene carboxylic acids,[151] meso-carboxy BODIPY,[152] and hydroxyflavone derivatives,[153] have all shown photoCORM properties. Due to the relatively recent development of organic CORMs, their biological applications are not established. Organic CORMs are also less advantageous than those containing metal centres due to the lower CO content and production of organic byproducts.[154]

1.7.2.3. Group 7 transition metal PhotoCORMs

The medicinal uses of light and its role in the activation of processes in metal complexes have been explored for over a decade.[155] The study of the photo-physics and photo-chemistry of CORMs led to the discovery of photoCORMs.[125] PhotoCORMs (photo-activated CO-releasing molecules) are CO donors that release CO upon illumination of light of the correct wavelength.[156]

In order for CO to be delivered to the biological target upon illumination, the metal carbonyl complex needs to be stable in aqueous solutions in the dark for long periods of time.[157] Upon illumination, one (or more) CO molecules will be released, while the remaining metal complex remains intact, as seen in **Figure 1.29**.[157] The released CO is transported to the biological target while the remaining metal complex is likely to bind to a solvent molecule in order to retain the correct coordination number and therefore stability.[157]

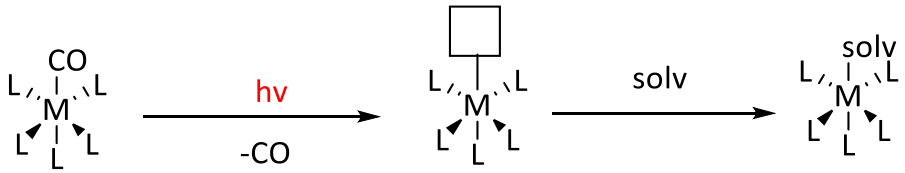

Figure 1.29. General method of photo-activated CO-release.[159]

Several metals are used in the synthesis of CORMs but the use of Mn(I) in photoCORMs is popular due to the thermal stability associated with the metal in this oxidation state, as well

as the easy synthesis and low toxicity of these compounds.[9] Mn(I) and Re(I) metal carbonyls have a low spin d^6 configuration and are studied due to their extensive photo-physical and photochemical properties.[158] These transition metal complexes exhibit a clear MLCT transition that favourably labilizes the metal-CO bond promoting CO-release. Mn carbonyls release CO quickly upon exposure to visible light, as opposed to its Re analogues which are only photoactivated upon exposure to UV light.[159] Several manganese photoCORMs have been reported, where CO-release was monitored intracellularly, using blue fluorescence.[125,156] Many manganese photoCORMs have mainly been studied for their physical properties and ability to release CO upon irradiation.[9,160] These complexes may potentially be studied further for the targeted release of CO into cellular systems.[160]

Dimanganese decacarbonyl [$Mn_2(CO)_{10}$) is one of the first Mn PhotoCORMs identified by Moterlinni *et al*.[139], although the complex was not referred to as a photoCORM at the time. [$Mn_2(CO)_{10}$] releases CO upon photodissociation and can cause heart vasoconstriction in rats.

Poole *et al.* synthesized a water-soluble Mn PhotoCORM, [$Mn(CO)_3$(tpa-κ^3N]Br (**Figure 1.30**).[161] The complex was found to be stable in solution and released CO upon illumination of light at 365 nm. The complex was also found to be toxic to the *Escherichia coli* strain K-12 upon photo-activation but had no effect in the dark.

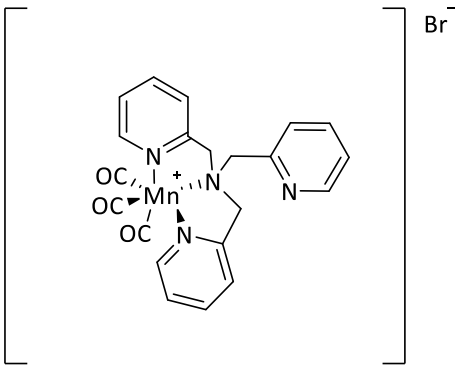

Figure 1.30. Structure of metal carbonyl complex, [$Mn(CO)_3$(tpa-κ^3N]Br synthesized by Poole *et al.*[163]

Tutar *et al*. synthesized several manganese photoCORMs, two of which are shown in **Figure 1.31**. These complexes were evaluated for their CO-releasing and anticancer properties against the human breast cancer cell line MCF-7. [116]

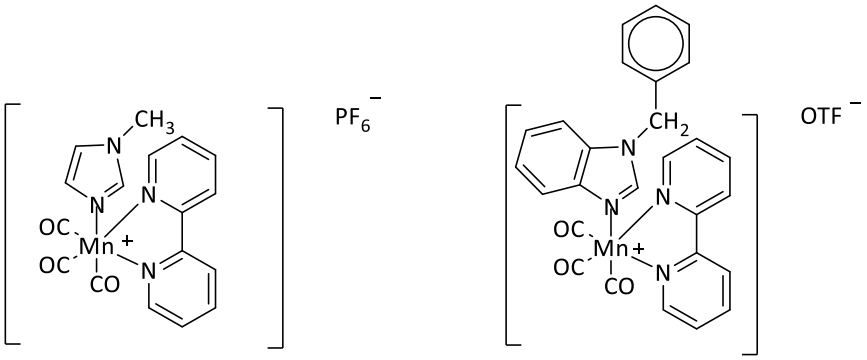

Figure 1.31. PhotoCORMs synthesized by Tutar et al. that show anticancer properties.[117]

In the absence of irradiation, the complexes exhibited low toxicity towards the cancer cells, but upon irradiation at 365 nm, the complexes inhibited cell proliferation.[116]

Kianfar *et al.* reports on three rhenium tricarbonyl compounds, shown in **Figure 1.32** that exhibits selective photochemical CO-release. These compounds all have low quantum yields, making them suitable for the potential study as photoCORMs without quickly reaching cytotoxic concentrations of CO.[162]

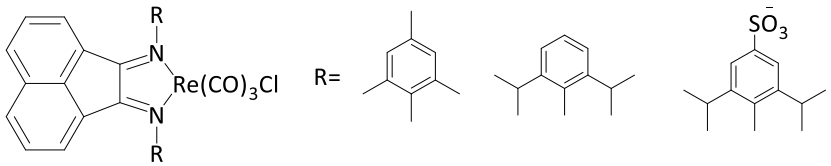

Figure 1.32. Rhenium PhotoCORMs that exhibits photochemical CO-release and non-cytotoxic CO concentrations.

1.7.2.4. CORMs used to treat malaria

No recorded reports were found in which group 7 transition metal CORMs are evaluated for the treatment of malaria. In general, the study of CORMs/photoCORMs revolves mostly around the treatment of cancer and its potential use as an antimalarial agent has only been explored in one study. Pena *et al.* synthesized a ruthenium-based metal carbonyl in **Figure 1.33** and evaluated its potential antiplasmodial activity in mice. [115]

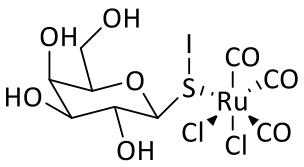

Figure 1.33. Ru (II) complex ((ALF492) that effectively protects mice against experimental cerebral malaria.

The Ru(II) complex (**ALF492**) protected mice from ECM (experimental cerebral malaria) and also induced the production of heme oxygenase 1 (HO-1) which has previously been proven to protect mice against ECM.[142] The study indicated that when the CORM was used in combination with the antimalarial drug artesunate, the efficacy of the combined compounds was increased and the immune response of the mice was enhanced.[115] This study becomes pivotal in drug design and certainly supports the investigation of CORMs as a new mode of action for antimalarial treatment.

1.8. Rationale and motivation for the current study

The prevalence and consistent emergence of resistant strains of malaria to all known antimalarial drugs is a clear indication that there is a need for new innovative treatments. It is essential that these compounds explore a new mode of action. The shocking statistics that the disease mainly claims the lives of pregnant women and children under the age of 5

motivates the investigation of new treatments. This study is also motivated by the fact that the majority of cases and fatalities occur on the African continent. Literature reports several beneficial biological activities of CORMs as well as the therapeutic use and extensive research into its anti-cancer properties. There is only a single study that evaluates a CORM for its antimalarial properties, despite the potential CO has as an antimalarial agent.

Chloroquine-triazole hybrids have proven to exhibit high potency against several strains of *P. falciparum*. For this reason, it is worth investigating the effects of incorporating these hybrid molecules into a CO-releasing framework. It is possible that in addition to the antimalarial properties of the two known antimalarial pharmacophores, CO-release may increase the potency of the parent molecules. While conducting this literature review, no metal carbonyl chloroquine-triazole hybrid molecules were found, but the several reports on chloroquine-derivative complexes make for a good argument in favor of a further investigation of such compounds. The addition of a triazole moiety is done on the basis that triazole compounds have also shown antiplasmodial activity against *P. falciparum.*

1.9. Aims and Objectives

1.9.1. General aims

As discussed in this chapter, there is a lack of research focussed on the antimalarial evaluation of carbon monoxide and CORMs/PhotoCORMs. The aims of this project were:

- To synthesize and characterize two quinoline-1,2,3-triazole ligands.
- To complex these ligands to an Mn(I) and Re(I) tricarbonyl core.
- To perform reactivity studies on the Mn(I) complexes.
- To evaluate the *in vitro* antiplasmodial activity of the parent ligand and their respective complexes.
- To evaluate the photoCORM properties of the metal tricarbonyl complexes.

1.9.2. Specific objectives

The specific objectives were to:

- Synthesize an aryl ether *via* a Schiff base condensation reaction followed by a Williamson ether reaction (**Scheme 1.1**)

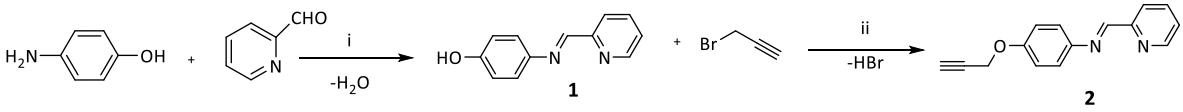

Scheme 1.1. Reaction scheme for the synthesis of the aryl ether (**2**). Reagents and conditions: (i) MeOH, reflux, 21 h; (ii) Acetone, K_2CO_3, 18-crown-6, reflux, 72 h.

- Synthesize 4-azido-7-chloroquinoline *via* a nucleophilic aromatic substitution reaction (**Scheme 1.2**)

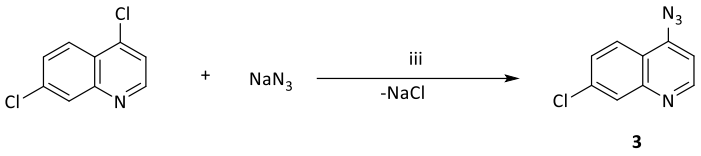

Scheme 1.2. Synthetic route for the synthesis of 4-azido-7-chloroquinoline (**3**). Conditions: (iii) DMF, reflux, 6 h.

- Synthesize *N*-(3-azidopropyl)-7-chloroquinolin-4-amine (**Scheme 1.3**)

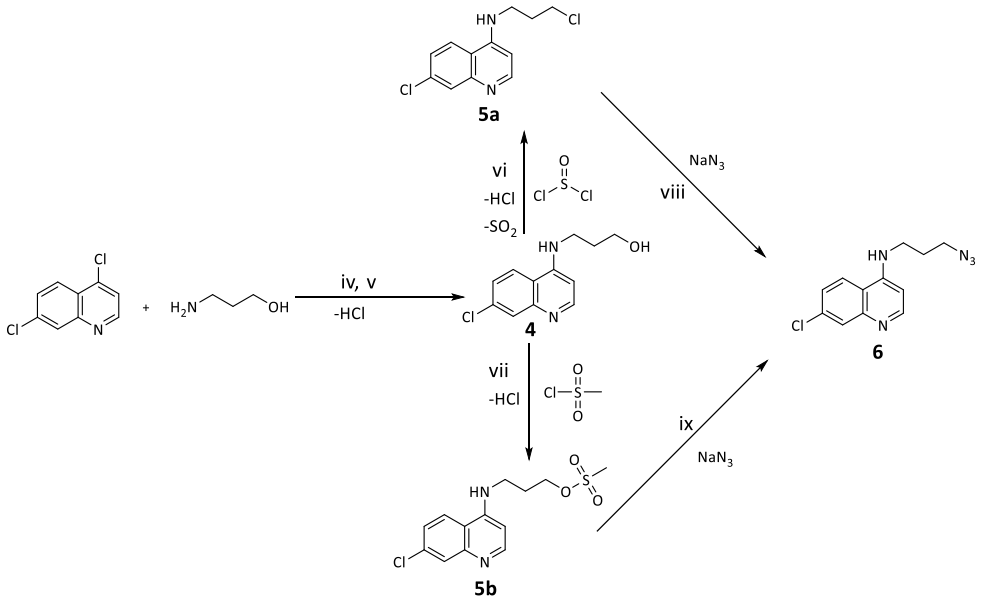

Scheme 1.3. Synthetic scheme for 4-amino-7-chloroquinoline intermediates **4**, **5a**,**5b** and **6**. Conditions: (iv) neat, 180 ℃, 1 h; (v) 130℃, 16 h; (vi) cat.DMF, reflux, 16 h; (vii) THF, NEt_3, 0℃, 3 h; (viii) DMF, relux, 18 h; (ix) DMF 4 h.

- Synthesize a 7-chloroquinoline-1,2,3-triazole and a 4-amino-7-chloproquinoline-1,2,3-triazole (**Scheme 1.4**).

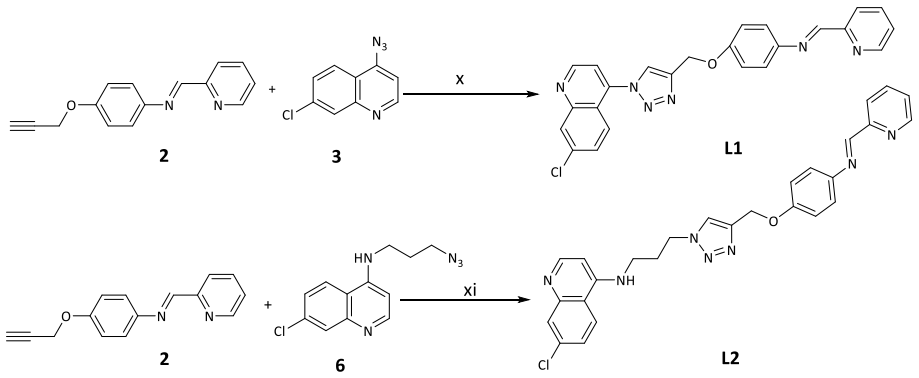

Scheme 1.4. Synthetic scheme for the CuAAC of **L1 and L2**. Conditions: (x) DCM,CuI, DIPEA, reflux, 4 h, (xi) DCM,CuI, DIPEA, reflux, 18 h.

- Synthesize Mn(I) and Re(I) tricarbonyl complexes of the quinoline-triazole ligands (**Scheme 1.5**).

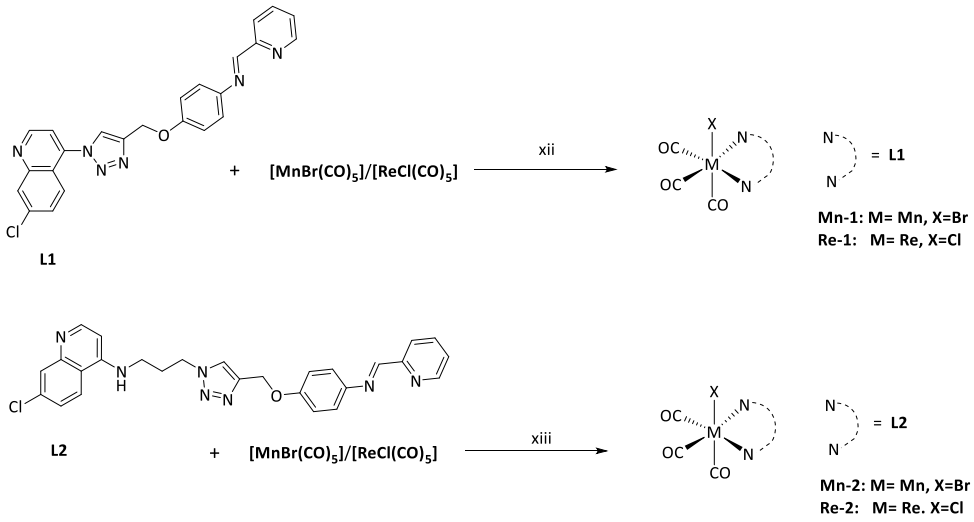

Scheme 1.5. Synthetic scheme for the complexation of ligands **L1 and L2**. Conditions: (xii) **Mn-1**: DCM, rt, 72 h. **Re-1**: DCM, reflux, 96 h. (xiii) **Mn-2**: DCM, 25, 24 h. **Re-2**: DCM, 40, 24 h.

- Perform reactivity studies on complex **Mn-1** using an [2+1] approach to synthesize a cationic species (**Scheme 1.6**)

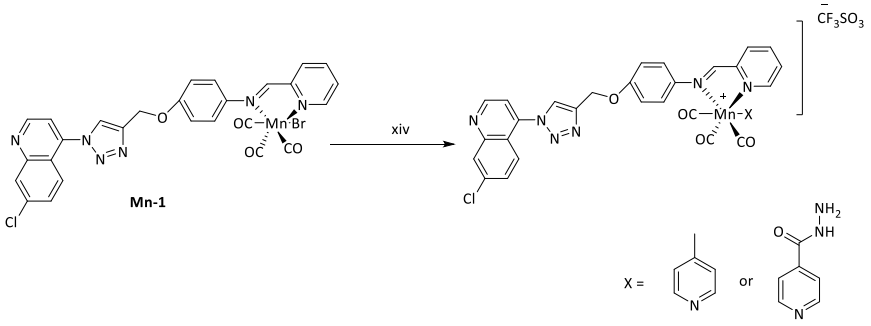

Scheme 1.6. Synthetic route taken for the synthesis of cationic **Mn-1.** Conditions: (xiv) MeCN, rt, 22.5 h.

- Characterize the compounds using various spectroscopic and analytical techniques such as Nuclear Magnetic Resonance spectroscopy (NMR), Fourier Transform-Infrared spectroscopy (FT-IR), Elemental Analysis (EA) and Electrospray Ionisation (ESI) mass spectrometry.
- Evaluate antimalarial and light-induced CO-releasing properties of metal tricarbonyl complexes to determine if the production of CO confers the compounds more toxic to the parasite.

1.10. References

1 F. E. Cox, *Parasites and Vectors*, 2010, **3**, 1–9.

2 K. A. H Gelband, CB Panosian, *Saving Lives, Buying Time*, National Academies Press, Washington, D.C., 2004.

3 L. J. Bruce-Chwatt, *J. R. Soc. Med.*, 1981, **74**, 531–536.

4 J. D. M. Mhlanga, M. Bentivoglio and K. Kristensson, *Brain Res. Bull.*, 1997, **44**, 579–589.

5 CDC, The History of Malaria, an Ancient Disease, https://www.cdc.gov/malaria/about/history/, (accessed 24 January 2018).

6 R. Ross, *Yale J. Biol. Med.*, 2002, **75**, 103–105.

7 WHO, 10 facts on malaria, http://www.int.features/factfiles/malaria, (accessed 24 January 2018).

8 World health organisation, World malaria report 2018, https://apps.who.int/iris/bitstream/handle/10665/275867/9789241565653-eng.pdf?ua=1, (accessed 5 November 2019).

9 B. J. Aucott, J. S. Ward, S. G. Andrew, J. Milani, A. C. Whitwood, J. M. Lynam, A. Parkin and I. J. S. Fairlamb, *Inorg. Chem.*, 2017, **56**, 5431–5440.

10 M. J. I. Nmadu P. M., Peter E., Alexander P., Koggie A. Z., *J. Heal. Sci.*, 2015, **5**, 47–51.

11 M. Navarro, W. Castro and C. Biot, *Organometallics*, 2012, **31**, 5715–5727.

12 P. F. Salas, C. Herrmann and C. Orvig, *Chem. Rev.*, 2013, **113**, 3450–3492.

13 R. Batista, A. De Jesus Silva Júnior and A. B. De Oliveira, *Molecules*, 2009, **14**, 3037–3072.

14 A. F. Cowman, D. Berry and J. Baum, *J. Cell Biol.*, 2012, **198**, 961–971.

15 P. J. Rosenthal, *N. Engl. J. Med.*, 2008, **358**, 1829.

16 C. Biot, W. Castro, C. Y. Botté and M. Navarro, *Dalton. Trans.*, 2012, **41**, 6335.

17 R. G. Ridley, A. Dorn, S. R. Vippagunta and J. L. Vennerstrom, *Ann. Trop. Med. Parasitol.*, 1997, **91**, 559–566.

18 S. Kumar, M. Guha, V. Choubey, P. Maity and U. Bandyopadhyay, *Life Sci.*, 2007, **80**, 813–828.

19 P. Parroche, F. N. Lauw, N. Goutagny, E. Latz, B. G. Monks, A. Visintin, K. A. Halmen, M. Lamphier, M. Olivier, D. C. Bartholomeu, R. T. Gazzinelli and D. T. Golenbock, *Proc. Natl. Acad. Sci. U. S. A.*, 2007, **104**, 1919–1924.

20 M. T. Shio, S. C. Eisenbarth, M. Savaria, A. F. Vinet, K. W. Harder, F. S. Sutterwala, D. S. Bohle, A. Descoteaux, A. Richard and M. Olivier, *PLoS Pathog.*, 2009, **5**, e100559.

21 T. J. Egan, *Mol. Biochem. Parasitol.*, 2008, **157**, 127–136.

22 D. J. S. Jr, I. Y. Gluzman and D. E. Goldberg, *Science (80-.).*, 2019, **271**, 219–222.

23 C. Y. H. Choi, E. L. Schneider, J. M. Kim, I. Y. Gluzman, D. E. Goldberg, J. A. Ellman, M. A. Marletta, A. Arbor and S. Louis, *Chem. Biol. Interface*, 2002, **9**, 881–889.

24 A. K. Tripathi, S. K. Garg and B. L. Tekwani, *Biochem. Biophys. Res. Commun.*, 2002, **290**, 595–601.

25 T. J. Egan, *Mini Rev. Med. Chem.*, 2001, **1**, 113–123.

26 T. J. Egan, *Trends Parasitol.*, 2002, **18**, 10–11.

27 J. Achan, A. O. Talisuna, A. Erhart, A. Yeka, J. K. Tibenderana, F. N. Baliraine, P. J. Rosenthal and U. D'Alessandro, *Malar. J.*, 2011, **10**, 144.

28 S. R. Meshnick and M. J. Dobson, *Antimalar. Chemother. Mech. Action, Resist. New*

Dir. Drug Discov., 2001, 15–25.

29 P. E. Guttmann, P. Ehrlich., *Berl Klin Wochenschr*, 1891, **28**, 953–956.

30 A. Zoungrana, B. Coulibaly, A. Sie, I. Walter-Sack, F. P. Mockenhaupt, B. Kouyate, R. H. Schirmer, C. Klose, U. Mansmann, P. Meissner, *PLoS One*, 2008, **3**, 23–26.

31 G. S. Hani Armma, Miriam Krugliuk, E. Deho and G. P. and H. Ginsbwg, *Biochem. Biophys. Res. Commun.*, 1996, **51**, 693–700.

32 M. Foley, *Pharmacol. Ther.*, 1998, **79**, 55–87.

33 M. Jeffery and G. R. Coatney, *Am. J. Trop. Med. Hyg.*, 1951, **2**, 949–957.

34 T. J. Egan and H. M. Marques, *Coord. Chem. Rev.*, 1999, **190**–**192**, 493–517.

35 K. N. Olafson, M. A. Ketchum, J. D. Rimer and P. G. Vekilov, *Proc. Natl. Acad. Sci. U. S. A.*, 2015, **112**, 4946–4951.

36 A. Dorn, S. R. Vippagunta, H. Matile, C. Jaquet, J. L. Vennerstrom and R. G. Ridley, *Biochem. Pharmacol.*, 1998, **55**, 727–736.

37 K. Kaur, M. Jain, R. P. Reddy and R. Jain, *Eur. J. Med. Chem.*, 2010, **45**, 3245–3264.

38 R. Pasupureddy, Atul, S. Seshadri, V. Pande, R. Dixit and K. C. Pandey, *Parasitol. Res.*, 2019, **118**, 29–42.

39 E. Y. Klein, *Int. J. Antimicrob. Agents*, 2013, **41**, 311–317.

40 M. Patra and G. Gasser, *Nat. Rev. Chem.*, 2017, **1**, 0066.

41 Glowicz, *Physiol. Behav.*, 2017, **176**, 139–148.

42 Y. Hu, C. Gao, S. Zhang, L. Xu, Z. Xu and L. Feng, *Eur. J. Med. Chem.*, 2017, **139**, 22–47.

43 M. Mushtaque and S. Shahjahan, *Eur. J. Med. Chem.*, 2015, **90**, 280–295.

44 V. A. Otelo, A. C. Sant'Ana, D. L. A. De Faria and C. M. S. Menezes, *Bioorganic Med. Chem. Lett.*, 2011, **21**, 250–254.

45 A. R. Parhizgar, *Iran. J. Med. Sci.*, 2017, **42**, 115–128.

46 D. Warhurst, J. Craig, I. Adagu, D. Meyer and S. Lee, *Malar. J.*, 2003, **2**, 26.

47 D. Lynch, *Trinity Student Sci. Rev.*, 2016, **2**, 196–210.

48 M. Chinappi, A. Via, P. Marcatili and A. Tramontano, *PLoS One*, 2010, **5**, e14064.

49 R. E. Martin, R. V. Marchetti, A. I. Cowan, S. M. Howitt, S. Bröer and K. Kirk, *Science (80-.).*, 2009, **325**, 1680–1682.

50 R. E. Martin and K. Kirk, *Mol. Biol. Evol.*, 2004, **21**, 1938–1949.

51 G. A. Biagini, P. M. O'Neill, A. Nzila, S. A. Ward and P. G. Bray, *Trends Parasitol.*, 2003, **19**, 479–487.

52 P. M. O'Neill, A. Mukhtar, P. A. Stocks, L. E. Randle, S. Hindley, S. A. Ward, R. C. Storr, J. F. Bickley, I. A. O'Neil, J. L. Maggs, R. H. Hughes, P. A. Winstanley, P. G. Bray and B. K. Park, *J. Med. Chem.*, 2003, **46**, 4933–4945.

53 P. M. O'Neill, A. C. Harrison, R. C. Storr, S. R. Hawley, S. A. Ward and B. K. Park, *J. Med. Chem.*, 1994, **37**, 1362–1370.

54 P. A. Stocks, K. J. Raynes, P. G. Bray, B. K. Park, P. M. O'Neill and S. A. Ward, *J. Med. Chem.*, 2002, **45**, 4975–4983.

55 P. B. Madrid, N. T. Wilson, J. L. DeRisi and R. K. Guy, *J. Comb. Chem.*, 2004, **6**, 437–442.

56 N. Sunduru, K. Srivastava, S. Rajakumar, S. K. Puri, J. K. Saxena and P. M. S. Chauhan, *Bioorganic Med. Chem. Lett.*, 2009, **19**, 2570–2573.

57 K. Kaur, M. Jain, T. Kaur and R. Jain, *Bioorganic Med. Chem.*, 2009, **17**, 3229–3256.

58 J. Han, J. G. Lee, S. S. Mi, S. H. Park, C. K. Angerhofer, G. A. Cordell and S. U. Kim, *J. Nat. Prod.*, 2001, **64**, 1201–1205.

59 S. Williams, *Confed. Aust. Crit. Care Nurses J.*, 1990, **3**, 20–21.

60 C. Sun and B. Zhou, *Microb. Cell*, 2016, **3**, 196–205.

61 J. Golenser, J. H. Waknine, M. Krugliak, N. H. Hunt and G. E. Grau, *Int. J. Parasitol.*, 2006, **36**, 1427–1441.

62 F. Nosten and N. J. White, *Am. J. Trop. Med. Hyg.*, 2007, **77**, 181–192.

63 L. E. Heller and P. D. Roepe, *Trop. Med. Infect. Dis.*, 2019, **4**, 89.

64 N. J. White, *Antimicrob. Agents Chemother.*, 1997, **41**, 1413–1422.

65 J. E. Hyde, *Acta Trop.*, 2005, **94**, 191–206.

66 A. Nzila, *J. Antimicrob. Chemother.*, 2006, **57**, 1043–1054.

67 Y. Yuthavong, *Microbes Infect.*, 2002, **4**, 175–182.

68 A. Nzila, S. A. Ward, K. Marsh, P. F. G. Sims and J. E. Hyde, *Trends Parasitol.*, 2005, **21**, 334–339.

69 I. B. Müller and J. E. Hyde, *Future Microbiol.*, 2010, **5**, 1857–1873.

70 A. E. P. Frosch, M. Venkatesan and M. K. Laufer, *Malar. J.*, 2011, **10**, 116.

71 A. M. Dondorp, F. Nosten, P. Yi, D. Das, A. P. Phyo, J. Tarning, D. Ph, K. M. Lwin, F. Ariey, W. Hanpithakpong, S. J. Lee, P. Ringwald, K. Silamut, T. Herdman, S. S. An, S. Yeung, D. Socheat and N. J. White, *Drug Ther. (NY).*, 2009, **361**, 455–467.

72 R. M. Fairhurst and A. M. Dondorp, *PLoS Pathog.*, 2016, **11**, 1–14.

73 A. M. Thu, A. P. Phyo, J. Landier, D. M. Parker and F. H. Nosten, *FEBS J.*, 2017, **284**, 2569–2578.

74 J. Le Bras and R. Durand, *Fundam. Clin. Pharmacol.*, 2003, **17**, 147–153.

75 R. L. Taylor, *J. Clin. Endocrinol. Metab.*, 1950, **10**, 1361–1362.

76 and D. A. F. Andrea Ecker, Adele M. Lehane, Jérôme Clain, *Trends Parasitol.*, 2012, **4**, 504–514.

77 L. Cui, S. Mharakurwa, D. Ndiaye, P. K. Rathod and P. J. Rosenthal, *Am. J. Trop. Med. Hyg.*, 2015, **93**, 57–68.

78 A. F. Cowman, M. J. Morry, B. A. Biggs, G. A. M. Cross and S. J. Foote, *Proc. Natl. Acad. Sci. U. S. A.*, 1988, **85**, 9109–9113.

79 M. Ouji, J. M. Augereau, L. Paloque and F. Benoit-Vical, *Parasite*, 2018, **25**, 24–36.

80 L. Paloque, A. P. Ramadani, O. Mercereau-Puijalon, J. M. Augereau and F. Benoit-

Vical, *Malar. J.*, 2016, **15**, 1–12.

81 V. Srivastava and H. Lee, *Eur. J. Pharmacol.*, 2015, **762**, 472–486.

82 J. Liu, C. Liu, X. Zhang, L. Yu, X. Gong and P. Wang, *J. Enzyme Inhib. Med. Chem.*, 2019, **34**, 1380–1387.

83 Z. Xu, S. Zhang, C. Gao, J. Fan, F. Zhao, Z. S. Lv and L. S. Feng, *Chinese Chem. Lett.*, 2017, **28**, 159–167.

84 S. S. Chauhan, M. Sharma and P. M. S. Chauhan, *Drug News Perspect.*, 2010, **23**, 632–646.

85 I. M. P. Doyle, G. Dale, H. Choi and B. City, *US Pat.*, 2015, **2**, 1–9.

86 R. Capela, G. G. Cabal, P. J. Rosenthal, J. Gut, M. M. Mota, R. Moreira, F. Lopes and M. Prudêncio, *Antimicrob. Agents Chemother.*, 2011, **55**, 4698–4706.

87 X. M. Chu, C. Wang, W. L. Wang, L. L. Liang, W. Liu, K. K. Gong and K. L. Sun, *Eur. J. Med. Chem.*, 2019, **166**, 206–223.

88 S. Manohar, S. I. Khan and D. S. Rawat, *Chem. Biol. Drug Des.*, 2011, **78**, 124–136.

89 V. Patil, W. Guerrant, P. C. Chen, B. Gryder, D. B. Benicewicz, S. I. Khan, B. L. Tekwani and A. K. Oyelere, *Bioorganic Med. Chem.*, 2010, **18**, 415–425.

90 N. Boechat, M. D. L. G. Ferreira, L. C. S. Pinheiro, A. M. L. Jesus, M. M. M. Leite, C. C. S. Júnior, A. C. C. Aguiar, I. M. De Andrade and A. U. Krettli, *Chem. Biol. Drug Des.*, 2014, **84**, 325–332.

91 E. M. Guantai, K. Ncokazi, T. J. Egan, J. Gut, P. J. Rosenthal, P. J. Smith and K. Chibale, *Bioorganic Med. Chem.*, 2010, **18**, 8243–8256.

92 G. R. Pereira, G. C. Brandão, L. M. Arantes, H. A. De Oliveira, R. C. De Paula, M. F. A. Do Nascimento, F. M. Dos Santos, R. K. Da Rocha, J. C. D. Lopes and A. B. De Oliveira, *Eur. J. Med. Chem.*, 2014, **73**, 295–309.

93 G. N. Kaluerović, S. Gómez-Ruiz, D. Maksimović-Ivanić, R. Paschke and S. Mijatović, *Bioinorg. Chem. Appl.*, 2012, **2012**, 2012–2014.

94 J. W. Alexander, *Surg. Infect. (Larchmt).*, 2009, **10**, 289–292.

95 S. Medici, M. Peana, V. Marina, J. I. Lachowicz, G. Crisponi and M. Antonietta, *Coord. Chem. Rev.*, 2015, **284**, 329–350.

96 J. Spencer and B. Walden, *Future Med. Chem.*, 2018, **10**, 607–609.

97 J. J. Wilson and S. J. Lippard, *Chem. Rev.*, 2014, **114**, 4470–4495.

98 C.S. Rajapakse; A. Martínez; B. Naoulou; A.A. Jarzecki; L. Suárez; C. Deregnaucourt; V. Sinou; J. Schrével; E. Musi; G. Ambrosini; G.K. Schwartz; R.A. Sánchez-Delgado, *Inorg. Chem.*, 2009, **48**, 1122–1131.

99 J. Meyerovitch, Z. Farfel, J. Sack and Y. Shechter, *J. Biol. Chem.*, 1987, **262**, 6658–6662.

100 I. B. Afanas'eva, E. A. Ostrakhovitch, E. V. Mikhal'chik, G. A. Ibragimova and L. G. Korkina, *Biochem. Pharmacol.*, 2001, **61**, 677–684.

101 A. R. Shaikh, R. Giridhar and M. R. Yadav, *Int. J. Pharm.*, 2007, **332**, 24–30.

102 S. P. Fricker, R. M. Mosi, B. R. Cameron, I. Baird, Y. Zhu, V. Anastassov, J. Cox, P. S. Doyle, E. Hansell, G. Lau, J. Langille, M. Olsen, L. Qin, R. Skerlj, R. S. Y. Wong, Z. Santucci and J. H. McKerrow, *J. Inorg. Biochem.*, 2008, **102**, 1839–1845.

103 M. Navarro, C. Gabbiani, L. Messori and D. Gambino, *Drug Discov. Today*, 2010, **15**, 1070–1078.

104 R. A. Sánchez-Delgado, M. Navarro, H. Pérez and J. A. Urbina, *J. Med. Chem.*, 1996, **39**, 1095–1099.

105 M. Navarro, F. Vásquez, R. A. Sánchez-Delgado, H. Pérez, V. Sinou and J. Schrével, *J. Med. Chem.*, 2004, **47**, 5204–5209.

106 M. Navarro, S. Pekerar and H. A. Pérez, *Polyhedron*, 2007, **26**, 2420–2424.

107 P. A. Ajibade and G. A. Kolawole, *Transit. Met. Chem.*, 2008, **33**, 493–497.

108 D. R. van Staveren and N. Metzler-Nolte, *Chem. Rev.*, 2004, **104**, 5931–5985.

109 F. Dubar, T. J. Egan, B. Pradines, D. Kuter, K. K. Ncokazi, D. Forge, J. F. Paul, C. Pierrot, H. Kalamou, J. Khalife, E. Buisine, C. Rogier, H. Vezin, I. Forfar, C. Slomianny, X. Trivelli, S. Kapishnikov, L. Leiserowitz, D. Dive and C. Biot, *ACS Chem. Biol.*, 2011, **6**, 275–287.

110 J. Xiao, Z. Sun, F. Kong and F. Gao, *Eur. J. Med. Chem.*, 2020, **185**, 111791.

111 E. Fourie, J. M. J. Van Rensburg and J. C. Swarts, *J. Organomet. Chem.*, 2014, **754**, 80–87.

112 F. Dubar, C. Slomianny, J. Khalife, D. Dive, H. Kalamou, Y. Guérardel, P. Grellier and C. Biot, *Angew. Chem - Int. Ed.*, 2013, **52**, 7690–7693.

113 B. S. Sekhon and N. Bimal, *Indian J. Pharm. Educ. Res.*, 2012, **3**, 52–63.

114 P. Chellan, S. Nasser, L. Vivas, K. Chibale and G. S. Smith, *J. Organomet. Chem.*, 2010, **695**, 2225–2232.

115 A. C. Pena, N. Penacho, L. Mancio-Silva, R. Neres, J. D. Seixas, A. C. Fernandes, C. C. Romao, M. M. Mota, G. J. L. Bernardes and A. Pamplona, *Antimicrob. Agents Chemother.*, 2012, **56**, 1281–1290.

116 E. Üstün, A. Özgür, K. A. Coşkun, S. Demir, İ. Özdemir and Y. Tutar, *J. Coord. Chem.*, 2016, **69**, 3384–3394.

117 M. Wrighton, *Chem. Rev.*, 1974, **74**, 401–430.

118 M. A. Gonzalez, M. A. Yim, S. Cheng, A. Moyes, A. J. Hobbs and P. K. Mascharak, *Inorg. Chem.*, 2012, **51**, 601–608.

119 S. Hostachy, C. Policar and N. Delsuc, *Coord. Chem. Rev.*, 2017, **351**, 172–188.

120 F. L. T.-G. and M. P. C. Vanesa Fernández-Moreira, *Chem. Commun.*, 2010, **46**, 186–202.

121 A. Leonidova, V. Pierroz, R. Rubbiani, J. Heier, S. Ferrari and G. Gasser, *Dalton. Trans.*, 2014, **43**, 4287–4294.

122 J. Oyarzo, A. Acuña, H. Klahn, R. Arancibia, C. P. Silva, R. Bosque, C. López, M. Font-Bardía, C. Calvis and R. Messeguer, *Dalton. Trans.*, 2018, **47**, 1635–1649.

123 P. Toro, A. H. Klahn, B. Pradines, F. Lahoz, A. Pascual, C. Biot and R. Arancibia, *Inorg. Chem. Commun.*, 2013, **35**, 126–129.

124 P. V. Simpson, C. Nagel, H. Bruhn and U. Schatzschneider, *Organometallics*, 2015, **34**, 3809–3815.

125 I. Chakraborty, S. J. Carrington, G. Roseman and P. K. Mascharak, *Inorg. Chem.*, 2017, **56**, 1534–1545.

126 S. Romanski, B. Kraus, U. Schatzschneider, J. M. Neudörfl, S. Amslinger and H. G. Schmalz, *Angew. Chem - Int. Ed.*, 2011, **50**, 2392–2396.

127 F. Zobi, A. Degonda, M. C. Schaub, A. Y. Bogdanova, Z. Ch-, Z. Ch- and Z. Ch-, *Inorg. Chem.*, 2010, 7313–7322.

128 R. Motterlini, P. Sawle, J. Hammad, S. Bains, R. Alberto, R. Foresti and C. J. Green, *FASEB J.*, 2005, **19**, 284–286.

129 J. S. Ward, J. M. Lynam, J. Moir and I. J. S. Fairlamb, *Chem. - A Eur. J.*, 2014, **20**, 15061–15068.

130 P. Peng, C. Wang, Z. Shi, V. K. Johns, L. Ma, J. Oyer, A. Copik, R. Igarashi and Y. Liao, *Org. Biomol. Chem.*, 2013, **11**, 6671–6674.

131 C. C. Roma, P. C. Roma and C. C. Roma, *Cem. Soc. Rev*, 2012, 3571–3583.

132 U. Schatzschneider, *Br. J. Pharmacol.*, 2015, **172**, 1638–1650.

133 I. Blumenthal, *J. R. Soc. Med.*, 2001, **94**, 270–272.

134 P. Govender, S. Pai, U. Schatzschneider and G. S. Smith, *Inorg. Chem.*, 2013, **52**, 5470–5478.

135 A. C. Kautz, P. C. Kunz and C. Janiak, *Dalton. Trans.*, 2016, **45**, 18045–18063.

136 S. K. Chiang, S. E. Chen and L. C. Chang, *Int. J. Mol. Sci.*, 2019, **20**, 1–18.

137 L. E. Otterbein, F. H. Bach, J. Alam, M. Soares, H. T. Lu, M. Wysk, R. J. Davis, R. A. Flavell and A. M. K. Choi, *Nat. Med.*, 2000, **6**, 422–428.

138 R. Song, M. Kubo, D. Morse, Z. Zhou, X. Zhang, J. H. Dauber, J. Fabisiak, S. M. Alber, S. C. Watkins, B. S. Zuckerbraun, L. E. Otterbein, W. Ning, T. D. Oury, P. J. Lee, K. R. McCurry and A. M. K. Choi, *Am. J. Pathol.*, 2003, **163**, 231–242.

139 R. Motterlini, J. E. Clark, R. Foresti, P. Sarathchandra, B. E. Mann and C. J. Green, *Circ. Res.*, 2002, **90**, e17–e24.

140 S. R. Thom, V. M. Bhopale, S. T. Han, J. M. Clark and K. R. Hardy, *Am. J. Respir. Crit. Care Med.*, 2006, **174**, 1239–1248.

141 L. S. Nobre, J. D. Seixas, C. C. Romão and L. M. Saraiva, *Antimicrob. Agents Chemother.*, 2007, **51**, 4303–4307.

142 A. Pamplona, A. Ferreira, J. Balla, V. Jeney, G. Balla, S. Epiphanio, Â. Chora, C. D. Rodrigues, I. P. Gregoire, M. Cunha-Rodrigues, S. Portugal, M. P. Soares and M. M. Mota, *Nat. Med.*, 2007, **13**, 703–710.

143 B. Chen, L. Guo, C. Fan, S. Bolisetty, R. Joseph, M. M. Wright, A. Agarwal and J. F. George, *Am. J. Pathol.*, 2009, **175**, 422–429.

144 A. Nakao, H. Toyokawa and A. Tsung, *Am. J. Transplant.*, 2006, **6**, 2243–2255.

145 L. K. Wareham, R. K. Poole and M. Tinajero-Trejo, *J. Biol. Chem.*, 2015, **290**, 18999–19007.

146 M. Kourti, W. G. Jiang and J. Cai, *Oxid. Med. Cell. Longev.*, 2017, **2017**, 1–12.

147 C. Chauveau and D. Bouchet, *Am. J. Transplant.*, 2002, **2**, 581–592.

148 T. I. Ayudhya, C. C. Raymond and N. N. Dingra, *Dalton. Trans.*, 2018, **46**, 882–889.

149 D. Wang, E. Viennois, K. Ji, K. Damera, A. Draganov, Y. Zheng, C. Dai, D. Merlin and B. Wang, *Chem. Commun.*, 2014, **50**, 15890–15893.

150 R. Mondal, A. N. Okhrimenko, B. K. Shah and D. C. Neckers, *J. Phys. Chem.*, 2008, **112**, 11–15.

151 G. Light, L. Angel and P. Antony, *Org. Lett.*, 2013, **15**, 2011–2014.

152 E. Palao, L. Muchova, V. Libor and P. Kla, *J. Am. Chem. Soc.*, 2016, **138**, 126–133.

153 S. N. Anderson, J. M. Richards, H. J. Esquer, A. D. Benninghoff, A. M. Arif and L. M. Berreau, *ChemistryOpen*, 2015, **4**, 590–594.

154 N. Abeyrathna, K. Washington, C. Bashur and Y. Liao, *Org. Biomol. Chem.*, 2017, **15**, 8692–8699.

155 G. Stochel, A. Wanat and E. Kuli, *Coord. Chem. Rev.*, 1998, **171**, 203–220.

156 J. Stenger-Smith, I. Chakraborty, S. Carrington and P. Mascharak, *Acta Crystallogr. Sect. C Struct. Chem.*, 2017, **73**, 357–361.

157 U. Schatzschneider, *Inorg Chim. Acta.*, 2011, **374**, 19–23.

158 I. Chakraborty, S. J. Carrington and P. K. Mascharak, *Acc. Chem. Res.*, 2014, **47**, 2603–2611.

159 J. Jimenez, I. Chakraborty, S. J. Carrington and P. K. Mascharak, *Dalton. Trans.*, 2016, **45**, 13204–13213.

160 S. E. McGlynn, D. W. Mulder, E. M. Shepard, J. B. Broderick and J. W. Peters, *Dalton. Trans.*, 2009, 4274.

161 M. Tinajero-Trejo, N. Rana, C. Nagel, H. E. Jesse, T. W. Smith, L. K. Wareham, M. Hippler, U. Schatzschneider and R. K. Poole, *Antioxid. Redox Signal.*, 2016, **24**, 765–780.

162 E. Kianfar, C. Scha¨fer, M. R. Lornejad-Scha¨fer, E. Portenkirchner and G. Knör, *Inorg. Chim. Acta.*, 2015, **435**, 174–177.

Chapter 2

Synthesis and characterization of quinoline-1,2,3-triazole ligands

2.1. Introduction

Chloroquine (CQ) (**Figure 2.1**) is one of the most significantly studied quinoline-containing antimalarial drugs due to its low toxicity, easy synthesis, good pharmacokinetic properties and few side effects.[1] However, its success and overuse have led to the development of CQ-resistant strains of *P.falciparum* and *P.vivax*, the two strains responsible for most malaria deaths.[2] Various structurally dissimilar alternative antimalarials have since been synthesized, including primaquine,[3] mefloquine[4] and artemisinins,[5] some of which are still used today. However, none of these drugs have shown the same pharmacological profile exhibited by CQ.[6] Due to the unmatched efficacy of chloroquine, scientists have focussed on the derivatization of CQ to attempt to synthesize compounds that avert resistance.

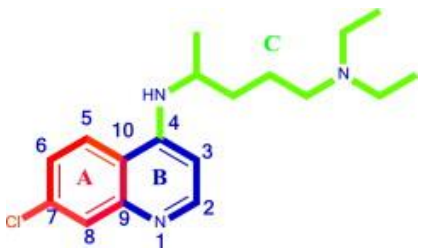

Figure 2.1**.** Chemical structure of chloroquine.[6]

Many chloroquine derivatives have been reported, including compounds where the side chain of CQ is modified with α,β-unsaturated amides and benzyl groups.[7] Kaschula *et al.* focussed on the derivatization of ring A on the quinoline scaffold of CQ, where the chloro group at position-7 was substituted with electron-withdrawing and electro-donating groups: NH_2, OH, OCH_3, H, CH_3.[8] Pou *et al.* modified the B ring with alkyl or aryl substituents in the 3-positon and altered the side chain in the 4-position. These compounds have relatively low IC_{50} values in the range 8-20 nm.[9]

Quinoline-containing antimalarials have been used as mainstays of chemotherapy against malaria.[10] A modern approach in drug design has been molecular hybridization, which involves covalent bonding between two or more known pharmacophores.[10] Many quinoline-based hybrid compounds have been synthesized and evaluated for their antimalarial activity, showing promising antiparasitic activity.[11] Wang *et al.* synthesized artesunate-quinoline hybrids, which showed greater antimalarial activity than the individual drugs.[12] N'Da *et al.* reported a series of quinoline-ferrocene hybrids that show greater antimalarial activity than equimolar amounts of the individual drugs in the Dd2-CQ-resistant strain of *P.falciparum*.[13] Other quinoline hybrid antimalarial compounds include quinoline-pyrimidines,[14] quinoline-trioxolanes,[15] and quinoline-triazole hybrids which have shown appreciable antimalarial activity in several studies.[16,17,18]

Triazoles, in particular, have shown to possess many pharmacological properties and have become widely used in medicinal chemistry due to their resistance to metabolic degradation and the capability of forming hydrogen bonds.[19] Triazoles can take part in various non-covalent interactions, improving their solubility and ability to bind to biomolecular targets.[20] Boechat *et al.* synthesized a series of quinoline-1,2,3-triazole compounds with varying R substituents in the 4-position of 1*H*-1,2,3-triazol-1-yl.[21] The compound bearing an aldehyde in the 4-position (**Figure 2.2.**) was the most active against the W2-CQ-resistant strain of *P.falciparum* with an IC_{50} value of 1.4 μM.

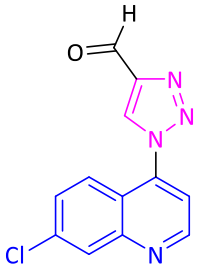

Figure 2.2. 1*H*-1,2,3-Triazole-Quinoline hybrid synthesised by Boechat *et al.* shown to have good antimalarial activity against W2-CQ-resistant strain *of P. falciparum*.[21]

Faidallah *et al.* synthesized a series of 1,2,3-triazole-quinine conjugates with varying R-substituents in the 1-position of the triazole ring.[22] The conjugate shown in **Figure 2.3**, shows the highest antimalarial activity with an IC_{50} value of 27 nM.

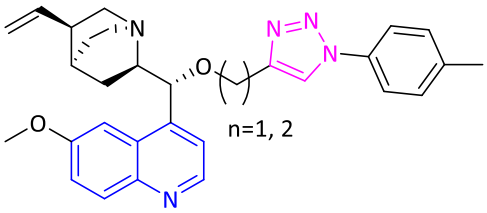

Figure 2.3. Quinoline-triazole conjugates synthesized by Faidallah *et al.* shown to have good antimalarial activity.[22]

Molecular hybridization is an exciting prospect and the good antimalarial activity exhibited by many quinoline-triazole hybrids reported in the literature motivates the current study. In this chapter, the synthesis and characterization of two new quinoline-triazole ligands (a molecule that binds to a central metal atom to form a complex) are discussed. These two triazole ligands vary in the 4-position, one having the triazole ring attached directly in the 4-position

whereas the second has the quinoline ring and triazole moiety separated by an amino-propyl chain. Several series of 7-chloroquinoline-triazole hybrids with varying substituents on the triazole moiety have been evaluated for their antiplasmodial activity in literature.[23,21] Some showing appreciable activity in CQ-resistant strains of *P.falciparum*. It has been established that the presence of an amino side chain on the quinoline ring plays an important role in the antimalarial activity of the hybrids.[16,24] It is for this reason that two 7-chloroquinoline-triazoles were synthesized. The difference in antimalarial activity exhibited by the compounds with the triazole moiety attached directly in the 4-position compared to those containing a basic amino-propyl chain in the 4-position of the quinoline ring is discussed in **Chapter 4**.

2.2. Synthesis of quinoline-1,2,3-triazole ligands using "click chemistry"

The 7-chloroquinoline-triazole ligands were synthesized *via* a copper-catalysed azide/alkyne 1,4-dipolar cycloaddition which makes use of two components: an alkyne and azide. These reactions have been called 'click chemistry', as coined by Sharpless in 2001.[25] Click chemistry has become a highly favourable synthetic route due to its reliability and selectivity.[26] Sharpless *et al*. defines click chemistry by the following criteria: high yielding, produces easily removable by-products, uses mild reaction conditions and makes use of benign solvents that are easily removed.[25] Among all the "click reactions", the Huisgen 1,3-dipolar cycloaddition between alkynes and azides is the leading example,[26] but it requires high temperatures and produces both regioisomers (1,4- and 1,5-disubstituted) when asymmetric alkynes are used. The copper-catalysed azide/alkyne 1,4-dipolar cycloaddition (CuAAC) reaction was developed as a method with a wider reaction scope.[27] The CuAA reaction succeeds under a wide range of temperatures and is insensitive to pH changes between 4 and 12. An organic azide and terminal alkyne is reacted together to regioselectively form a 1,4-disubstituted 1,2,3-triazole.[28] Herein is reported the copper-catalysed cycloadditions of a terminal alkyne to two different azido-chloroquinolines to produce two new quinoline-1,2,3-triazole ligands.

2.2.1. Synthesis of terminal alkyne.[29]

The alkyne component (**2**) of the triazole was synthesized from a precursor, 4-(pyridinylimine)phenol (**1**). Compounds **1** and **2** were synthesized following published methods,[29] as shown in **Scheme 2.1.**

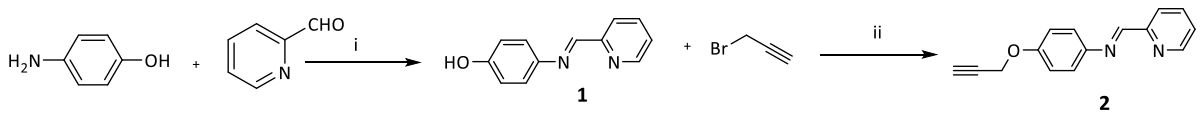

Scheme 2.1. Reaction scheme for the synthesis of the aryl ether (**2**). Conditions: (i) MeOH, reflux, 21 h; (ii) Acetone, K_2CO_3, 18-crown-6, reflux, 72 h.

For the synthesis of compound **1**, a Schiff base condensation was carried out by reacting 4-aminophenol with 2-pyridinecarboxaldehyde. A Schiff base condensation reaction occurs between an aldehyde/ketone and primary amine to form an imine or "Schiff base "as shown in **Scheme 2.2**.[30] Compound **1** was isolated as a yellow crystalline solid in high yield of 84% with a melting point range of 186.2-187.8 ℃ that correlates with that reported in the literature of 186.2-187.8 ℃.[29]

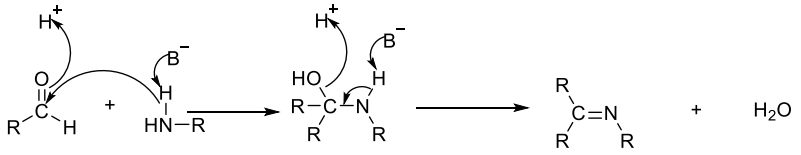

Scheme 2.2. General mechanism for the Schiff base condensation reaction between aldehydes and primary amines.[31]

Propargylation of compound **1**, involved the reaction with K_2CO_3 as the base and 18-crown-6 as the phase-transfer catalyst *via* a Williamson-ether reaction. Propargyl bromide was subsequently added and the reaction proceeded *via* an S_N2 reaction mechanism. Compound

2 was isolated as brown crystals in a high yield of 81%. It has a melting point range of 104.4-106.2 °C. The Williamson-ether reaction follows an S_N2 mechanism in which an alkyl halide reacts with an alcohol under basic conditions to form an ether.[31] Under these conditions, the alcohol is deprotonated to form a phenoxide, which reacts faster with the alkyl halide. This is due to an increased electron density on the nucleophile which attacks the electrophilic carbon center of the alkyl halide as seen in **Scheme 2.3**.[32]

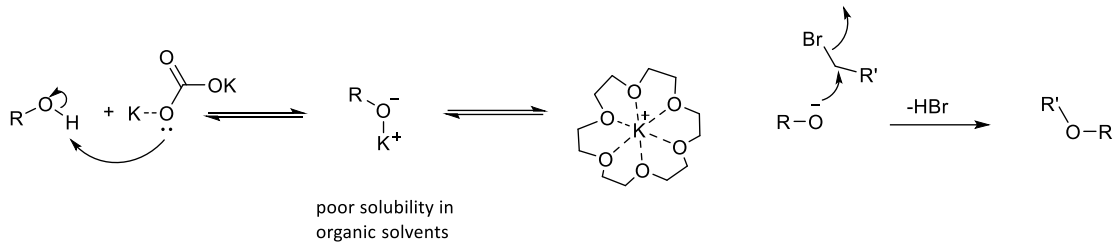

Scheme 2.3. General mechanism of a Williamson ether reaction.[33]

18-Crown-6 is added due to the poor solubility of the phenoxide intermediate in organic media. The phase transfer catalyst facilitates the migration of the solid into the solvent so the reaction may proceed. 18-Crown-6 encapsulates K^+ subsequently improving the solubility and nucleophilicity of the phenoxide intermediate.[33]

2.2.2. Characterization

The Schiff base (**1**) and aryl ether (**2**) were characterized using ^{1}H NMR, $^{13}C\{^1H\}$ NMR and infrared (IR) spectroscopy. The carbon signals were assigned using HSQC.

2.2.2.1. ^{1}H and $^{13}C\{^1H\}$ NMR spectroscopy

The ^{1}H NMR spectrum of compound **1** (**Figure 2.4**) shows a distinctive singlet at 9.61 ppm for the phenolic proton and another singlet at 8.67 ppm corresponding to the imine proton (H-

6). The α-N_{pyr} proton appears as a doublet at 8.67 ppm with a coupling constant of $^{3}J_{HH}$= 4.8 Hz. Protons H-9 and H-8 are observed as doublets at 7.28 ppm and 6.82 ppm respectively, with coupling constants of $^{3}J_{HH}$= 8.70 ppm. Each signal integrates for the expected two protons due to the equivalent chemical environment of each set of protons. In the $^{13}C\{^{1}H\}$ NMR spectrum of compound **1**, the most deshielded signal at 156.99 ppm corresponds to C-10. The imine carbon C-6 appears as a singlet at 156.88 ppm, while the quaternary carbons C-5 and C-7 are seen at 141.49 ppm and 154.52 ppm respectively.

In the ^{1}H NMR spectrum of compound **2** (**Figure 2.4**) the phenolic proton signal seen in the spectrum of compound **1** is no longer present. H-11 is assigned to the doublet integrating for two protons and H-13 to the triplet integrating for one proton in the aliphatic region at 4.83 ppm and 3.56 ppm respectively. Each signal has a coupling constant of $^{4}J_{HH}$= 2.4 Hz. The presence of protons H-11 and H-13 in the respective aliphatic region is indicative of successful propargylation. The imine proton (H-6) is assigned as the singlet at 8.69 ppm, showing a shift from 8.58 ppm for compound **1**. The C-10 singlet has shifted upfield from 156.99 ppm (compound **1**) to 156.39 ppm (compound **2**) in the $^{13}C\{^{1}H\}$ spectrum of compound **2**. This shift is a result of the increased electron density in the alkyne substituent. Three signals appear in the aliphatic region at 79.27 ppm, 78.34 ppm and 55.77 ppm for carbons C-12, C-13 and C-11 respectively.

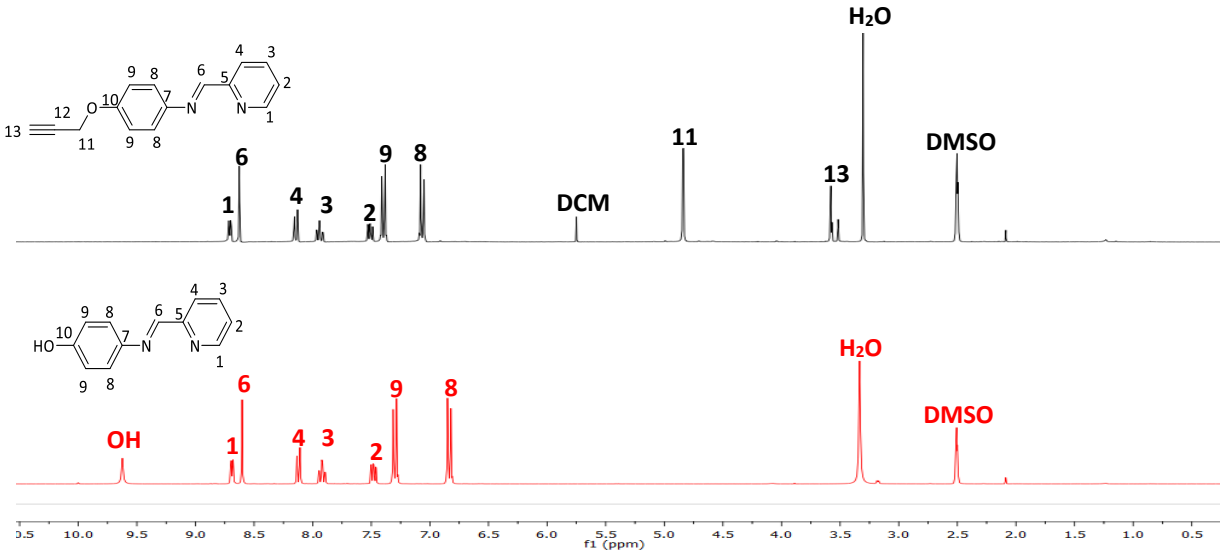

Figure 2.4. Stacked ^{1}H NMR spectra of compounds **1** (bottom) and **2** (top).

2.2.2.2. IR spectroscopy

The IR spectrum of compound **1** shows characteristic absorption bands at 1623 cm^{-1} and 1581 cm^{-1}, corresponding to the imine C=N and pyridyl C=N functional groups respectively, further confirming the formation of the Schiff base. A broad absorption band is seen between 2465-2988 cm^{-1} and is assigned to the aromatic C-H's and the hydroxyl (OH) functionality. In the IR spectrum of compound **2**, diagnostic absorption bands at 3171 cm^{-1} and 2964 cm^{-1} are seen for the H-C≡ and C≡C functional groups respectively. The imine and pyridyl C=N absorption bands appear at 1623 cm^{-1} and 1600 cm^{-1} respectively. The asymmetric stretch of the ether (C-O-C) appears as a strong absorption band at 1239 cm^{-1}.

2.2.3. Synthesis of 4-azido-7-chloroquinoline (3).[34]

The first azide components for the CuAAC reaction was synthesized using a method adapted from literature.[34] The azido-quinoline, compound **3** was synthesized *via* a Nucleophilic Aromatic substitution (S_NAr) reaction between 4,7-dichloroquinoline and sodium azide, as shown in **Scheme 2.4**. Compound **3** was isolated as yellow needle-like crystals in a moderate yield (62%) with a melting point range of 116.3-118.5 ℃. This experimental range corresponds to the literature value of 115℃,[34] supporting successful azidation.

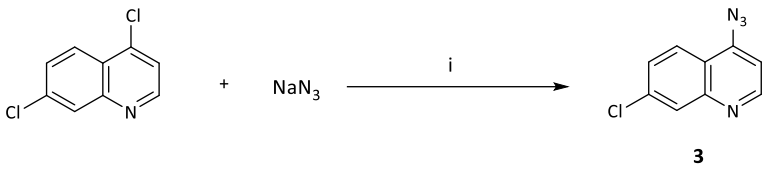

Scheme 2.4. Synthesis of 4-azido-7-chloroquinoline (**3**). Conditions: (i) DMF, reflux, 6 h.

An S_NAr reaction is an organic substitution reaction in which a nucleophile replaces a leaving group on an aromatic ring. The substitution of aromatic rings containing a heteroatom is more likely to occur when an electron-withdrawing group is *ortho* or *para* to the leaving group.

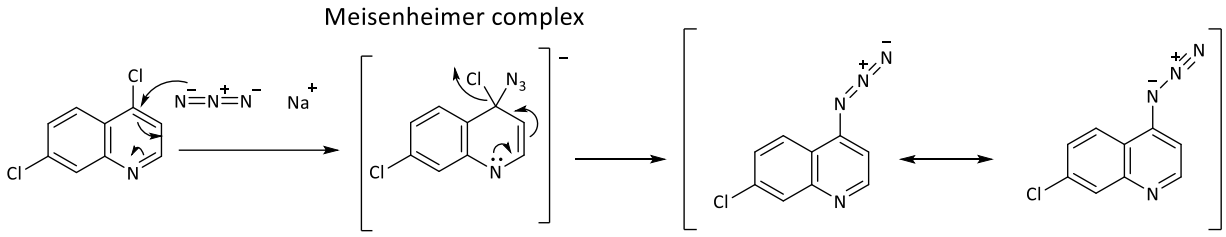

Scheme 2.5. Mechanism for the azidation of 4,7-dichloroquinoline *via* S_NAr.

Substitution, therefore, occurs exclusively at the 4-position as opposed to the 7-position of 4,7-dichloroquinoline. The para-electron-withdrawing nitrogen stabilizes the Meisenheimer intermediate through resonance as shown in **Scheme 2.5**. This stabilization results in substitution occurring in the 4- as opposed to the 7-position.

2.2.4. Characterization

2.2.4.1. ^{1}H and $^{13}C\{^{1}H\}$ NMR spectroscopy

The proton resonance of H-2 shifts upfield from 7.49 ppm in 4,7-dichloroquinoline to 7.13 ppm for compound **3**, as seen in the ^{1}H NMR spectra in **Figure 2.5**. This upfield shift is indicative of the weaker electron-withdrawing effect of the azido entity compared to the stronger electron-withdrawing inductive effect caused by the chloride. Protons H-5, H-6, H-8 all undergo upfield shifts upon azidation due to the same phenomenon. H-5 appears as a doublet of doublets at 7.49 ppm with coupling constants $^{3}J_{HH}$= 8.94 Hz and $^{5}J_{HH}$= 2.07 Hz, indicating that it couples to H-6 as well as H-8. H-1 undergoes a downfield shift from 8.78 ppm to 8.83 ppm. The $^{13}C\{^{1}H\}$ NMR spectrum of compound **3** shows the C-1 singlet as the most deshielded carbon at 151.37 ppm.

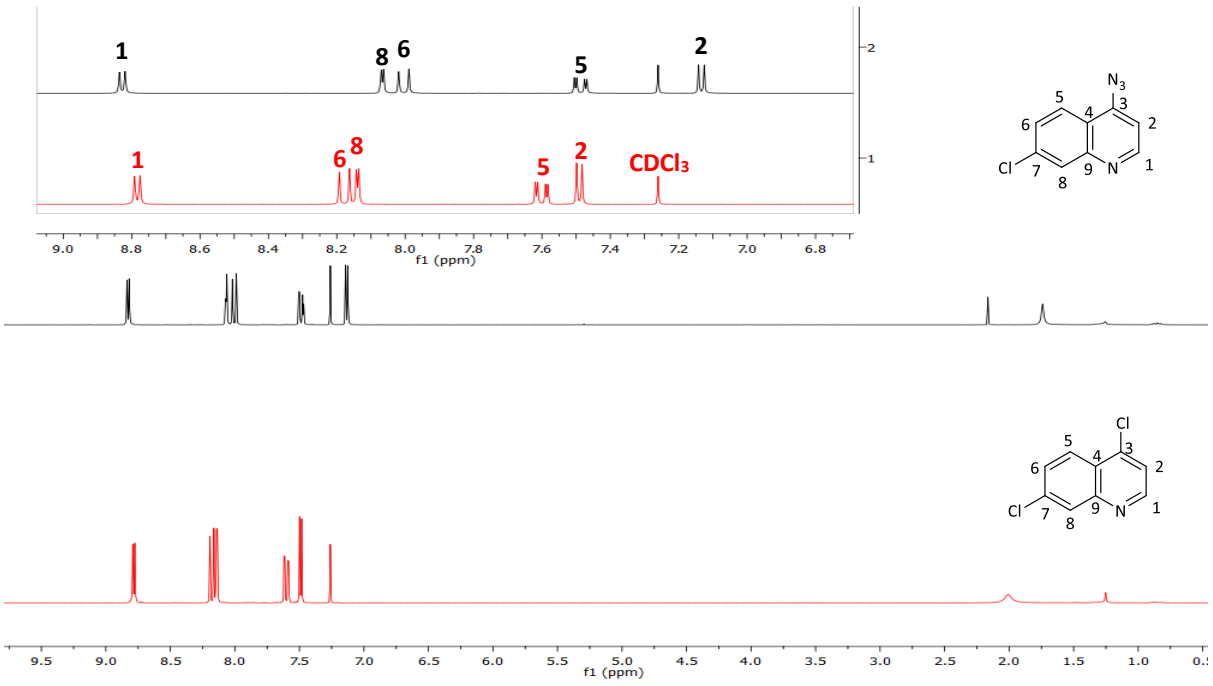

Figure 2.5. Stacked ^{1}H NMR spectra of 4,7-dichloroquinoline (bottom) and compound **3** (top).

2.2.4.2. IR spectroscopy

The IR spectrum of compound **3** shows an azide (N_3) absorption band in the characteristic region at 2117 cm^{-1}, a quinoline C=N band at 1608 cm^{-1} and a C-Cl absorption band at 766 cm^{-1}.

2.2.5. Synthesis of *N*-(3-azidopropyl)-7-chloroquinolin-4-amine.[35]

A second azido-quinoline was synthesized, in which the azide entity is on the terminal end of an amino-propyl chain on the quinoline ring (**6**). A series of intermediates (compounds **4**, **5a** and **5b**) were first synthesized.

4,7-Dichloroquinoline was reacted with 3-aminopropan-1-ol following a known method, [35] to form the amino alcohol compound **4** as shown in **Scheme 2.6** (conditions i and ii). This afforded a beige powder in a moderate yield (62%).

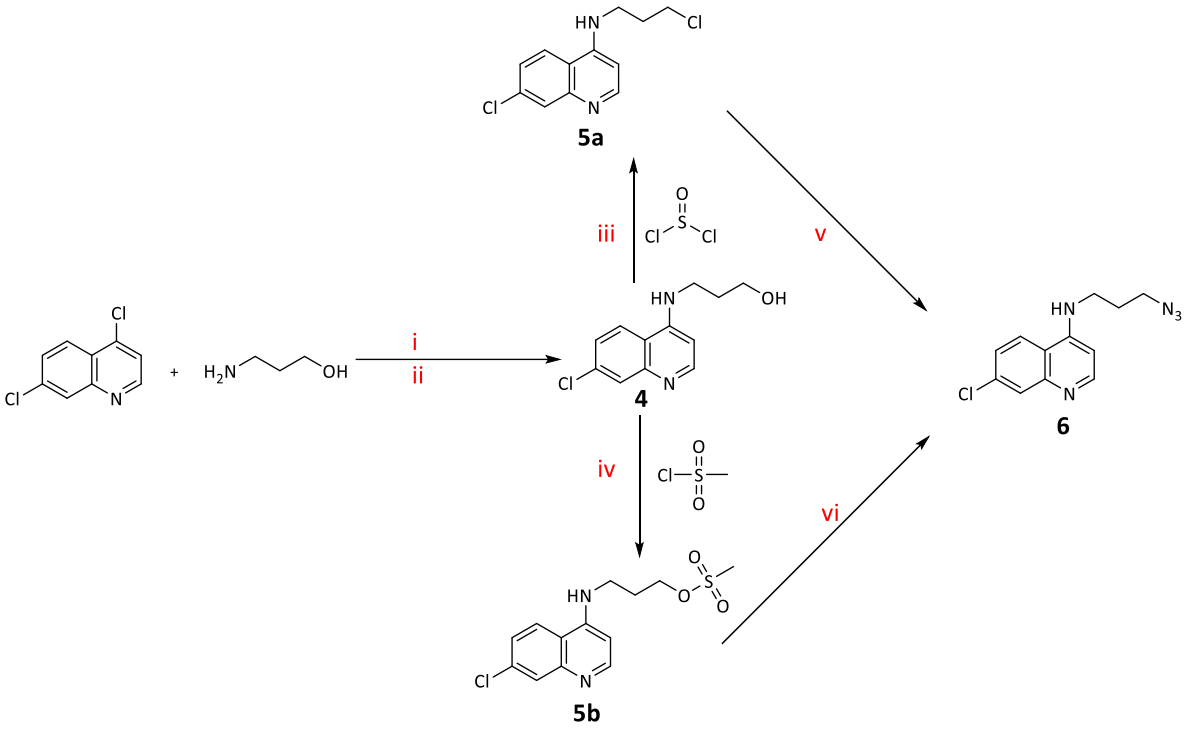

Scheme 2.6. Synthetic scheme for 4-amino-7-chloroquinoline intermediates **4**, **5a**,**5b** and the final product compound **6**. Conditions: (i) 180 °C, 1 h; (ii) 130 °C, 16 h; (iii) cat. DMF, reflux, 16 h; (iv) THF, NEt_3, 0 °C, 3 h; (v) NaN_3, DMF, 80 °C, 18 h; (vi) NaN_3, DMF, 55 °C 4 h.

Two routes were explored for the synthesis of the azido precursor in order to optimize the reaction. The first route involved the synthesis of a chloro intermediate (**5a**) whereas the second route involved the synthesis of a methanesulfonyl intermediate (**5b**). The reaction of the chloro intermediate (**5a**) with NaN_3 produced a low yield of the final azide (**6**), hence the second intermediate (**5b**) was synthesized. Compound **4** was reacted with either thionyl chloride ($SOCl_2$) or methanesulfonyl chloride (MsCl) *via* Nucleophilic substitution (S_N2) reactions described in the literature.[35,36] These reactions afforded beige solids in moderate yields of 67% for **5a** and 53% for **5b**. Compounds **5a** and **5b** were reacted with NaN_3 under similar conditions shown in **Scheme 2.6** (conditions v and vi). These reactions afforded compound **6** as pale-yellow solids in a low yield of 23% using **5a** as a precursor and a moderate yield of 56% using **5b** as the precursor.

2.2.6. Characterization

The 4-amino-7-chloroquinoline intermediates (**4**, **5a** and **5b**) and azide (**6**) were characterized using ^{1}H NMR, ^{13}C{^{1}H} NMR and infrared (IR) spectroscopy.

2.2.6.1. ^{1}H and ^{13}C{^{1}H} NMR spectroscopy

In the ^{1}H NMR spectrum of compound **4** (**Figure 2.6**), the most deshielded signal at 8.39 ppm is assigned to H-7. The amine proton H-4 is observed as a broad signal at 7.27 ppm and the hydroxyl proton as a broad signal at 4.56 ppm. The propyl chain protons are identified as the triplet at 3.55 ppm, a signal at 3.33 ppm, not well resolved from the H_2O resonance and the quintet at 1.82 ppm. These signals correspond to protons H-1, H-3 and H-2 respectively. The H-1 and H-2 signals integrate for the expected two protons. The presence of the H-3 signal was confirmed using HSQC, indicated by a cross peak at 3.33 ppm; 117.74 ppm. The cross peak is assigned to that of H-3; C-3. Protons H-6, H-9 and H-11 are seen as doublets at 6.47 ppm, 7.77 ppm, and 8.24 ppm. The doublet of doublets at 7.43 ppm with coupling constants $^{3}J_{HH}$= 9.00 Hz and $^{5}J_{HH}$= 1.6 Hz is assigned to H-12. The coupling constants suggest that H-12 couples to H-11 and H-9. C-5 is observed as the most deshielded signal at 151.91 ppm in the ^{13}C{^{1}H} NMR spectrum of compound **4**. All remaining aromatic carbon signals are accounted for and appear as singlets between 150.4 ppm and 98.56 ppm. Aliphatic carbons C-1, C-3, and C-2 are assigned to the signals at 48.46 ppm, 40.94 ppm, and 31.23 ppm respectively.

Analysis and comparison of the ^{1}H NMR spectra of compounds **4**, **5a** and **5b** (**Figure 2.6**) show the successful transformation of the hydroxyl (OH) functionality to a chloride and methanesulfonyl. The hydroxyl proton signal seen in the ^{1}H NMR spectrum of compound **4**, is no longer present in the spectra of compounds **5a** and **5b**. The amine proton (H-4) shifts downfield from 7.27 ppm to 9.50 ppm upon the formation of the alkyl halide, due to the greater inductive electron-withdrawing effect of the chloride compared to that of the hydroxyl group. There are significant downfield shifts of the aromatic proton resonances of compound **5a**, as seen in **Figure 2.6**. These shifts may be due to the possible reaction of the quinoline nitrogen with the sulfur of $SOCl_2$. This would explain the low yield of compound **6**

produced from reaction condition v in **Scheme 2.6**. Further analysis such as mass spectrometry of compound **5a** would be needed to confirm this.

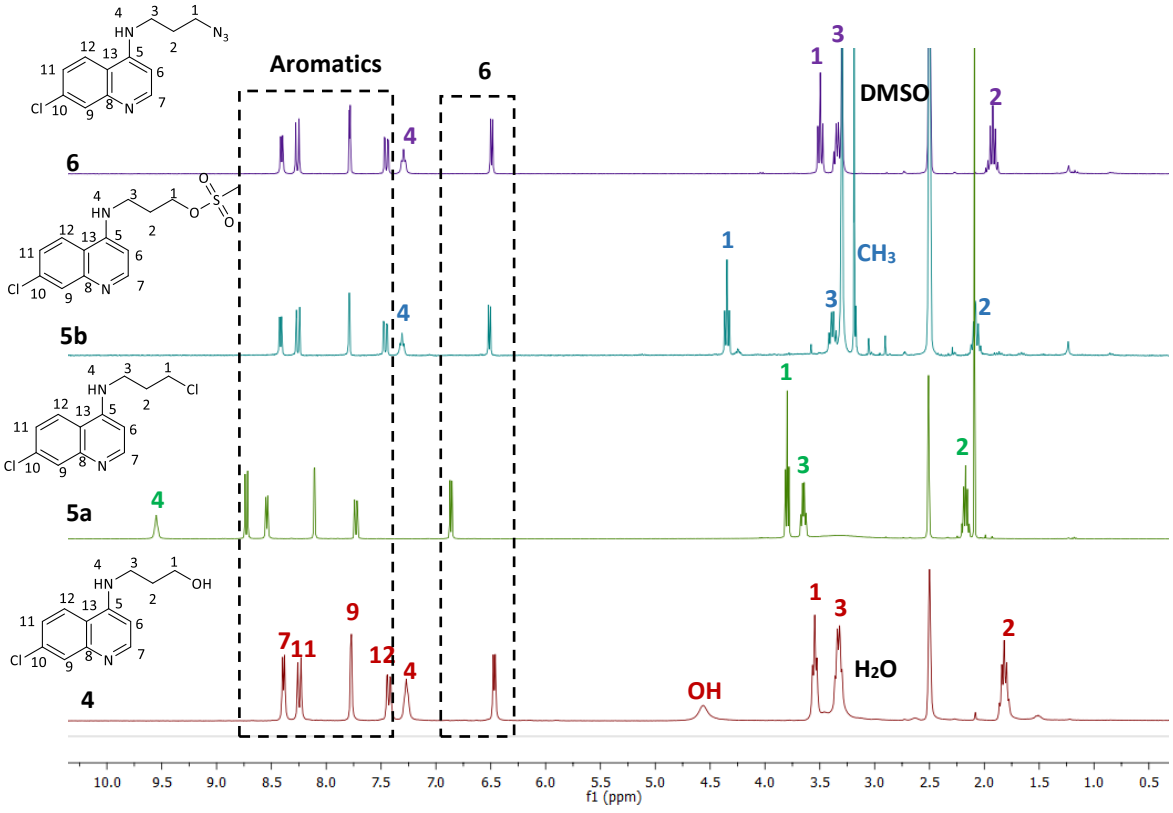

Figure 2.6. Stacked ^{1}H NMR spectra of compounds **4**, **5a**, **5b** and **6**

Upon the formation of the methanesulfonyl intermediate (**5b**), the amine proton (H-4) signal is observed at a similar frequency (7.31 ppm) to the precursor alcohol (7.27 ppm). The intense singlet at 3.19 ppm, integrating for three methyl protons in the spectrum of **5b**, is the diagnostic signal for the successful mesylation. In the $^{13}C\{^{1}H\}$ NMR spectrum of compound **5a**, C-5 resonates downfield at 155.11 ppm. C-1, C-3 and C-2 signals have shifted upfield to 44.20 ppm, 39.88 and 30.96 ppm, owing to the electron-withdrawing nature of the Cl. All carbon signals in the $^{13}C\{^{1}H\}$ NMR spectrum of **5b** are accounted for and only undergo slight shifts due to their similar electronic environments in the alcohol precursor and methanesulfonyl intermediate. The methyl carbon ($\underline{C}H_3$) is observed as a singlet at 27.45 ppm.

Azidation of compound **5a** was more apparent in the ^{1}H NMR spectroscopy than that of **5b**. Comparison of the ^{1}H NMR spectra of **5a** and **6** shows an upfield shift of the imine proton (H-4) from 9.50 ppm to 7.30 ppm. All aromatic and aliphatic protons shift upfield with chemical shifts resembling those observed for the aminopropanol precursor, compound **4**. The aliphatic protons H-1, H-3, and H-2 are observed as a triplet at 3.50 ppm, a doublet of doublets at 3.63 ppm and a quintet at 1.93 ppm. This upfield shift of the aliphatic protons is attributed to the weaker electron-withdrawing nature of the azide moiety in comparison to the chloride.^{1}H NMR spectral analysis of **5b** and **6**, indicates that the aliphatic protons all undergo upfield shifts upon azidation. The proton resonance of H-1 shifts from 4.34 ppm to 3.50 ppm, H-3 from 3.39 ppm to 3.38-3.33 ppm and H-2 from 2.08 ppm to 1.93 ppm. The ^{13}C{^{1}H} NMR spectrum of compound **6**, shows the aliphatic carbon signal C-1, C-3, and C-2 at 48.53 ppm, 40.10 ppm, and 27.09 ppm respectively.

2.2.6.2. IR spectroscopy

A broad absorption band at 3312 cm^{-1} is seen in the IR spectrum of compound **4**, corresponding to the hydroxy (OH) functionality. A weak sharp absorption band is seen at 3058 cm^{-1} corresponding to the secondary amine and a strong sharp band at 1609 cm^{-1} for the quinoline C=N. The electronic properties of the chloride are seen in the IR spectrum of compound **5a**, as the amine absorption band shifts to a higher wavenumber of 3219 cm^{-1} and that of the quinoline shifts to a higher wavenumber of 1614 cm^{-1}.The distinctive OH band is no longer present in the IR spectrum of compound **5a** while there is an absorption band at 734 cm^{-1} for the C-Cl stretch. The IR spectrum of compound **5b** shows the secondary amine absorption band at 3065 cm^{-1} and the absorption band observed at 1609 cm^{-1} is assigned to the quinoline C=N stretch. The IR spectrum of **6** has a strong sharp absorption band at 2111 cm^{-1} corresponding to the azide moiety and a sharp strong band at 3191 cm^{-1} for the secondary amine. The quinoline C=N absorption band is observed at 1609 cm^{-1}.These values are similar to those found in the literature.[35]

2.2.7. Synthesis of the 7-chloroquinoline-1,2,3-triazole ligand (L1) using "click chemistry".

Click chemistry has also been said to be "green" as it often proceeds in aqueous media, making this type of chemistry appealing.[37, 38] However, in order to synthesize the desired ligands, DCM was required as a solvent.

The quinoline-1,2,3-triazole ligand **L1** was synthesized using the CuAAC reaction.[39] **4-Azido-7-chloroquinoline** (**3**) was reacted with **(*E*)-*N*-(4(prop-2-yn-1-yloxy)phenyl)-1-(pyridine-2-yl)methanimine** (**2**) as outlined in **Scheme 2.7**. **L1** was isolated as a beige solid in a moderate yield of 56% and is soluble in chlorinated solvents like DCM and chloroform, partially soluble in DMSO, but insoluble in ethyl acetate, methanol, ethanol, hexane, pentane, diethyl ether, and toluene.

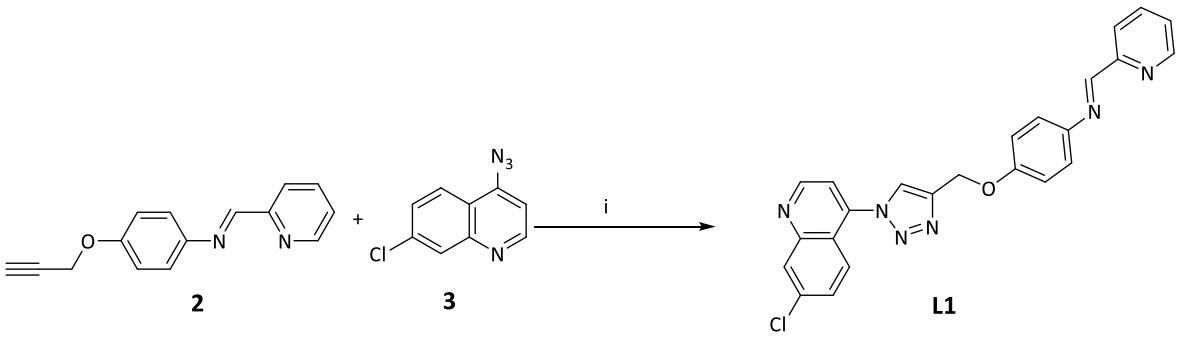

Scheme 2.7. Reaction scheme for the synthesis of **L1** using a copper-catalysed azide/alkyne cycloaddition. Conditions: (i) DCM, CuI, *N,N*-diisopropylethylamine (DIPEA), reflux, 4 h.

CuAAC or 'click' reactions are copper-catalysed reactions between terminal alkynes and azides to regioselectively form a 1,4-disubstituted 1,2,3-triazole.[40] Cu(I) is the active catalyst that leads to the exclusive synthesis of the 1,4-disubstituted regioisomer.[41] CuI exists in an inactive polymeric form and therefore is dissociated by an amine to form the active Cu(I) species.[39] *N, N*-diisopropylethylamine (DIPEA) is used as a base to pre-activate CuI by forming

a copper(I)-acetylide complex as shown in **Scheme 2.8**.[40,42] The formation of a Cu(I) acetylide is an essential activation step for the regioselective formation of 1,4-disubstituted triazoles.[43]

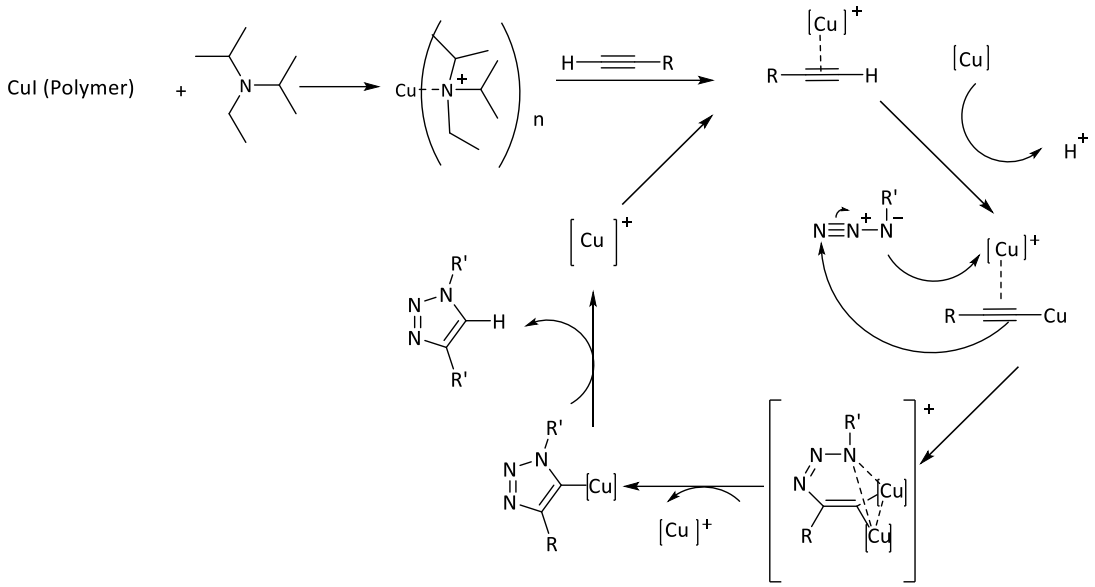

Scheme 2.8. General mechanism of CuAAC reactions.[40]

The σ-bound Cu(I) acetylide has a π-bound copper which coordinates to the azide forming a six-membered copper metallacycle. The second Cu atom acts as a stabilizing donor ligand. Ring contraction occurs forming a triazolyl-copper intermediate which then undergoes protonolysis yielding the desired triazole.

2.2.8. Characterization

2.2.8.1. *^{1}H and $^{13}C\{^{1}H\}$ NMR spectroscopy*

The diagnostic triazole proton signal H-13 is seen in the ^{1}H NMR spectrum of **L1** as a singlet at 9.00 ppm. The methylene protons H-11 appear as a singlet at 5.37 ppm but as a doublet with a coupling constant of $^{3}J_{HH}$= 2.4 Hz in the ^{1}H NMR spectrum of compound **2**. Upon cycloaddition, protons H-11 no longer couple to H-13 as was observed for compound **2**. All

quinoline aromatic protons except H-18 shifts downfield upon cycloaddition, as the triazole ring is more electron-withdrawing than the azide. The H-15(*) doublet has shifted to a higher frequency at 7.95 ppm compared to its initial frequency at 7.13 ppm in **3**. The H-20 (*) doublet of doublets is observed at a lower frequency (7.86 ppm) compared to its initial chemical shift at 8.94 ppm in compound **2**. Spectral analysis of the $^{13}C\{^{1}H\}$ NMR spectrum of **L1** shows the triazole carbon C-13 signal at 124.32 ppm. This lies in the characteristic region of 1,4-disubstituted triazole rings.[44] The imine carbon C-6 appears at 168.78 ppm and C-1 at 153.48 ppm.

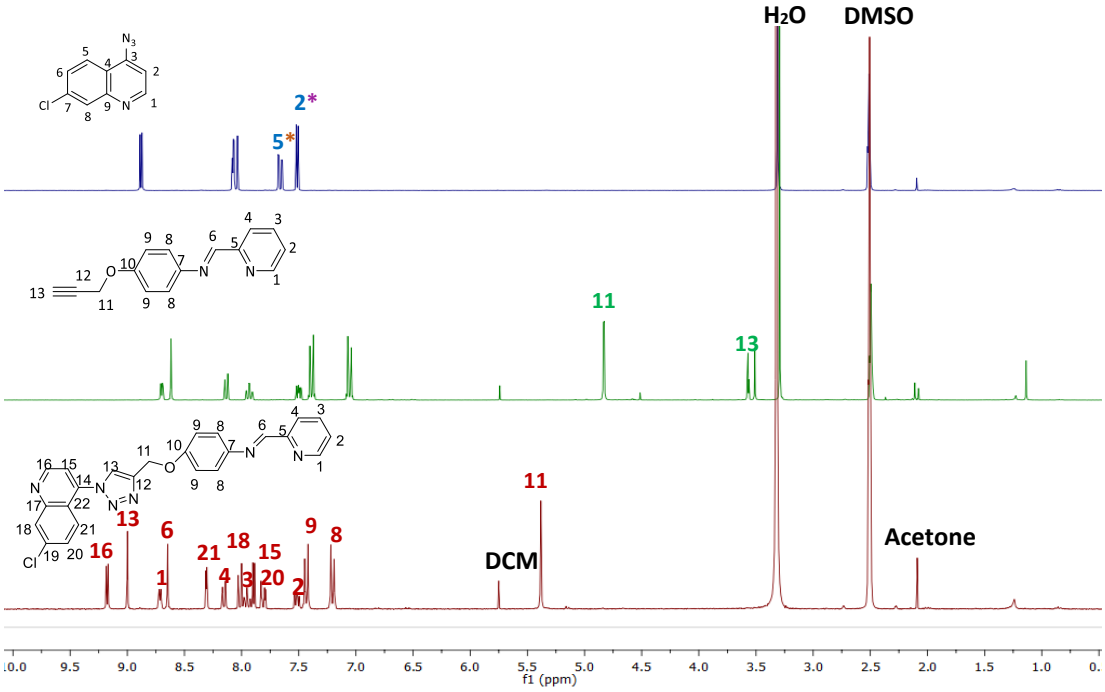

Figure 2.7. Stacked ^{1}H NMR spectra of azido-quinoline (**3**) (top), the precursor alkyne (**2**) (middle) and the quinoline-triazole **L1** (bottom).

2.2.8.2. IR spectroscopy

IR spectroscopy is a useful technique for the elucidation of successful synthesis of the quinoline-triazole ligand. The azide absorption band at 2117 cm^{-1} (compound **3**) is no longer present in the spectrum of **L1**, as seen in **Figure 2.8**. The quinoline C=N absorption band shifts

slightly from 1608 cm^{-1} to 1610 cm^{-1}. The imine and pyridyl C=N bands are found at 1623 cm^{-1} and 1595 cm^{-1}.

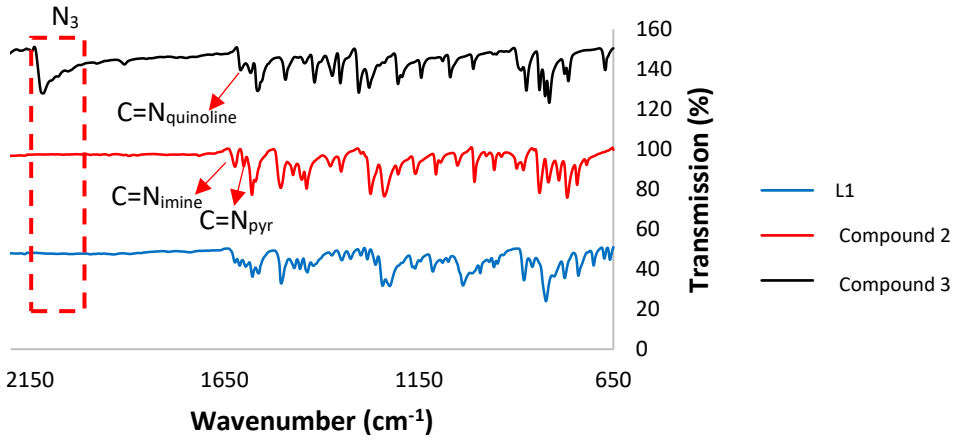

Figure 2.8. Stacked IR spectra of compounds **2**, **3** and **L1**

2.2.9. Synthesis of 4-amino-7-chloroquinoline-1,2,3-triazole ligand (L2)

L2 was synthesized *via* a CuAAC reaction between compounds **6** and **2**, as outlined in **Scheme 2.9**. The reaction follows the same mechanism described in **Section 2.2.6**. **L2** was isolated as an off-white powder in a moderate yield of 42%.

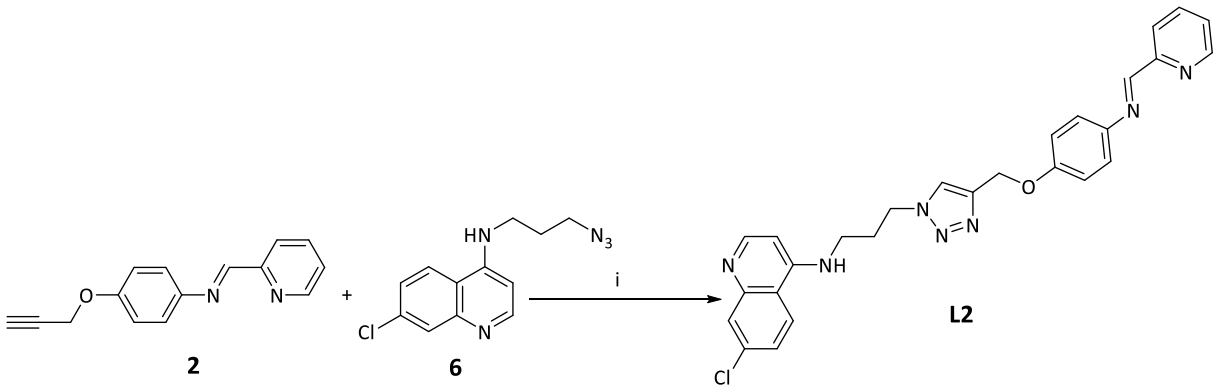

Scheme 2.9. Synthetic scheme for the CuAAC of **L2**. Conditions: (i) DCM,CuI, DIPEA, reflux, 18 h.

L2 is a new aminoquinoline-1,2,3-triazole that is soluble in most polar organic solvents like DCM, DMSO, ethyl acetate, methanol, acetone, ethanol, and chloroform. Contradictory to what is expected from click reactions, the synthesis of ligand **L2** was slightly more challenging than **L1**. Ligand **L2** was isolated *via* the slow diffusion out of diethyl ether and gave a moderate yield of 42%. The reaction time was longer than expected, taking 18 hours for the reaction to proceed to completion.

2.2.10. Characterization

2.2.10.1. ^{1}H and $^{13}C\{^{1}H\}$ NMR spectroscopy

The ^{1}H NMR spectrum of **L2** (**Figure 2.9**) shows the diagnostic triazole H-13 proton signal as a singlet at 8.28 ppm. The methylene protons H-11 are observed as a singlet at 5.18 ppm and has undergone a downfield shift from 4.83 ppm (compound **2**). This shift is attributed to the more electron-withdrawing nature of the triazole ring. H-11 no longer appears as a doublet, as was seen in the spectrum of compound **2** and therefore no longer couples to H-13. The amine proton H-17 experiences a negligible migration from 7.30 ppm in **6** to 7.34 ppm. Protons H-15 and H-14 undergo a downfield shift from 1.93 ppm and 3.50 ppm to 2.25 ppm and 4.54 ppm respectively. As observed for compound **4**, proton H-16 is not well resolved from the H_2O resonance at 3.33 ppm, which was confirmed by HSQC. A cross peak is seen at (3.33 ppm; 39.74 ppm) corresponding to that of (H-16; C-16). In the $^{13}C\{^{1}H\}$ NMR spectrum of **L2**, C-13 appears in the characteristic region at 125.67 ppm. C-1 appears as a singlet at 149.97 ppm and C-6 at 158.54 ppm.

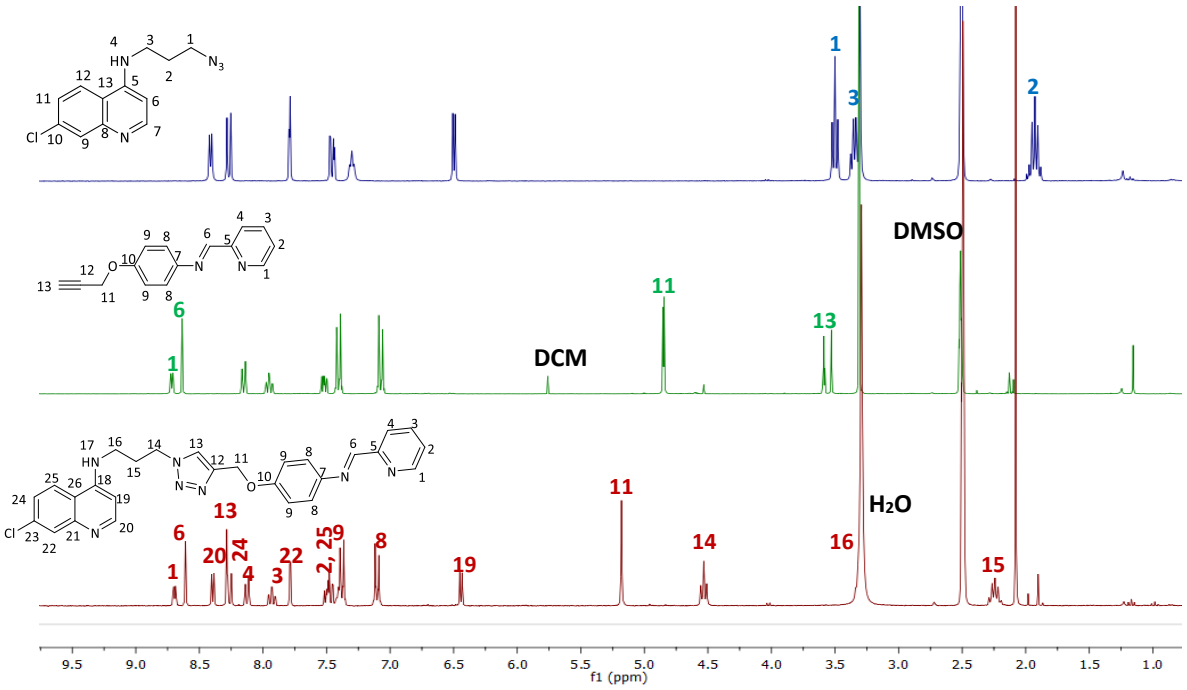

Figure 2.9. Stacked 1H NMR spectra of compounds **2** (middle), **6** (top) and **L2** (bottom)

2.2.10.2. IR Spectroscopy

The imine C=N and quinoline C=N functional groups are observed as a weak sharp absorption band at 1612 cm^{-1} in the IR spectrum of **L2**, as seen in **Figure 2.10**. The pyridyl absorption band appears as a strong sharp absorption band at 1592 cm^{-1}.

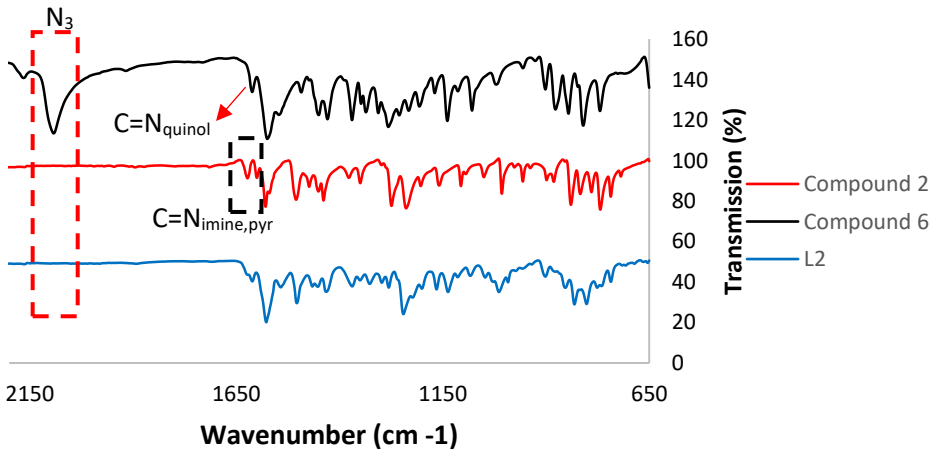

Figure 2.10. Stacked IR spectra of compounds **2**, **6** and **L2**.

2.3. Summary

A quinoline-1,2,3-triazole and an aminoquinoline-1,2,3-triazole ligand were successfully synthesized *via* CuAAC reactions to yield 1,4-disubstituted ligands **L1** and **L2**. These ligands were characterized using ^{1}H NMR, ^{13}C{^{1}H} NMR and FT-IR spectroscopy. Both ligands were isolated in moderate yields and were air and moisture stable. The click reactions have been described as "green" aqueous reactions in literature.[37] This is due to the often mild conditions needed and compatibility in H_2O.[38] It was however found that the CuAAC reactions reported herein required DCM as a solvent and slightly longer reaction times for **L2**. The synthesis and purification of these quinoline-triazole ligands were relatively easy as expected from "click chemistry". Easy isolation of the click product is one of the criteria defining "click chemistry", as the reaction produces easily removed by-products and purification should not require column chromatography. The yields of these reactions were moderate and could possibly be improved in the future by using tris-hydroxypropyltriazolylmethylamine (THPTA). THPTA is a water-soluble ligand that is often used in CuAAC reactions to help increase the rate of reaction and possibly improve its yield. The antimalarial properties of the synthesized quinoline-triazoles were evaluated and are discussed in **Chapter 4**.

2.4. References

1 P. Bray, B. Park, E. Asadollaly, G. Biagini, J. Jeyadevan, N. Berry, S. Ward and P. O' Neill, *Curr. Top. Med. Chem.*, 2006, **6**, 479–507.

2 T. E. Wellems and C. V Plowe, *J. Infect. Dis.*, 2019, **184**, 770–776.

3 K. K. Singh and S. K. Vingkar, *Int. J. Pharm.*, 2008, **347**, 136–143.

4 C. C. C. Hans O. Lobel, Mark Miani, Tom Eng, Kenneth W. Bernard, Allen W.Hightower, *Lancet*, 1992, **341**, 848–851.

5 D. L. Klayman, *Am. Assoc. Adv. Sci.*, 2016, **228**, 1049–1055.

6 M. Mushtaque and S. Shahjahan, *Eur. J. Med. Chem.*, 2015, **90**, 280–295.

7 S. J. Yeo, D. X. Liu, H. S. Kim and H. Park, *Malar. J.*, 2017, **16**, 1–9.

8 C. H. Kaschula, T. J. Egan, R. Hunter, N. Basilico, S. Parapini, D. Taramelli, E. Pasini and D. Monti, *J. Med. Chem.*, 2002, **45**, 3531–3539.

9 S. Pou, R. W. Winter, A. Nilsen, J. X. Kelly, Y. Li, J. S. Doggett, E. W. Riscoe, K. W. Wegmann, D. J. Hinrichs and M. K. Riscoe, *Antimicrob. Agents Chemother.*, 2012, **56**, 3475–3480.

10 Y. Hu, C. Gao, S. Zhang, L. Xu, Z. Xu and L. Feng, *Eur. J. Med. Chem.*, 2017, **139**, 22–47.

11 X. Nqoro, N. Tobeka and B. A. Aderibigbe, *Molecules*, 2017, **22**, 2268.

12 N. Wang, K. J. Wicht, E. Shaban, T. A. Ngoc, M. Q. Wang, I. Hayashi, M. I. Hossain, Y. Takemasa, M. Kaiser, I. El Tantawy El Sayed, T. J. Egan and T. Inokuchi, *Medchemcomm*, 2014, **5**, 927–931.

13 D. D. N'Da and P. J. Smith, *Med. Chem. Res.*, 2014, **23**, 1214–1224.

14 M. Tripathi, S. I. Khan, P. Ponnan, R. Kholiya and D. S. Rawat, *ChemistrySelect*, 2017, **2**, 9074–9083.

15 F. B. El Garah, C. Claparols, F. Benoit-Vical, B. Meunier and A. Robert, *Antimicrob. Agents Chemother.*, 2008, **52**, 2966–2969.

16 S. Manohar, S. I. Khan and D. S. Rawat, *Chem. Biol. Drug Des.*, 2011, **78**, 124–136.

17 E. M. Guantai, K. Ncokazi, T. J. Egan, J. Gut, P. J. Rosenthal, P. J. Smith and K. Chibale, *Bioorganic Med. Chem.*, 2010, **18**, 8243–8256.

18 R. Raj, P. Singh, P. Singh, J. Gut, P. J. Rosenthal and V. Kumar, *Eur. J. Med. Chem.*, 2013, **62**, 590–596.

19 R. C. N. R. Corrales, N. B. de Souza, L. S. Pinheiro, C. Abramo, E. S. Coimbra and A. D. Da Silva, *Biomed. Pharmacother.*, 2011, **65**, 198–203.

20 X. M. Chu, C. Wang, W. L. Wang, L. L. Liang, W. Liu, K. K. Gong and K. L. Sun, *Eur. J. Med. Chem.*, 2019, **166**, 206–223.

21 N. Boechat, M. D. L. G. Ferreira, L. C. S. Pinheiro, A. M. L. Jesus, M. M. M. Leite, C. C. S. Júnior, A. C. C. Aguiar, I. M. De Andrade and A. U. Krettli, *Chem. Biol. Drug Des.*, 2014, **84**, 325–332.

22 H. M. Faidallah, S. S. Panda, J. C. Serrano, A. S. Girgis, K. A. Khan, K. A. Alamry, T. Therathanakorn, M. J. Meyers, F. M. Sverdrup, C. S. Eickhoff, S. G. Getchell and A. R. Katritzky, *Bioorganic Med. Chem.*, 2016, **24**, 3527–3539.

23 G. R. Pereira, G. C. Brandão, L. M. Arantes, H. A. De Oliveira, R. C. De Paula, M. F. A. Do Nascimento, F. M. Dos Santos, R. K. Da Rocha, J. C. D. Lopes and A. B. De Oliveira, *Eur. J. Med. Chem.*, 2014, **73**, 295–309.

24 L. Taleli, C. De Kock, P. J. Smith, S. C. Pelly, M. A. L. Blackie and W. A. L. Van Otterlo, *Bioorg. Med. Chem.*, 2015, **23**, 4163–4171.

25 M. G. F. and K. B. S. H. C. Kolb, *Angew. Chem - Int. Ed.*, 2001, **40**, 2004–2021.

26 J. E. Moses and A. D. Moorhouse, *Chem. Soc. Rev.*, 2007, **36**, 1249–1262.

27 F. Himo, T. Lovell, R. Hilgraf, V. V. Rostovtsev, L. Noodleman, K. B. Sharpless and V. V. Fokin, *J. Am. Chem. Soc.*, 2005, **127**, 210–216.

28 J. E. Hein and V. V. Fokin, *Chem. Soc. Rev.*, 2010, **39**, 1302–1315.

29 Q. Zhang, H. Su, J. Luo and Y. Wei, *Catal. Sci. Technol.*, 2013, **3**, 235–243.

30 D. A. Xavier, 1 and N. Srividhya, *J. Appl. Chem.*, 2014, **7**, 06–15.

31 H. C. Aspinall, N. Greeves, W. M. Lee, E. G. McIver and P. M. Smith, *Tetrahedron Lett.*, 1997, **38**, 4679–4682.

32 R. N. B. Robert Thornton Morrison, in *Organic chemistry*, Prentice Hall, 6th edn., 1992, pp. 241–242.

33 D. J. Sam and H. E. Simmons, *J. Am. Chem. Soc.*, 1974, **96**, 2252–2253.

34 G. C. Brandão, F. C. Rocha Missias, L. M. Arantes, L. F. Soares, K. K. Roy, R. J. Doerksen, A. Braga de Oliveira and G. R. Pereira, *Eur. J. Med. Chem.*, 2018, **145**, 191–205.

35 P. M. Njogu, J. Gut, P. J. Rosenthal and K. Chibale, *ACS Med. Chem. Lett.*, 2013, **4**, 637–41.

36 M. P. Kristina Starcevic, Dijana Pesic, Ana Toplak, Goran Landek, Sulejman Alihodzic, Esperanza Herreros, Santiago Ferrer, Radan Spaventi, *Eur. J. Med. Chem.*, 2012, **49**, 365–378.

37 L. Chen and C. J. Li, *Adv. Synth. Catal.*, 2006, **348**, 1459–1484.

38 L. Li and Z. Zhang, *Molecules*, 2016, **21**, 1–22.

39 Y. H. Changwei Shao, Xinyan Wang, Qun Zhang, Sheng Luo, Jichen Zhao, *J. Org. Chem.*, 2011, **76**, 6832–6836.

40 A. A. H. A. Fuaad, F. Azmi, M. Skwarczynski and I. Toth, *Molecules*, 2013, **18**, 13148–13174.

41 J. E. Arg, *R. Soc. Chem.*, 2017, **7**, 33967–33973.

42 V. O. Rodionov, V. V. Fokin and M. G. Finn, *Angew. Chem - Int. Ed.*, 2005, **44**, 2210–2215.

43 V. A. Online, H. Ben, E. Ayouchia, L. Bahsis, L. R. Domingo and S. Stiriba, *R. Soc. Chem.*, 2018, **8**, 7670–7678.

44 X. Creary, A. Anderson, C. Brophy, F. Crowell and Z. Funk, *J. Org. Chem.*, 2012, **77**, 8756–8761.

Chapter 3

Quinoline-triazole Mn(I), Re(I) complexes

3.1. Introduction

Carbon monoxide (CO) is well known for its toxic effects on the oxygen metabolism.[1] Despite CO's well-known toxicity, it is reportedly produced in miniscule amounts in mammalian cells under stress conditions.[2] The gaseous small molecule plays an important physiological role as a molecular messenger under stress conditions.[3] CO has demonstrated several therapeutic effects such as anti-inflammatory,[4] antiproliferative[5] and antiapoptotic.[6] In addition to the therapeutic effects displayed by the gasotransmitter (a gaseous compound with a biochemical function), the medicinal application of CO extends much further. CO has received significant acknowledgement in the medical field for its application and progress in organ transplants, including the heart,[7] lungs,[8] kidneys,[9] liver[10] and the small intestine.[11] However, the administration of CO in its gaseous form does not allow for control over localisation, concentration or selectivity of CO,[12] as shown in **Figure 3.1.** The toxicity of CO and the unpredictability of its administration through inhalation prompted the research of Carbon Monoxide-Releasing Molecules (CORMs).

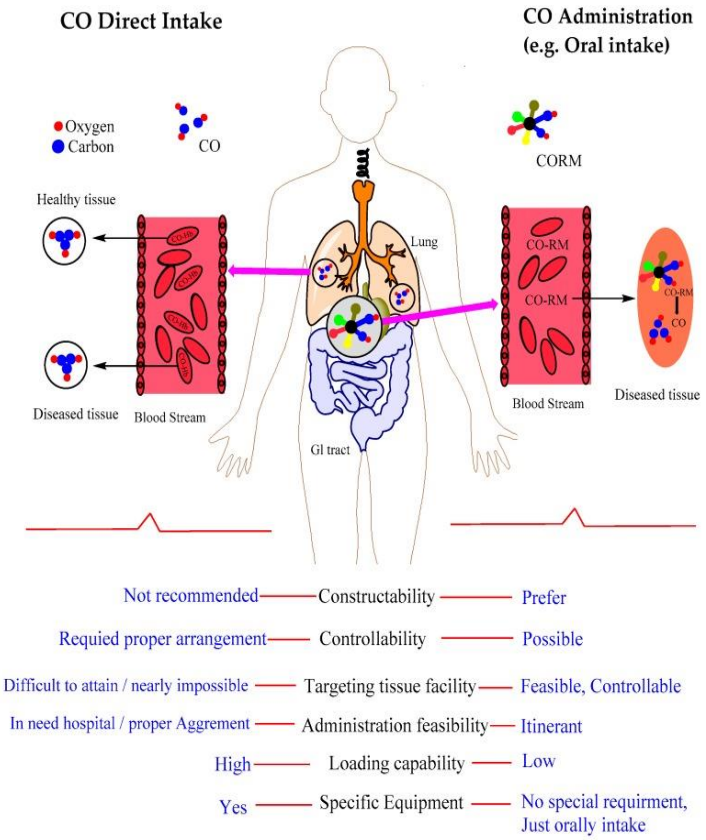

Figure 3.1. Feasibility of using gaseous CO *vs*. administration using CORMs.[13]

The development of CORMs by Motterlini *et al*.[13] has presented an alternative mode of transporting CO *via* a controllable mechanism.[14] CORMs release CO upon exposure to external stimuli such as solvent,[15] enzymes,[16] pH,[17] and light (PhotoCORMs).[18] Although CORMs that release CO spontaneously in aqueous media are popular, this method makes it difficult to control the starting time of action.[19] PhotoCORMs allow for CO-release to be targeted and time-specific. PhotoCORMs release CO upon exposure to light at a specific wavelength and present a favourable method of spatial and temporal CO-release control. The majority of PhotoCORMs reported to date are based on group 7 transition metals, attributing to their extensively studied photochemical and photophysical properties.[20] CORMs have been evaluated for their antimicrobial activity and have displayed potential against many microorganisms including *Escherichia coli*,[21] *Staphylococcus aureus,*[21] and *Pseudomonas aeruginosa*.[22] CO has also been used as an effective cancer treatment strategy, due to its antiproliferative properties.[23] CO has been found to prevent the development of cerebral

malaria in mice, making the mice tolerant to *P.falciparum*.[24] The development of CORMs has thus presented a novel form of treating the before-mentioned diseases and has become of great interest in both the scientific and medical field.

There are several methods that can be used to test the CO-releasing properties of a CORM, but the most widely used is a Myoglobin (Mb) assay.[25] The Myoglobin assay is based on the UV/vis detection of the conversion of deoxymyoglobin (deoxy-Mb) to carbonmonoxy-Mb (COMb). Mb serves as the oxygen transport protein in live muscles,[26] but it has been established that it has a higher affinity for CO than it does for O_2.[27] During the assay, Mb is reduced using sodium dithionite to form deoxy-Mb, as shown in **Scheme 3.1**.

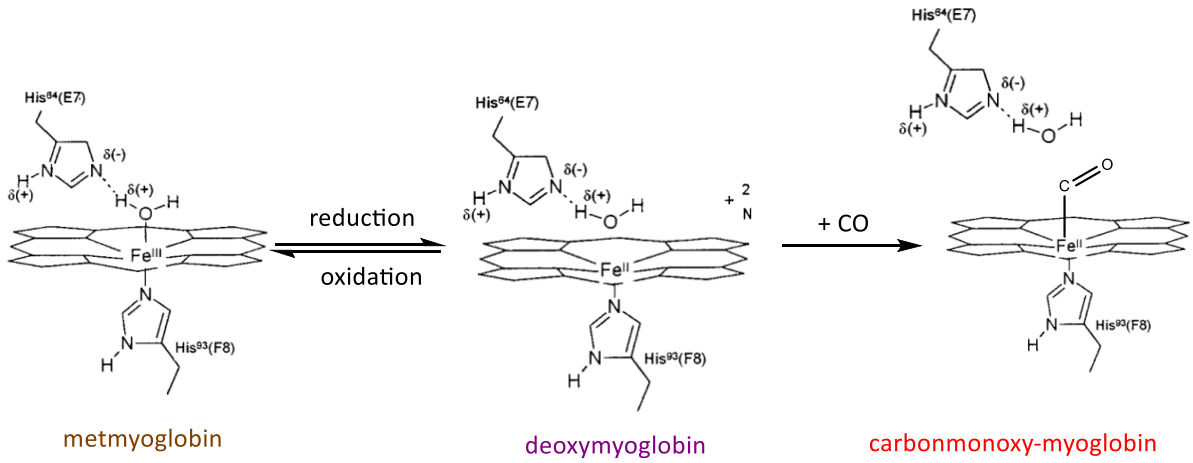

Scheme 3.1. Reduction, oxidation and addition of CO onto myoglobin.

Deoxy-Mb absorbs at 557 nm and therefore exhibits a single maxima at this point in the UV/vis spectrum. In the presence of CO, deoxy-Mb preferentially binds to CO and is therefore converted to COMb. COMb has two absorbance maximums at 544 nm and 570 nm. This conversion and therefore the change in the electronic absorption spectra can be observed over time.

Manganese and rhenium carbonyl complexes are often used to form cationic species to add various substituents in place of one of its ligands. These complexes have been studied for

their ability to take part in agostic C-H interactions,[28,29] for the functionalisation of [ReX(CO)$_3$(N-N)] complexes,[30] and to synthesise luminescent manganese complexes.[20,31] Developing a method for the synthesis of a cationic species of the manganese complexes reported herein will be useful for future work. Manganese complexes are not inherently luminescent and cannot be visualized intracellularly. Through salt metathesis, fluorescent ligands can be added to the complex potentially rendering the complexes fluorescent.

In this chapter, the synthesis and characterisation of two manganese and rhenium tricarbonyl complexes are reported. The reactivity of one manganese complex was evaluated *via* salt metathesis in order to attempt to synthesize a cationic manganese complex with two N-donor ligands: isoniazid and 4-picoline. The manganese complexes were further evaluated for their photochemical properties using IR spectroscopy, UV/Vis and a Myoglobin assay.

3.2. Synthesis and characterisation of Quinoline-1,2,3-triazole Mn(I) and Re(I) tricarbonyl complexes

3.2.1. Synthesis

New Mn(I) and Re(I) complexes, **Mn-1** and **Re-1** were synthesised under similar conditions using a modified literature method where similar compounds were synthesised.[1] The ligand **L1** was reacted with either [MnBr(CO)$_5$] or [ReCl(CO)$_5$] as shown in **Scheme 3.2** to afford either an orange or yellow powder in good yields of 93% (**Mn-1**) and 84% (**Re-1**). Due to the known photosensitivity of most Mn(I) tricarbonyl complexes and potential photosensitivity of their Re(I) analogues, both complexes were synthesised and isolated in the dark.

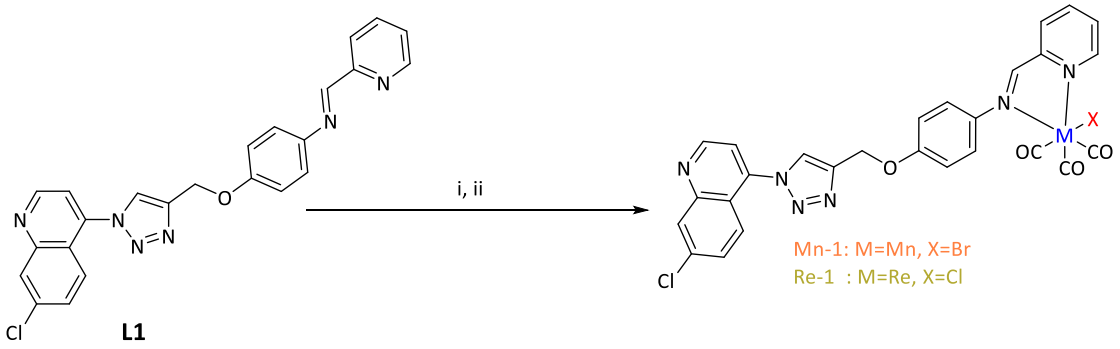

Scheme 3.2. Reaction scheme for the synthesis of **Mn-1** and **Re-1.** Reagents and conditions: (i) $[MnBr(CO)_5]$, DCM, rt, 72 h. (ii) $[ReCl(CO)_5]$, DCM, 40 °C 96 h.

The chelation of the bidentate ligand **L1** occurs *via* a dissociative substitution method,[32] similar to that of an S_N1 reaction in organic chemistry. Initially, the halide atom acts as a cis-labilizing ligand,[33] allowing for the dissociation of a carbonyl *cis* to the bromide (*cis*-CO) and the subsequent association of either the imine or pyridyl nitrogen forming a 16-electron $[MnBr(CO)_4\mathbf{L1}]$ intermediate as shown in **Equation 3.1**. With one nitrogen atom already complexed to the metal centre, it becomes easier for the second nitrogen atom to displace another CO and coordinate to the metal (**Equation 3.2**).

$$[MnBr(CO)_5] + L2 \rightarrow [MnBr(CO)_4L2] + CO \quad \ldots\ldots \text{Eqn } 3.1$$

$$[MnBr(CO)_4L2] \rightarrow [MnBr(CO)_3L2] + CO \quad \ldots\ldots \text{Eqn } 3.2$$

Imine and pyridyl nitrogens are both weaker π-acceptors than CO and are therefore likely to once again labilize a *cis*-CO as opposed to a trans one,[33] resulting in the formation of a *fac*-$[MX(CO)_3\mathbf{L1}]$ complex as shown in **Figure 3.2**.

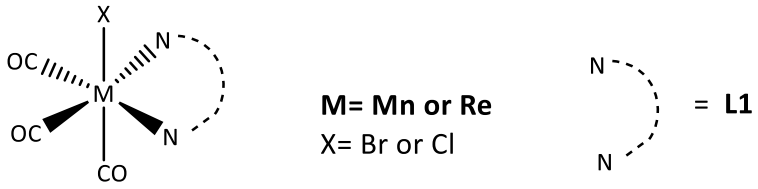

Figure 3.2. Representative structure of the *fac*-**[MX(CO)$_3$L1]** complex

Transition metal complexes can form two kinds of geometric isomers, either *cis/trans* isomers or *fac/mer* isomers. *Cis/trans* isomers refer to the spatial arrangement of two species whereas *fac/mer* refers to the spatial arrangement of three species. As previously mentioned, the *cis*-effect of the bromide results in the formation of the *cis*-isomer with regards to **L1**. In turn, this effect resulted in the formation of the *fac*- as opposed to the *mer*-isomer with regards to the attached carbonyls, which will be confirmed in **Section 3.2.2.2**.

3.2.2. Characterisation

*3.2.2.1. ^{1}H and $^{13}C\{^{1}H\}$ NMR spectroscopy of **Mn-1** and **Re-1***

The ^{1}H NMR spectrum of **Mn-1** (**Figure 3.3**) shows a shift from 8.77 ppm (in ligand **L1**) and 8.70 ppm to 9.22 ppm and 8.87 ppm for the pyridyl (H-1) and the imine (H-6) protons respectively. Spectroscopic analysis of metal complexes and their parent ligand indicates that upon metalation, the synergic effect causes the resonance of protons on the carbon adjacent to the nitrogens to undergo upfield shifts. This synergic effect is caused by the donation of electrons from a filled π-orbital of the ligand to an empty metal orbital. Electrons are synergistically back-donated from a filled d-orbital of the metal centre into an empty π^*-antibonding orbital of the ligand.[34] This back-donation has a shielding effect on protons surrounding the atom receiving to which electrons are back-donated, resulting in an upfield shift of the directly affected protons.

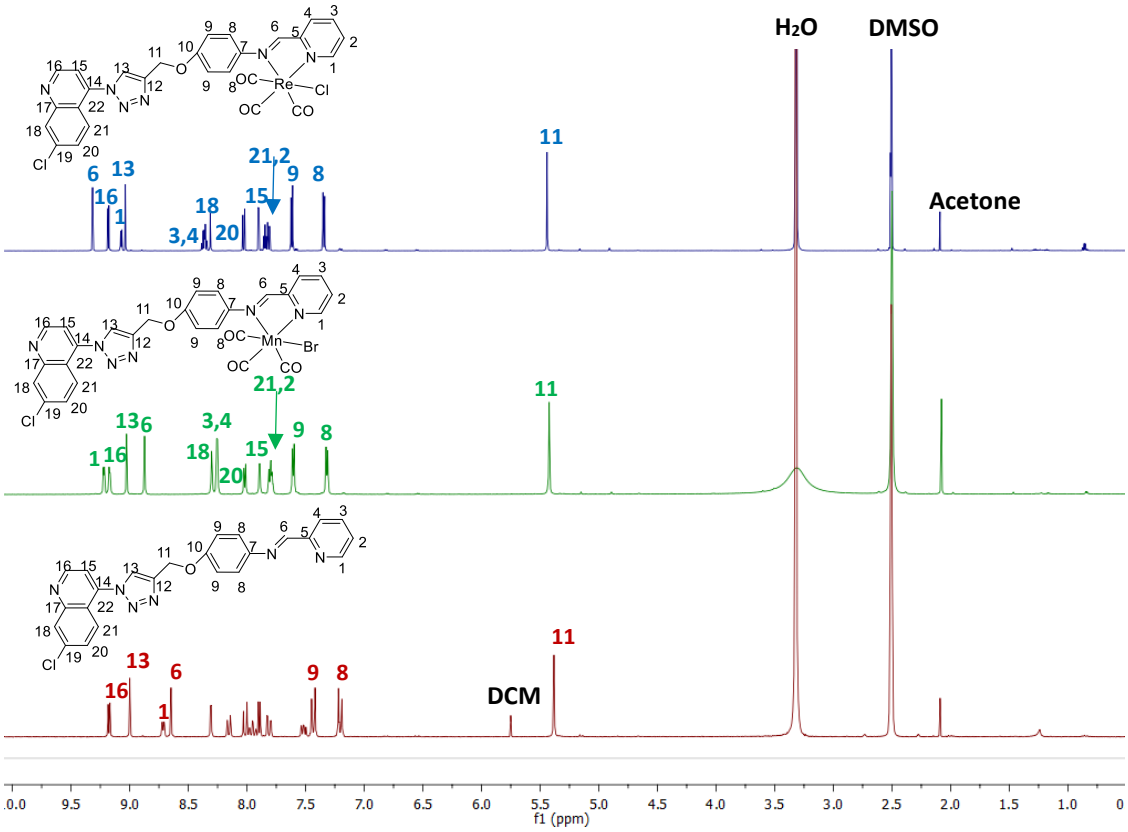

Figure 3.3. Stacked ^{1}H NMR spectra of **L1**, **Mn-1** and **Re-1** in DMSO-d6

However, carbonyls are better π-acceptors than nitrogen, causing a stronger back-donation of electrons into C=O (**Figure 3.4**) rather than N=CH, deshielding protons H-1 and H-6. Subsequently, all aromatic protons on the pyridyl and phenyl ring undergo downfield shifts.

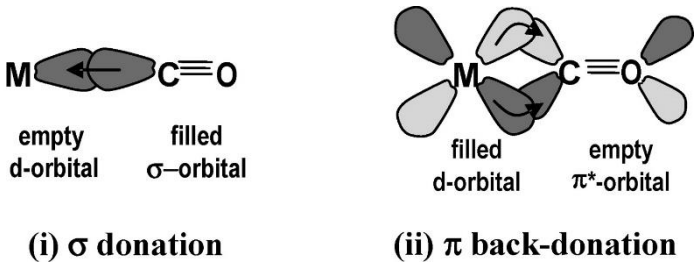

Figure 3.4. σ Donation and π back-donation in transition metal carbonyl compounds.[33]

The same characteristic downfield shifts of protons H-1 and H-6 are seen in the ^{1}H NMR spectrum of **Re-1**. The chemical shifts of protons H-1 and H-6 shift from 8.77 ppm and 8.70 ppm (**L1**) to 9.07 ppm and 9.31 ppm respectively. These downfield shifts are expected, due to the better π-accepting capacity of the CO ligands as explained for complex **Mn-1**. These shifts confirm that the bidentate ligand chelates to the metal centre *via* the pyridyl and amine nitrogens. All aromatic protons on the pyridyl and phenyl ring undergo a slight downfield shift as well, further confirming successful complexation. **L1** chelates to the Re centre in a *cis*-configuration with *facially* arranged carbonyls as described in for the Mn analogue. The ^{13}C {^{1}H} NMR spectrum of **Mn-1** has three singlets of low intensity at 222.22 ppm, 221.18 ppm and 218.3 ppm, corresponding to the three carbonyl carbons. There are three singlets of low intensity at 197.73 ppm, 197.19 ppm and 187.81 ppm, corresponding to the three carbonyl carbons in the ^{13}C{^{1}H} NMR spectrum of **Re-1**.

*3.2.2.2. IR spectroscopy of **Mn-1** and **Re-1***

The IR spectrum of **Mn-1** and **Re-1** (**Figure 3.5**) both show absorption bands of strong intensity for the CO ligands at 2024 cm^{-1} and 2019 cm^{-1}respectively. Broad absorption bands with a shoulder are seen at 1914 cm^{-1} and 1886 cm^{-1} in the IR spectra of complexes **Mn-1** and **Re-1** respectively, corresponding to two CO ligands. These wavenumbers appear in the range common to *facially* arranged carbonyls suggesting that the three carbonyls lie on one face of the proposed octahedral geometry.[35] The imine C=N band shifts to a lower wavenumber from 1623 cm^{-1} in the ligand to 1610 cm^{-1} in complex **Mn-1**, overlapping with that of the quinoline C=N absorption band. This was unexpected and contradicts the downfield shift observed for the imine proton in the ^{1}H NMR spectrum. If back-donation were directed towards the imine C=N, the bond length would increase. This increase in bond length and decrease in bond order would result in a shift in the frequency of the C=N absorption band to a lower wavenumber and what is observed would be expected. However, back-donation is directed towards the carbonyls due to them being better π-acceptors. No similar examples of this occurrence were found in literature and further experiments will need to be performed to explain it. The pyridine C=N band shifts from 1595 cm^{-1} to a higher wavenumber of 1598 cm^{-1} in complex **Mn-1**. In the IR spectrum of **Re-1**, the imine C=N band shifts from 1623 cm^{-1} to 1614 cm^{-1},

overlapping with that of the quinoline C=N band. The pyridyl C=N band shifts from 1595 cm^{-1} in the ligand to 1598 cm^{-1} in the metal complex.

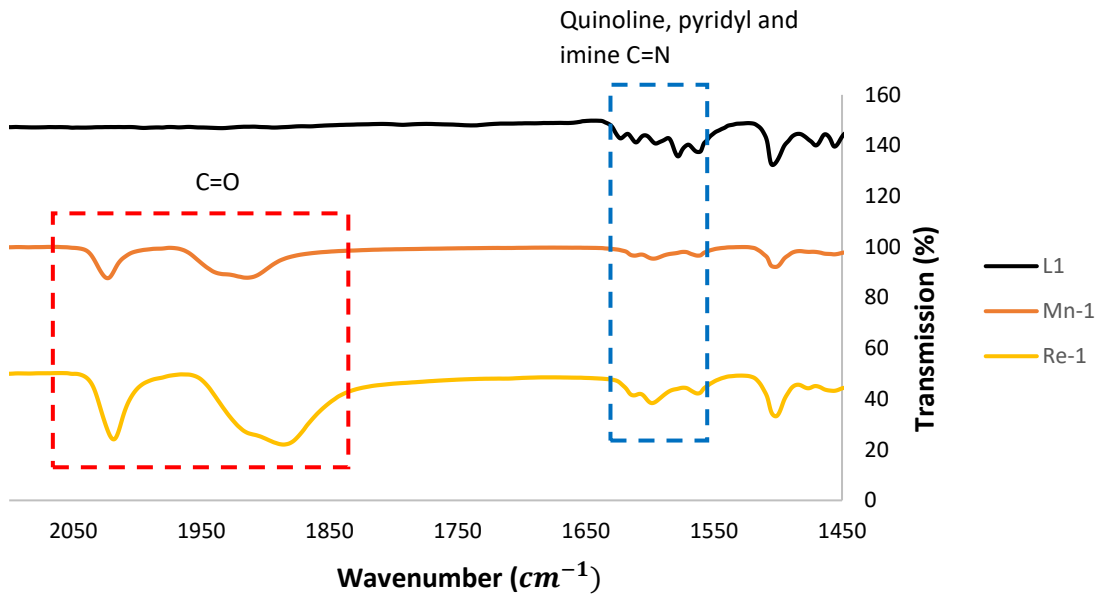

Figure 3.5. Stacked IR spectra of **L1**, **Mn-1** and **Mn-2**

3.2.2.3. Mass Spectrometry

Complexes **Mn-1** and **Re-1** were analysed using high-resolution ESI-MS. The mass spectrum of **Mn-1** shows the protonated molecular ion peak at *m/z* 660.9620 attesting to the integrity of the complex, correlating with the calculated value of 660.7680. A protonated molecular ion peak was observed at *m/z* 747.0309 in the mass spectrum of **Re-1**, corresponding with the calculated value of 747.5880.

3.3. Synthesis and characterisation of aminoquinoline-1,2,3-triazole Mn(I) and Re(I) complexes

3.3.1. Synthesis

The ligand **L2** was reacted with either $[MnBr(CO)_5]$ or $[ReCl(CO)_5]$ under the conditions shown in **Scheme 3.3**, to afford the new metal tricarbonyl complexes **Mn-2** and **Re-2**. **Mn-2** was isolated as an orange powder in a good yield of 70%. **Re-2** was isolated as a yellow powder comprised of some unreacted ligand and the desired complex in a yield of 73%. **L2** was reacted with $[ReCl(CO)_5]$ under several conditions, optimizing for solvents, equivalents of $[ReCl(CO)_5]$, reaction times and temperatures, where DCM at 40℃ for 24 hours produced the best results.

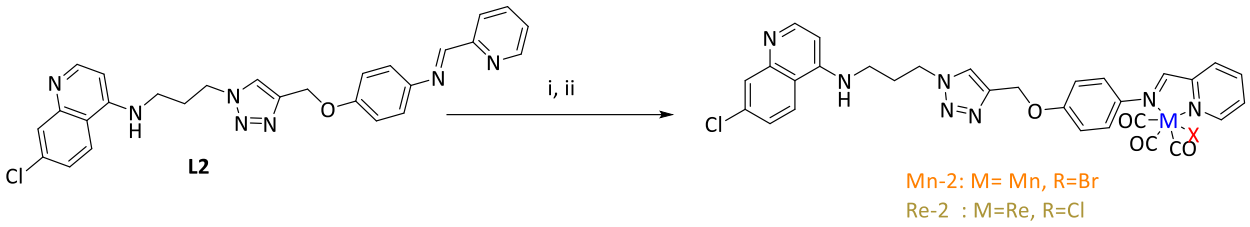

Scheme 3.3. Synthetic scheme for the synthesis of **Mn-2** and **Re-2.** Reagents and conditions: (i) $[MnBr(CO)_5]$, DCM, 25 ℃, 24 h. (ii) $[ReCl(CO)_5]$, DCM, 40 ℃, 24 h.

Attempts to separate unreacted **L2** from **Re-2** were challenging, as both compounds were soluble in the same organic solvents and thus using recrystallisation/ trituration was unsuccessful. Both **L2** and **Re-2** displayed the same Rf value on silica TLC plates despite using varying mobile phases which included MeOH/DCM and EtOAc/petroleum ether. It was therefore not feasible to employ column chromatography. It should also be noted that **L2** produced multiple spots on silica TLC plates, due to possible degradation of the imine. Further attempts to purify **Re-2** were not explored and, instead, the focus was shifted to attempting to synthesize a cationic Mn(I) species.

3.3.2. Characterisation

3.3.2.1. ^{1}H and $^{13}C\{^{1}H\}$ NMR spectroscopy

The ^{1}H NMR spectra of **Mn-2** and crude **Re-2** are shown in **Figure 3.6**. Proton resonances of H-1 and H-6 undergo the expected downfield shifts from 8.69 ppm and 8.60 ppm (in **L2**) to 9.22 ppm and 8.87 ppm respectively in the spectrum of **Mn-2**. H-8 and H-9 resonate downfield at 7.22ppm and 7.56 ppm respectively. Protons H-3, H-4 shift downfield and resonates in the same region as H-24. This results in a multiplet that integrates for three protons in the range of 8.29-8.24 ppm.

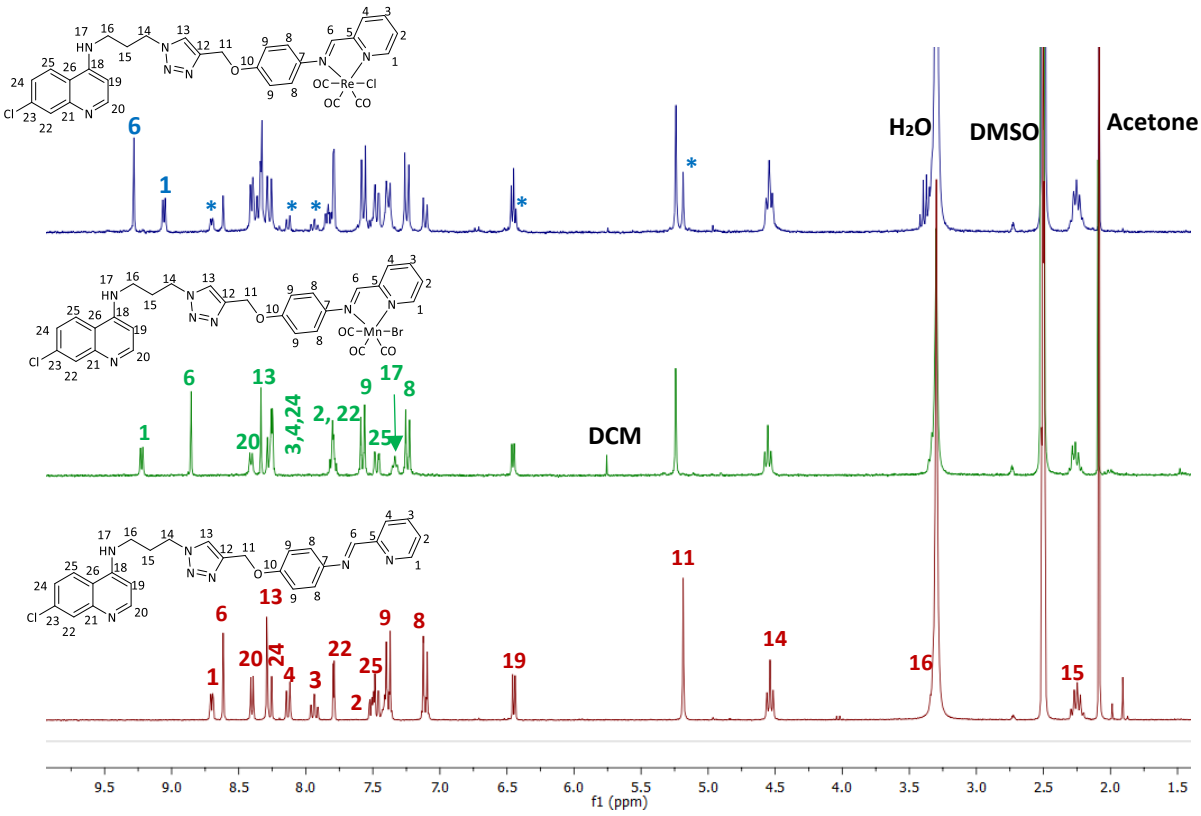

Figure 3.6. Stacked ^{1}H NMR spectra of **L2**, **Mn-2** and crude **Re-2.** The asterix (*) represents **L2** signals.

In the $^{13}C\{^{1}H\}$ NMR spectrum of **Mn-2**, three carbonyl carbon signals are observed as low-intensity singlets at 222.33 ppm, 221.22 ppm and 219.25 ppm. C-13 appears at 124.72 ppm, C-1 at 153.69 ppm and C-6 at 167.85 ppm.

The ^{1}H NMR spectrum of crude **Re-2** sample does attest to successful chelation of **L2** *via* the imine and pyridyl nitrogens to form **Re-2**. Upon complexation, protons H-1 and H-6 shift downfield to 9.06 ppm and 9.29 ppm respectively. H-9 and H-8 appear as doublets at 7.57 ppm and 7.25 ppm respectively. Proton signals corresponding to unreacted **L2** are indicated with an Asterix (*) and analysis of the ligand to complex ratio using ^{1}H NMR spectroscopy indicates that there is a 0.5/1 ratio of ligand/complex.

3.3.2.2. IR spectroscopy

A sharp strong absorption band is observed at 2024 cm^{-1} and 2019 for one carbonyl in the IR spectra of complexes **Mn-2** and **Re-2** respectively (**Figure 3.7**). A broader strong band is observed at 1914 cm^{-1} and 1889 cm^{-1} for two carbonyls in the IR spectrum of **Mn-2** and **Re-2** respectively. The range of these wavenumbers confirms that the *fac*-isomer has been synthesised. The imine C=N absorption band appears as a weak sharp absorption band at 1603 cm^{-1} and the pyridyl C=N absorption band has not shifted, still residing at 1592 cm^{-1} in the spectra of both complexes.

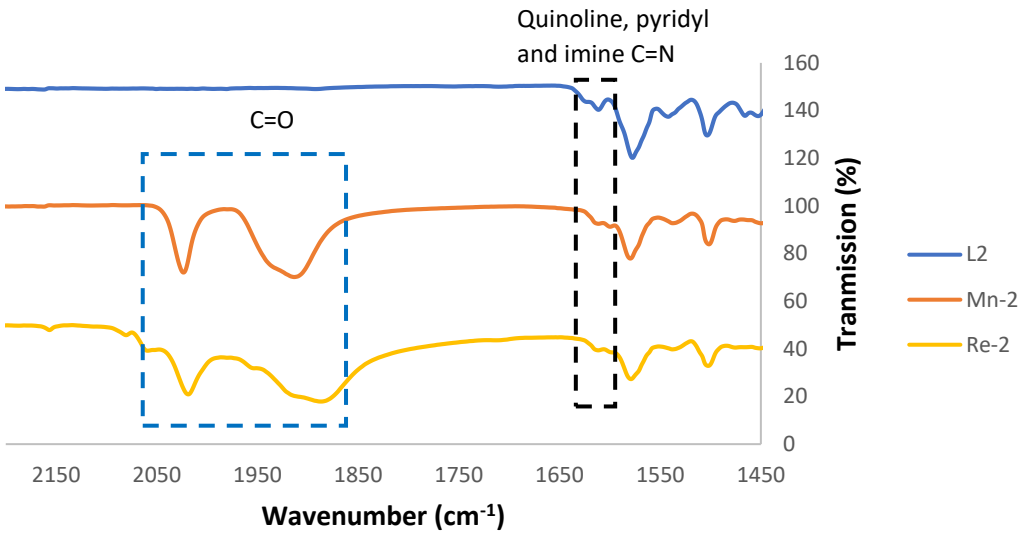

Figure 3.7. Stacked IR spectra of compounds **L2**, **Mn-2** and **Re-2**.

3.3.2.3. Mass spectrometry

Mn-2 was analysed using high-resolution ESI-MS. The mass spectrum of **Mn-2** shows a $[M+MeCN+Na]^+$ peak corresponding to the molecular ion plus acetonitrile and a sodium molecule at *m/z* 736.4257 correlating with the calculated value of 736.4400. The Mass spectrum of Re-2 was not obtained, due to the known presence of **L2** in the sample.

3.4. Reactivity studies of complex Mn-1 using a [2+1] approach

Reactivity studies were done using complex **Mn-1** in an attempt to synthesize a cationic manganese species that could potentially be further functionalized. The method used for the [2+1] reactivity studies was a salt metathesis. **Mn-1** has an *N*-*N*-bidentate ligand chelating to the metal centre, hence 2 and a single *N*-donor ligand will subsequently be attached, representing the 1 in [2+1]. Salt metathesis involves a halogen abstraction,[36] and exchange with a donor ligand. Mn complexes are not inherently luminescent like their Re analogues.

The Mn complexes reported herein cannot be tracked intracellularly.The purpose of the reactivity study was to develop a method in which the bromide can be extracted from the metal centre and a simple *N*-donor ligand added in its place. This method could then be followed in future to add a fluorescent ligand such as dansyl imidazole,[20] to potentially allow the compound to be visualized intracellularly.

3.4.1. Attempted synthesis of cationic Mn-1 complex

A [2+1] synthetic approach was followed whereby a halogen abstraction from complex **Mn-1** was conducted using $AgCF_3SO_3$. An *N*-donor was then added to the reaction mixture. The intermediate was either isolated as the triflate complex or underwent a counterion exchange with several inorganic salts as shown **Scheme 3.4**.

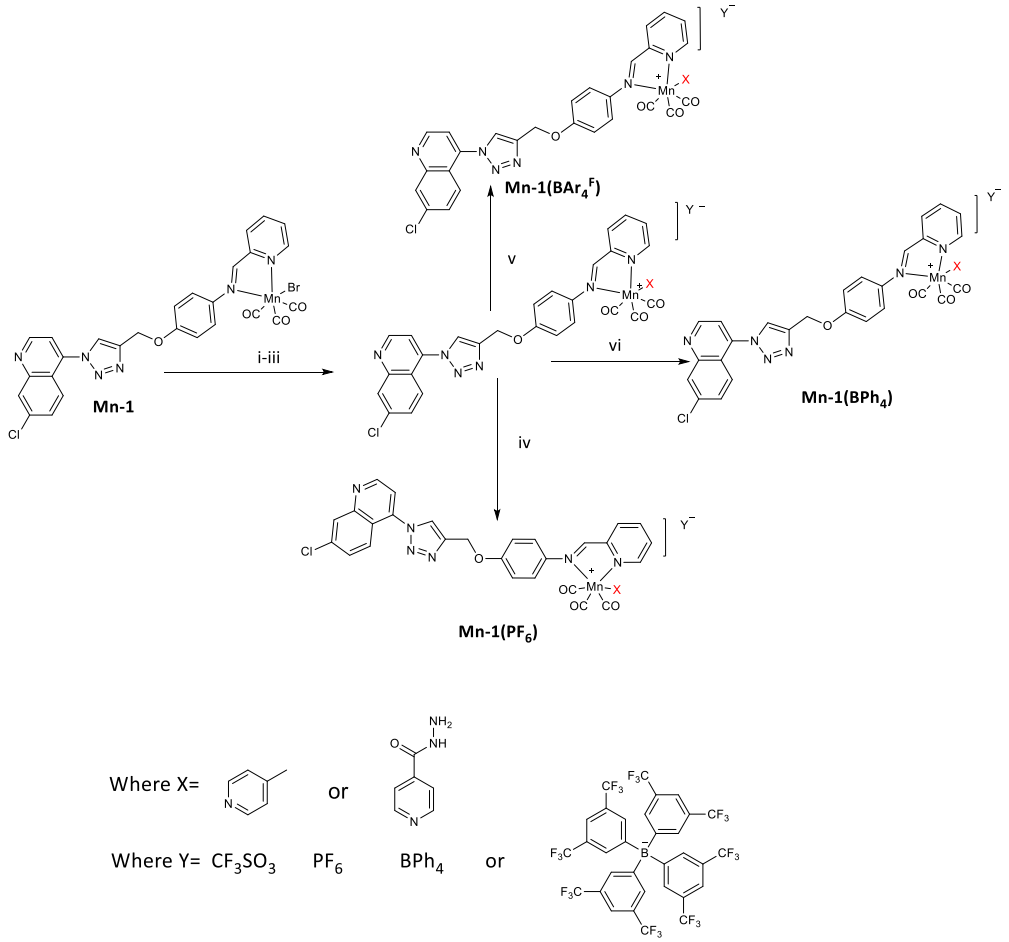

Scheme 3.4. Synthetic routes taken for the attempted synthesis of cationic **Mn-1**. See **Table 3.1** for conditions i-vi.

Several reaction conditions were used to synthesize and isolate a cationic **Mn-1** species substituted with two different *N*-donors: isoniazid or 4-picoline. These reaction conditions are outlined in **Table 3.1**. These *N*-donors were chosen based on availability, 4-picoline was used as a simple *N*-donor and isoniazid as a structurally more complex one.

Table 3.1 Optimisation of the synthesis of cationic **Mn-1**

Condition	Solvent	Inorganic salt	Equivalence of inorganic salt	N-donor	Equivalence of N-donor	Duration of reaction
i	MeCN	$AgCF_3SO_3$	1.1	isoniazid	1.1	4 h
	DCM					20 h
ii	MeCN	$AgCF_3SO_3$	2	isoniazid	2	22.5 h
iii	MeCN	$AgCF_3SO_3$	2	4-picoline	2	22.5 h
iv	MeCN	$AgCF_3SO_3$	2	isoniazid	2	2.5 h
	MeOH:DCM	NH_4PF_6	2			20 h
v	MeCN	$AgCF_3SO_3$	2	4-picoline	2	2.5 h
		$NaBAr_4^F$	1.3			20 h
vi	MeCN	$AgCF_3SO_3$	2	4-picoline	2	2.5 h
		$NaB(Ph)_4$	1.3			22 h

3.4.2. Attempted synthesis and characterisation of ***[Mn-1(isoniazid)](CF$_3$SO$_3$/PF$_6$)***

Isoniazid was used as an *N*-donor in the [2+1] reaction of complex **Mn-1** with silver triflate ($AgCF_3SO_3$), however, the purification of the **[Mn-1(isoniazid)](CF$_3$SO$_3$)/PF$_6$)** complexes were challenging. Analysis of the ^{1}H NMR spectra of these complexes pointed to their possible synthesis. It was challenging to isolate the complexes from the impurities that were present. **Mn-1** was reacted with $AgCF_3SO_3$ *via* a halogen abstraction and isoniazid was subsequently added under two different conditions, outlined in **Table 3.1**. Condition iv involved a counterion exchange reaction with NH_4PF_6.

3.4.2.1. ^{1}H NMR spectroscopy

The ^{1}H NMR spectrum of **[Mn-1(isoniazid)](CF$_3$SO$_3$)** (**Figure 3.8**) alludes to the synthesis of the complexes under both conditions i and ii. There is a downfield shift of the signal identified as H-1 from 9.22 ppm in **Mn-1** to 9.39 ppm in the spectra of both cationic species. Proton resonances for H-a, H-b and NH are observed but due to the poor resolution, cannot be identified with absolute clarity. A cation exchange between CF_3SO_3 and PF_6 yielded a more resolute spectrum, but the presence of multiple additional aromatic signals are observed in all three spectra. These peaks do not correlate to any of the starting material and suggest the possible formation of side products. Pike and co-workers compared various methods in which arenes and heteroarenes can be reacted with $[MnBr(CO)_5]$ to form $[MnBr(CO)_3]^+$ species.[37] They found that highly electron-deficient aromatics or aromatics containing electron-withdrawing groups do not metalate at all or do so to a small degree. They also found that aromatics containing electron-donating alkyl substituents metalate readily.

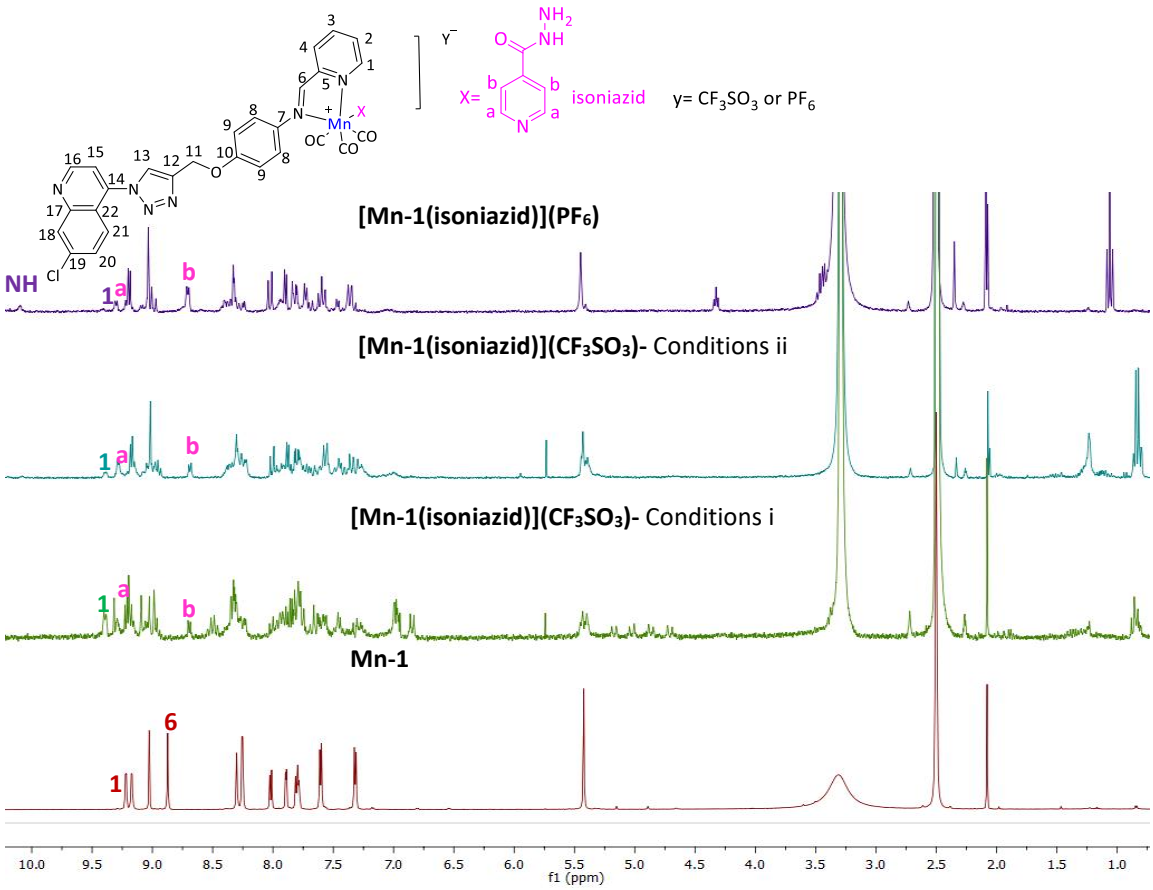

Figure 3.8. Stacked ^{1}H NMR spectra of **Mn-1**, **[Mn-1]isoniazid(CF$_3$SO$_3$)**-conditions i, **[Mn-1] isoniazid (CF$_3$SO$_3$)**- conditions ii and **[Mn-1]isoniazid(PF$_6$)**

This may explain the reluctance of isoniazid to react with **Mn-1** under three different conditions. Although metalation does occur to a certain degree, the reaction does not appear to go to completion with the possible formation of side products. Isoniazid contains the highly electron-withdrawing amide functional group, which may hinder metalation as described by Pike and co-workers.[37] The **[Mn-1(CO)$_3$]$^+$** is electron-deficient and the likelihood of coordination depends on the degree to which the *N*-donor donates its electrons.

3.4.3. Synthesis and characterisation of [Mn-1(4-picoline)](Y)

Due to the difficulty in isolating the cationic species from unreacted **Mn-1**, numerous inorganic salts were used in the hopes of generating a cationic complex that could easily be separated from **Mn-1**. A simpler *N*-donor (4-picoline) was also used to determine if the amide functionality of isoniazid hinders the reaction. **Mn-1** was reacted with $AgCF_3SO_3$ in MeCN to undergo a halogen abstraction, after which 4-picoline was subsequently added. The product was either isolated as the triflate species or a counterion exchange was done using $NaBAr_4^F$ or $NaB(Ph)_4$.

3.4.3.1. ^{1}H NMR spectroscopy

Comparison of the ^{1}H NMR spectra of **[Mn-1(4-picoline)](BAr$^F_4$)** and **[Mn-1(4-picoline)](B(Ph$_4$))** shows that synthesis of both cationic **Mn-1** species does occur. In both spectra, the diagnostic downfield shifts of H-1 and H-6 are observed. In the ^{1}H NMR spectrum of **[Mn-1(4-picoline)](BAr$^F_4$)**, the methyl (C$\underline{H}_3$) protons signal is observed as a singlet at 2.35 ppm. Aromatic protons belonging to 4-picoline can be identified, as indicated in **Figure 3.9.** The BAr_4^F aromatic protons H-d appear as a broad signal at 7.73 ppm, integrating for eight protons and H-c appears as a broad signal at 7.62 ppm integrating for four protons.

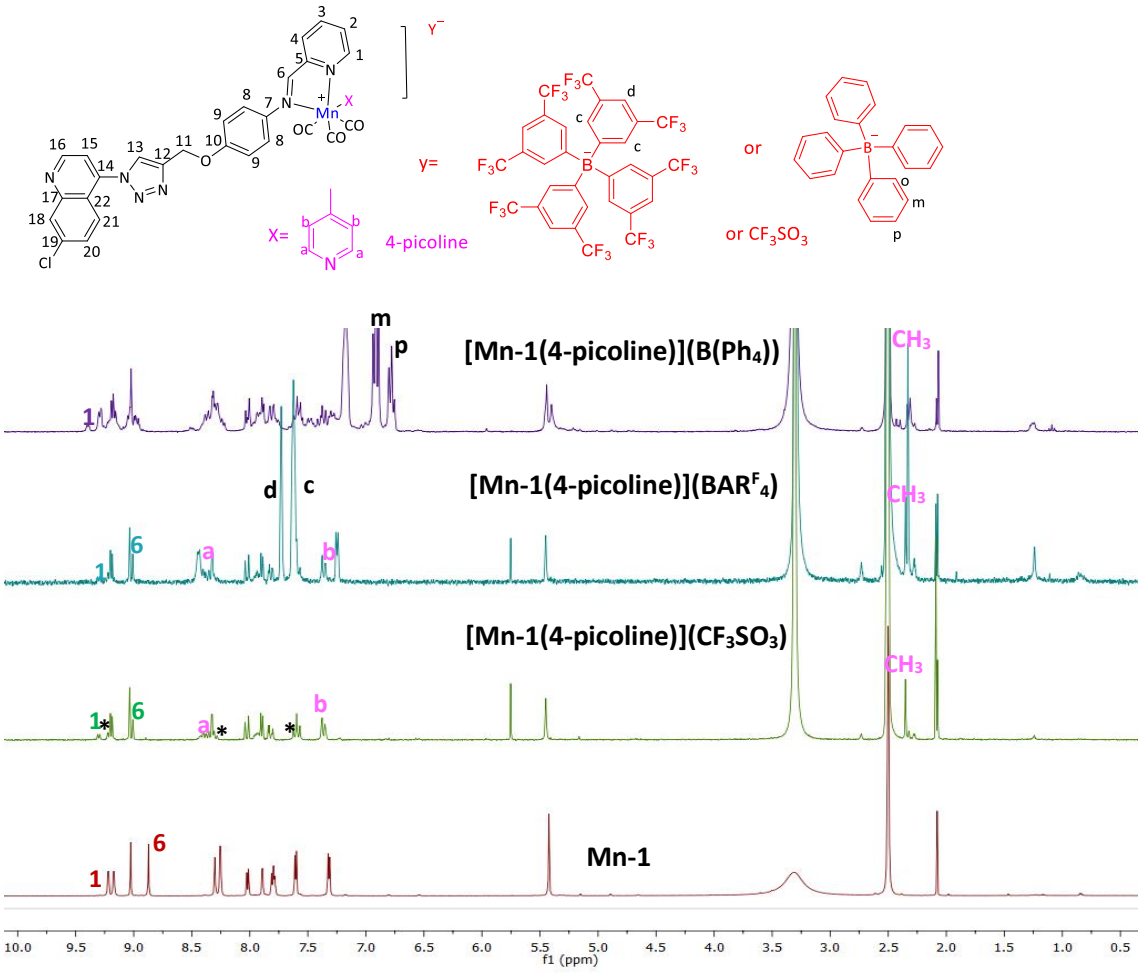

Figure 3.9. Stacked ^{1}H NMR spectra of **Mn-1**, **[Mn-1(4-picoline)](CF$_3$SO$_3$)**, **[Mn-1(4-picoline)](BAR^F$_4$)** and **[Mn-1(4-picoline)](B(Ph$_4$))**

Proton signals in the ^{1}H NMR spectrum of **[Mn-1(4-picoline)](B(Ph)$_4$)** are less distinguishable than seen in the spectrum of the BAr$_4^F$ or CF_3SO_3 analogues. The ortho-H(BPh$_4$) appears as a broad signal at 7.17 ppm, the meta-H(BPh$_4$) appears as a triplet at 6.92 ppm and the para-H(BPh$_4$) appears as a triplet at 6.78 ppm. The methyl protons appear as a singlet at 2.33 ppm, but the 4-picoline aromatic signals cannot be identified. **[Mn-1(4-picoline)](CF$_3$SO$_3$)** produced the more resolute ^{1}H NMR spectrum. The methyl protons are observed as a singlet at 2.35 ppm, the H-1 doublet occurs at 9.31 ppm and the H-6 singlet appears at 9.00 ppm. H-a of 4-picoline is identified as the doublet at 8.39 ppm and H-b as the doublet at 7.35 ppm. The multiplicity of H-a and integration of both proton signals do not correlate to the structure of 4-picoline, as one expects two sets of doublets each integrating for two protons. Unreacted

Mn-1 is identified by the asterix (*). The use of larger inorganic salts did not simplify purification, despite attempts to purify using recrystallization, water-washing, column chromatography and Preparative Thin Layer chromatography.

4-Picoline is more strongly electron-donating in comparison to isoniazid and should, therefore, complex with ease, which was indeed observed. Comparing the numerous inorganic salts used reveals a trend; Non-coordinating or weakly coordinating anions such as PF_6, BAr_4^F and BPh_4, produced ^1H NMR spectra with signals that do not correspond to any of the starting materials or expected products. The triflate (CF_3SO_3) anion is slightly coordinating compared to the other anions used and may, therefore, form a more stable intermediate, allowing for metathesis to occur easier.

It is clear that the formation of the cationic species does occur under all conditions but the use of silver triflate and 4-picoline produced a comprehensive ^1H NMR spectrum with diagnostic peaks of the expected product. The general purification method used in literature for cationic manganese complexes is recrystallisation. However, this method was unsuccessful for the cationic **Mn-1** species synthesised herein. Purification via recrystallization was unsuccessful, despite the use of several polar and non-polar solvents at various room temperatures. The synthesis of cationic **[Mn-1(4-picoline)](CF_3SO_3)** but difficulty in purifying the complex prompted further investigation using a simpler neutral complex as a starting material.

3.4.4. Synthesis and characterization of a cationic pyridyl Mn complex [Mn-4(4-picoline)](CF_3SO_3/PF_6)

In order to identify any structural hindrance caused by the large size of complex **Mn-1**, a simpler system was employed to find an alternate route of synthesis and purification. The aim of this was to establish a method for the synthesis of a cationic manganese complex of the structurally smaller precursor compounds **1** and **2**. Once a method is established for the simpler system, it could potentially be replicated using the larger complex **Mn-1**. Complexation was attempted using compounds **1** and **2** (discussed in **Chapter 2**) to subsequently form the cationic species thereof, as shown in **Scheme 3.5**. Complexation of

compound **2** was not successful despite reacting **2** with $[MnBr(CO)_5]$ at room temperature nor upon refluxing for 24 or 72 hours. Compound **1** was therefore reacted with $[MnBr(CO)_5]$ to form **Mn-4** as a dark orange powder in good yield (87%).

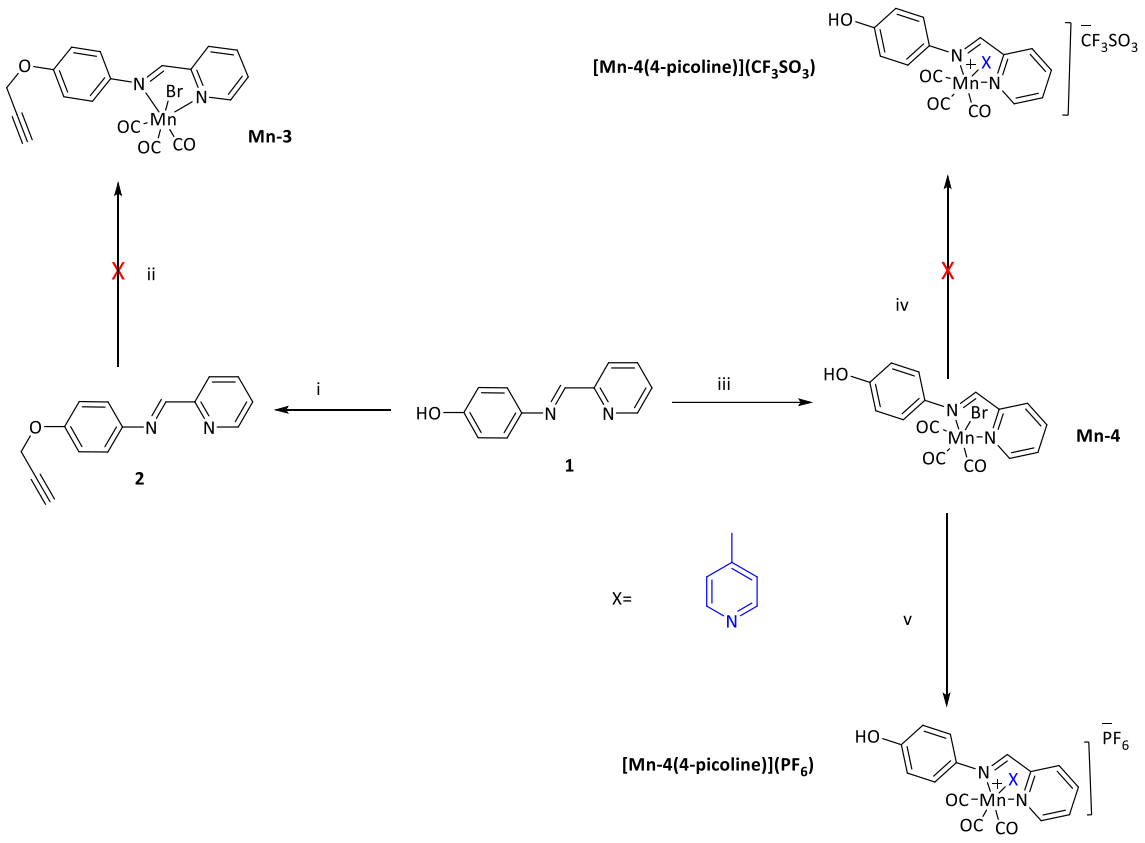

Scheme 3.5. Synthetic routes taken for the attempted synthesis of **Mn-3** and cationic **[Mn-4(4-picoline)](CF$_3$SO$_3$)**and the synthesis of **Mn-4** and **[Mn-4(4-picoline)](PF$_6$)**. Reagents and conditions: (i) K_2CO_3, 18-crown-6, acetone, propargyl bromide, reflux, 72 h. (ii) $[MnBr(CO)_5]$, DCM, reflux, 24/72 h. (iii) $[MnBr(CO)_5]$, MeOH, reflux, 24 h. (iv) a) MeCN, $AgSF_3SO_3$, 2.5 h, b) 4-picoline, 20 h. (v) a) DCM, AgPF6, 18 h, b) 4-picoline, 48 h.

3.4.4.1. ^{1}H NMR spectroscopy

In the ^{1}H NMR spectrum of **Mn-4** (**Figure 3.10**) the H-1 doublet and H-6 singlet have both shifted downfield from 8.67 ppm and 8.58 ppm in **1** to 9.88 ppm and 8.79 ppm respectively, confirming successful complexation. The hydroxyl proton is observed as a broad signal at 9.88 ppm. All aromatic protons experience the electron back-donation towards the carbonyls, as all shift slightly downfield.

Upon reaction of **Mn-4** with $AgCF_3SO_3$ and 4-picoline, the ^{1}H NMR spectrum shows clear upfield shifts in the proton resonances of H-1 and H-6 to 9.39 ppm and 8.89 ppm. The 4-picoline proton resonances are observed at 7.99 ppm for H-a and 7.31 ppm for H-b. These shifts suggest successful metathesis, but as was observed for the cationic **Mn-1** species, the resolution of the spectrum is poor. A second salt metathesis method was attempted whereby **Mn-4** was reacted with $AgPF_6$ following a literature method for a different complex,[38] as shown in **Scheme 3.5**. In the ^{1}H NMR spectrum of **[Mn-4(4-picoline)](PF$_6$)** the H-1 doublet and H-6 singlet appear at 1.93 ppm and 8.89 ppm. 4-Picoline protons H-a appears as a doublet at 7.99 ppm, H-b as a doublet at 7.33 ppm and the methyl protons as a singlet at 2.30 ppm integrating for three protons. The resolution of the ^{1}H NMR spectrum is far better than observed for the triflate derivative and all protons are accounted for with the expected downfield shifts and presence of 4-picoline proton signals. Thus, using compound **1** as a ligand for complexation and the subsequent complex **Mn-4** provides an easy method for the synthesis and isolation of a pure cationic manganese complex.

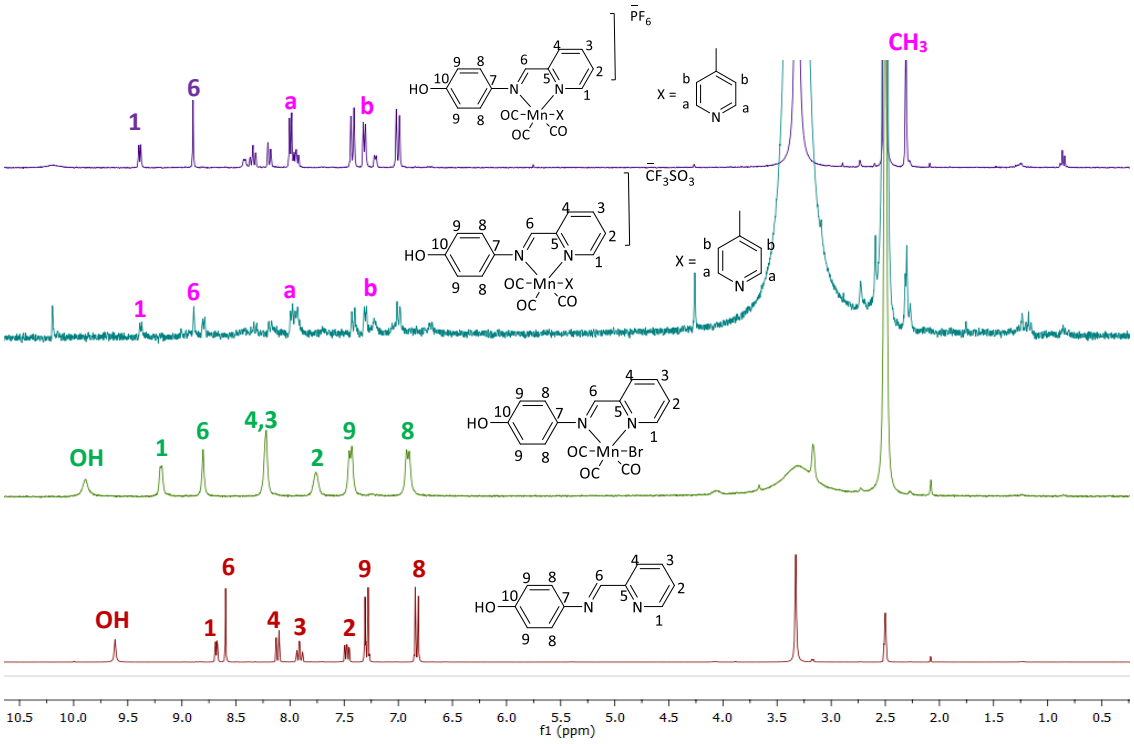

Figure 3.10. Stacked ^{1}H NMR spectra of compound **1**, **Mn-4**, **[Mn-4(4-picoline)](CF$_3$SO$_3$)** and **[Mn-3(4-picoline)](PF$_6$)**

3.4.4.2. IR spectroscopy

In the IR spectrum of **Mn-4**, the imine C=N absorption band is observed at 1604 cm^{-1} and the pyridyl C=N absorption band at 1591 cm^{-1}. A sharp strong band is seen at 2027 cm^{-1} in **Figure 3.11**, corresponding to one carbonyl. A strong absorption broad band is seen at 1918 cm^{-1} with a shoulder and corresponds to two carbonyl functionalities. The range in which these carbonyl bands appear is characteristic of a *fac*-isomer, as discussed earlier in this chapter.

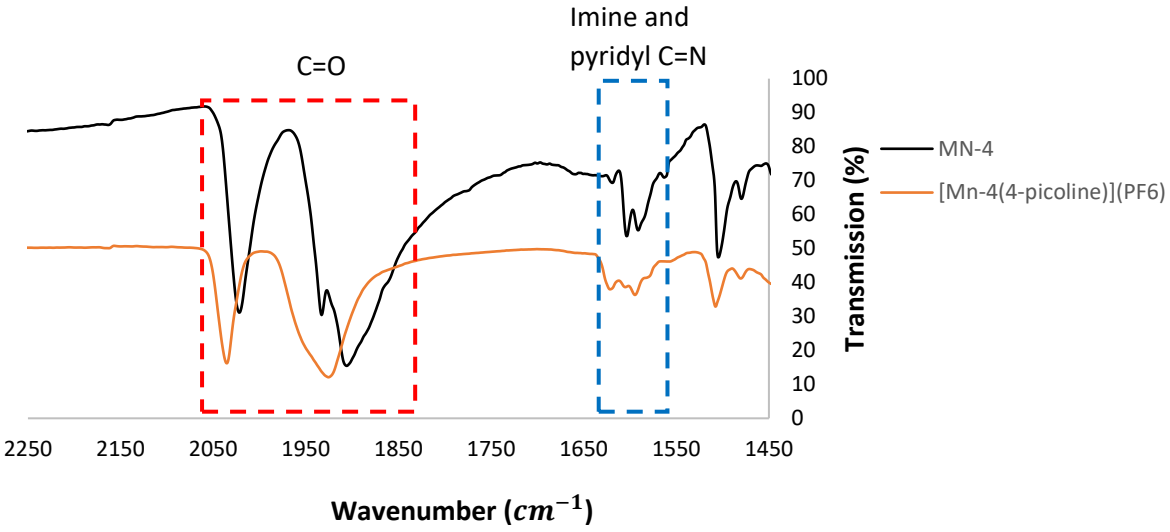

Figure 3.11. Stacked IR spectra of **Mn-4** and **[Mn-4(4-picoline)](PF$_6$)**

Upon the formation of the cationic **[Mn-4(4-picoline)](PF$_6$)** complex, the carbonyl bands shift to higher wavenumbers at 2036 cm^{-1} and 1926 cm^{-1}. The cationic nature of the metal centre reduces the back-donation to the carbonyls. The imine and pyridyl C=N absorption bands also shift to higher wavenumbers at 1622 $cm^{-1}$and 1595 cm^{-1} respectively.

3.4.5. Synthesis and characterisation of [Mn-1(4-picoline)](PF$_6$)

As a consequence of the successful synthesis of **[Mn-4(4-picoline)](PF$_6$)** using the reaction conditions outlined in **Scheme 3.6**, these conditions were replicated in the attempted synthesis of the quinoline-containing **[Mn-1(4-picoline)](PF$_6$)** complex as shown in **Scheme 3.6**. **Mn-1** was reacted with AgF_6 in DCM and subsequently with 4-picoline under inert conditions.

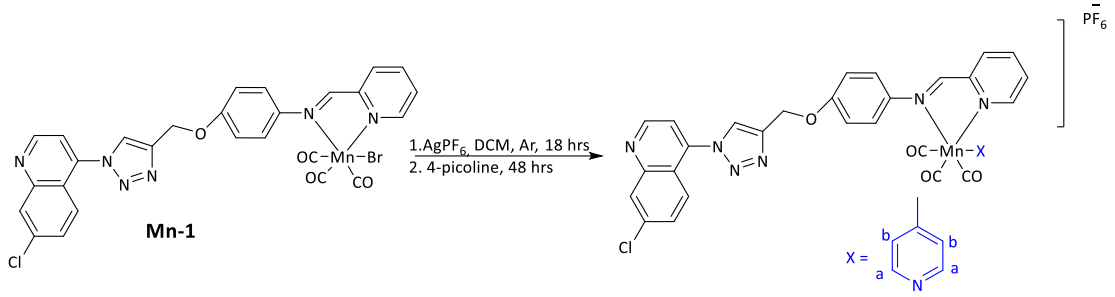

Scheme 3.6. Synthetic route for the attempted synthesis of cationic **[Mn-1(4-picoline)](PF$_6$)**

3.4.5.1. ^{1}H NMR spectroscopy

The ^{1}H NMR spectrum of **[Mn-1(4-picoline)](PF$_6$)** (**Figure 3.12**) shows the distinctive downfield shifts in proton resonance of H-1 and H-6 to 9.40 ppm and 8.96 ppm. The methyl protons are observed as a singlet at 2.32 ppm. H-a appears as a triplet at 8.43 ppm and H-b at 7.24 ppm. The resolution of the peaks is poor with unidentified peaks present in the aromatic region. These peaks do not correlate to any of the starting material and once again suggests possible decomposition of the product. The downfield shifts in the discussed proton resonances and the presence of 4-picoline proton signals indicate that the reaction was partially successful. Due to the higher success of using the triflate salt, the method which makes use of PF_6 as a counterion was not developed further.

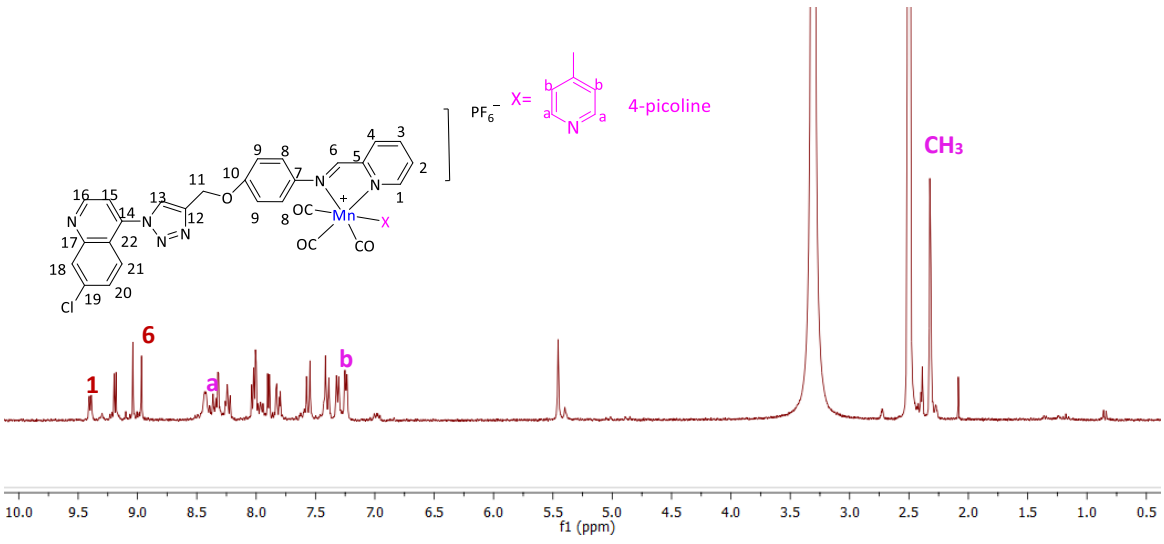

Figure 3.12. ^{1}H NMR spectrum of **[Mn-1(4-picoline)](PF$_6$)**

Thus, the method used to synthesise **[Mn-4(4-picoline)](PF_6]** could not be used to isolate a pure cationic **Mn-1** species.

3.4.6. A brief summary of attempted synthesis of a cationic Mn(I) species

In summary, several synthetic pathways were followed in an attempt to synthesize a cationic manganese complex. Two different *N*-donor ligands were used, isoniazid which contains an electron-withdrawing amide functionality and 4-picoline which contains the more electron-donating methyl group. The difficulty at which isoniazid reacted under the salt metathesis reaction conditions is determined by Pike *et al*. who found that electron-deficient aromatics do not perform well in these reactions.[37] The use of various anions for the salt metathesis reactions revealed a trend in which the more coordinating anion CF_3SO_3 performed better under the reaction conditions than the less coordinating anions. The use of the smaller pyridyl phenol complex **Mn-4** allowed for the successful synthesis of a cationic **[Mn-4(4-picoline)](PF_6)** complex. The same method used to synthesize the cationic **Mn-4** complex could not be replicated to successfully synthesize **[Mn-1(4-picoline)](PF_6).**

3.5. Photochemistry of Mn(I) complexes

Manganese tricarbonyl complexes are well-known for their photosensitive properties and their ability to release CO upon exposure to light. It is necessary to evaluate the photochemical properties of the synthesised compounds to establish their photosensitive wavelength and the degree of CO-release. The CO-releasing properties of complexes **Mn-1** and **Mn-2** were evaluated using infrared spectroscopy, UV/Vis spectroscopy and a Myoglobin assay for **Mn-1**. The Re analogues did not express the same photo-dissociative properties as their Mn analogues under the tested conditions.

3.5.1. Solution dark stability and CO-release of Mn-1 and Mn-2

3.5.1.1. Electronic Absorption

The absorbance maxima of complexes **Mn-1** and **Mn-2** were determined in a solution of DMSO and PBS buffer (pH 7.4) (5:95% v/v). Complexes **Mn-1** and **Mn-2** display two broad bands at ~240 nm and ~365 nm for the intraligand charge transfer (ILCT) and the metal to ligand charge transfer (MLCT) bands (**Figure 3.13**). These bands were assigned based on *N*-*N*-manganese tricarbonyl complexes reported in the literature.[39,1,40]

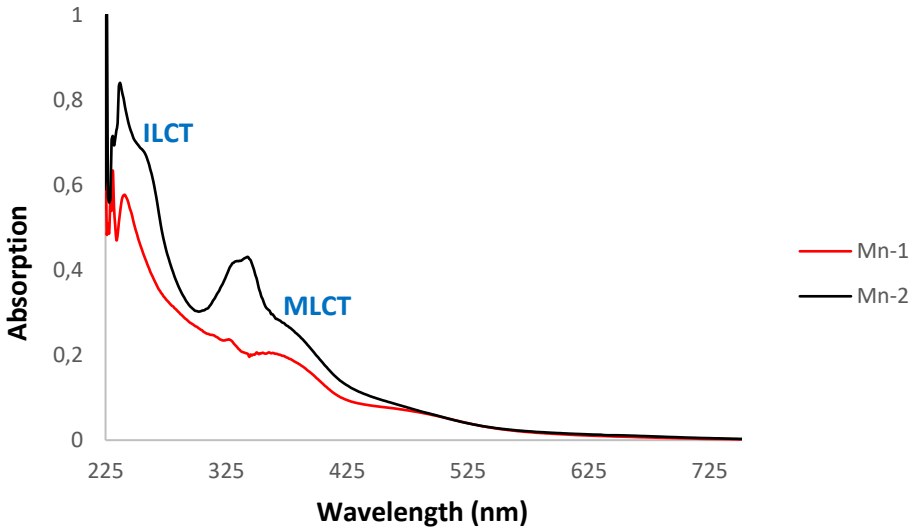

Figure 3.13. Stacked electronic absorption spectra of complexes **Mn-1** and **Mn-2**

The MLCT band provides the wavelength at which these complexes are most likely to release CO and thus the CO-release studies were done using light of 365 nm. Upon photodissociation of the carbonyls, the intensity of the MLCT bands are expected to decrease indicating that CO is being released.

3.5.1.2. CO-release using infrared spectroscopy

To gain further insights into the CO-release properties from complexes **Mn-1** and **Mn-2**, the spectral changes upon irradiation of solutions of these complexes in DCM were investigated. Solution state Infrared spectroscopy was used to evaluate photo-induced CO-release from complexes **Mn-1** and **Mn-2**. Complexes **Mn-1** and **Mn-2** were dissolved in DCM and an IR spectrum was obtained at time zero (**Figure 3.14**). The solution was then irradiated with light of 365 nm in 30-minute increments after which an IR spectrum was recorded. The carbonyl absorption bands are seen at 2030 cm^{-1}, 1945 cm^{-1} and 1925cm^{-1} for **Mn-1**. In the IR spectrum of complex **Mn-2**, the carbonyl absorption bands are observed at 1463 cm^{-1}, 1379 cm^{-1} and 1366cm^{-1}.

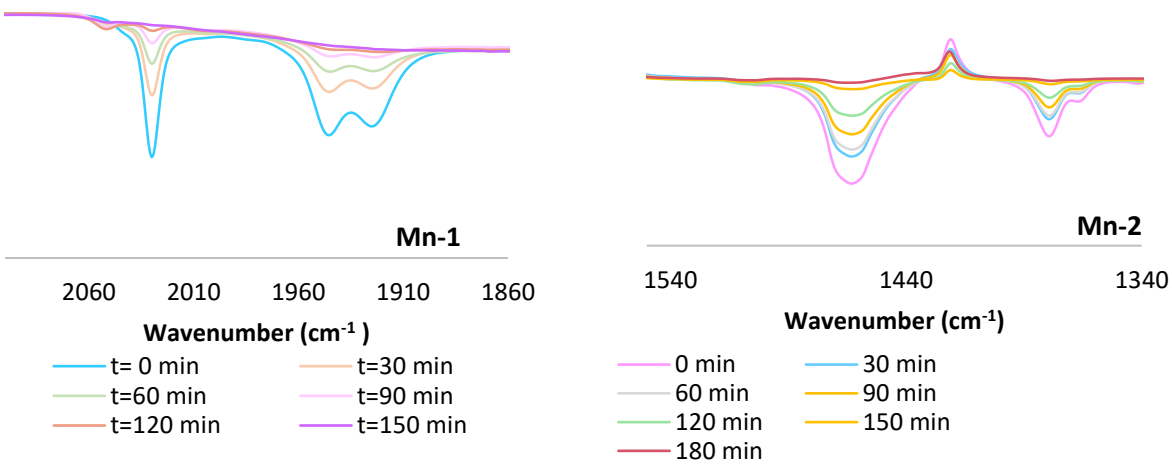

Figure 3.14. IR Spectral changes in the carbonyl region of complexes **Mn-1** (left) and **Mn-2** (right) in DCM upon irradiation of 365 nm.

Upon irradiation of solutions of complexes **Mn-1** and **Mn-2** in DCM, the carbonyl absorption bands at their respective wavenumbers decrease in intensity (**Figure 3.14**). No intermediate carbonyl species can be observed. After 150 and 180 minutes of irradiation, the carbonyl bands can no longer be seen in the spectra of complexes **Mn-1** and **Mn-2** respectively. This suggests that the rate of CO-release is slower for complex **Mn-2** compared to that of **Mn-1**, although no kinetic studies have been done as part of this study. The disappearance of the carbonyl absorption bands in both spectra is indicative of the structural changes these complexes undergo upon irradiation. As a consequence of the structural changes that occur, both solutions of complex **Mn-1** and **Mn-2** in DCM change colour from bright orange to brown upon prolonged exposure to light.

The possible photosensitivity of **Re-1** was evaluated following the same method used for the manganese complexes. **Re-1** did not display photodissociation of its carbonyls upon prolonged exposure to light at 365 nm and natural daylight. This was confirmed using IR spectroscopy.

3.5.1.3. Solution dark stability and CO-release

It has been established that complexes **Mn-1** and **Mn-2** release CO in the presence of light, but it is necessary to investigate if they are stable in the dark. The CO-releasing properties of complexes, **Mn-1** and **Mn-2** were investigated using a Myoglobin assay. The Myoglobin assay is performed at 37 ℃ and makes use of DMSO/PBS as the medium, thus it is necessary to investigate the dark stability of the manganese complexes at body temperature in DMSO/PBS. Complexes **Mn-1** and **Mn-2** were dissolved in DMSO/PBS (pH 7.4) (5/95% v/v) and an electronic absorption spectrum of each solution was obtained at time zero. The mixtures were kept in the dark at 37 ℃ and an electronic absorption spectrum obtained every 1 hour for 6 hours and after 24 hours.

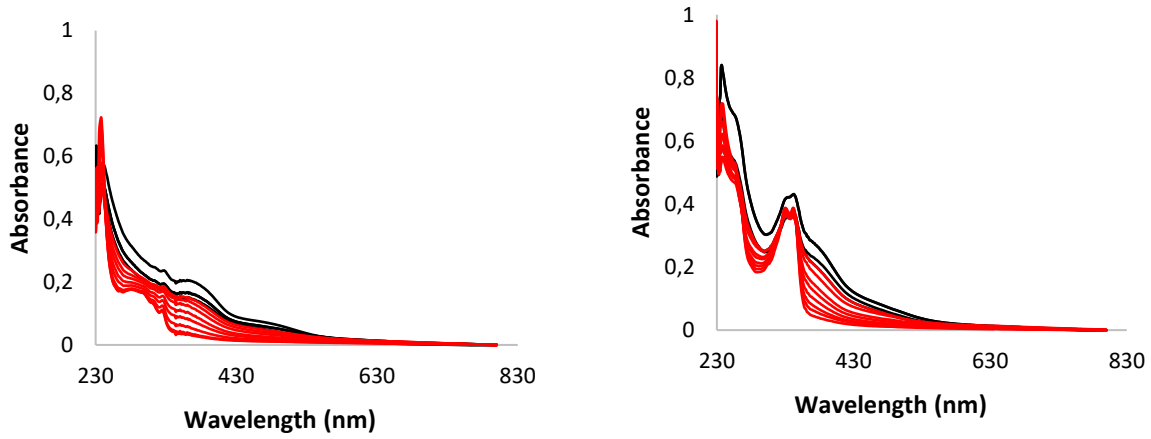

Figure 3.15. Electronic Absorption spectra of **Mn-1** (left) and **Mn-2**(right) in DMSO and PBS (5/95% v/v) at 37 ℃. Stability over 24 hours (black) and irradiation of increasing time at 365 nm (red).

Both complexes **Mn-1** and **Mn-2** display long-term dark stability in DMSO/PBS (pH 7.4), as shown by the black spectra in **Figure 3.15**. Any changes seen in the spectra over 24 hours can be attributed to precipitation of the complex out of solution. The complexes were then irradiated at 365 nm in 1-minute, 2-minute and 5-minute increments over a 1-hour period. Irradiation was halted after each irradiation period to record an electronic absorption spectrum, shown by the red spectra in **Figure 3.15**. Upon irradiation, a distinct decrease in the absorption at the MLCT band is observed, indicative of photo-induced CO-release. This study shows that the complexes are stable in solution in the dark and releases CO only upon irradiation.

The antiplasmodial activity of complexes **Mn-1** and **Mn-2** in the dark and upon photo-excitation is evaluated in **Chapter 4**. The antiplasmodial activity was tested using a pLDH assay which makes use of DMSO and growth medium. Thus, to investigate the dark stability and photolysis behaviour of complexes **Mn-1** and **Mn-2** in a mixture of DMSO/growth medium (5/95% v/v), the complexes were incubated at 37 ℃ for 24 hours. An electronic absorption spectrum was recorded every 1 hour for 5 hours and after 24 hours (**Figure 3.16,** black spectra). The **Mn-1** solution was irradiated with light at 365 nm in 1-minute increments for 5

minutes, after each irradiation period an electronic absorption spectrum was recorded (**Figure 3.16 (left)**). The **Mn-2** solution was irradiated at 365 nm in 1-minute, 2-minute and 5-minute increments for an hour. After each irradiation period, an electronic absorption spectrum was obtained (**Figure 3.16 (right)**). The irradiation times were subject to the complex.

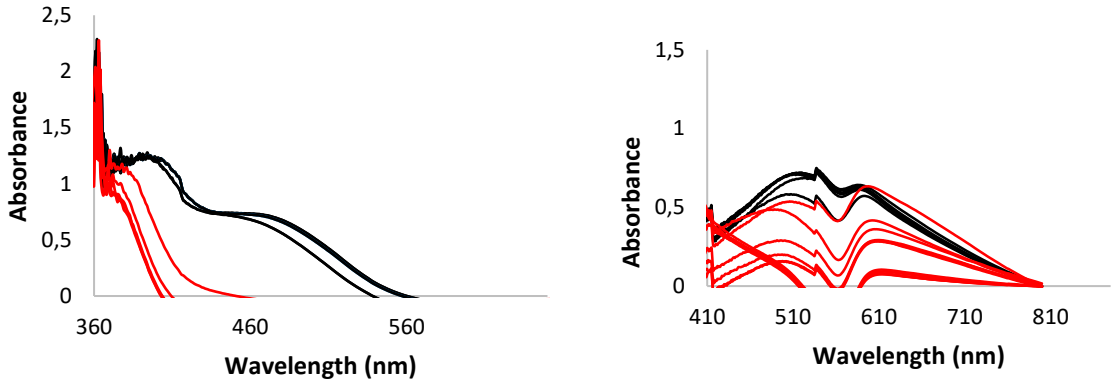

Figure 3.16. Electronic Absorption spectra of **Mn-1** (left) and **Mn-2**(right) in DMSO and growth medium (5/95% v/v). Stability over 24 hours (black) and irradiation of increasing time at 365 nm (red).

Complexes **Mn-1** and **Mn-2** both show dark stability in a mixture of DMSO and growth medium over a 24-hour period, as shown by the black spectra in **Figure 3.15**. The MLCT bands are observed at higher wavenumbers in the growth medium. The broad MLCT bands are seen at 480 nm and 601 nm for **Mn-1** and **Mn-2** respectively. The solvent used in Ultraviolet-visible spectroscopy affects the wavelength at which the MLCT band is observed. The position of the MLCT band is related to the solvating ability of the solvent being used. Upon irradiation of these solutions of complexes, the absorbance at the MLCT band of both complexes decreases in intensity, as seen by the red spectra. The release of CO occurs more rapidly for **Mn-1** compared to that of **Mn-2**, as after 5 minutes no MLCT band is observed in the electronic absorption spectrum of **Mn-1**. In the electronic absorption spectrum of **Mn-2**, no change in

the MLCT band is seen after 35 minutes. Comparison of **Figures 3.15** and **3.16** suggests that the rate of CO-release is dependent on the medium in which the complex is in at the time of photolysis. It is clear that CO-release from both complexes **Mn-1** and **Mn-2** occurs faster in the DMSO/growth medium mixture than it does in the DMSO/PBS mixture.

3.5.1.4. CO-release using the Myoglobin assay

The Myoglobin assay allows for the detection and quantification of CO-release. The Myoglobin assay is the most widely used assay for the quantification and determination of the rate of CO-release. The assay is based on the UV/Vis detection of the conversion of deoxy-myoglobin (deoxy-Mb) to carboxy-myoglobin (COMb). In the presence of CO, myoglobin irreversibly binds to CO, resulting in the formation of COMb. The source of CO comes from the complex which photo-actively releases CO, resulting in a change in the Q-band region of the UV/vis spectrum as shown in **Figure 3.17**.[41]

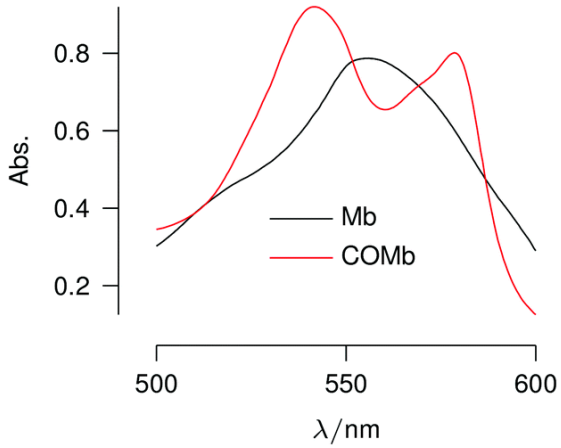

Figure 3.17. Visible spectra of Mb and COMb.[39]

Myoglobin in PBS (0.01 M, pH 7.4) was reduced with a solution of sodium dithionite in PBS (0.01M, pH 7.4) and degassed by bubbling argon into the solution. A solution of complex **Mn-1** in DMSO (10 μM, 10 μL) was added and an initial electronic absorption spectrum was

obtained, as shown in **Figure 3.18**. At time zero, only deoxy-Mb is present, as shown by the parabolically shaped spectrum with a maximum at 557 nm. The mixture was then irradiated at 365 nm in 1-minute increments for 10 minutes, 2-minute increments for 10 minutes and 5-minute increments for the remainder of an hour. As irradiation proceeds, the absorbance at 557 nm shows a steady decrease while the absorbance at 544 nm and 577 nm increase rapidly. This is indicative of the conversion of deoxy-myoglobin to COMb, confirming that CO-release does occur upon photo-excitation.

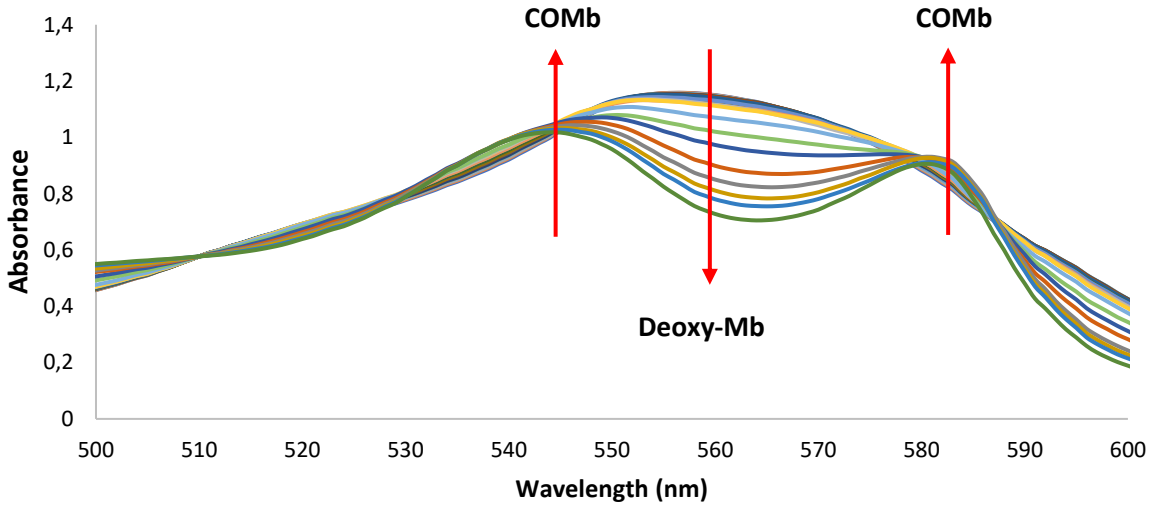

Figure 3.18. UV/vis spectral changes in the Q-band region of myoglobin upon irradiation at 365 nm in the presence of **Mn-1.**

The concentration of COMb formed was determined *via* calculation using the molar extinction coefficient for COMb (15.4 $mM^{-1}\,cm^{-1}$).[25] A graph of [COMb] *vs* time was plotted and is shown in **Figure 3.19**. The concentration of COMb increases over the irradiation period, plateauing at *ca.* 21.5 μM, after approximately 40 minutes of irradiation. A 10 μM solution of complex **Mn-1** is used in the assay, indicating that on average, approximately 2 equivalents of CO molecules is released per **Mn-1** molecule present. CORMS are able to release varying equivalents of CO per CORM present, as those synthesised by Brückmann *et al*.[42] It is not

uncommon for Mn(I) tricarbonyl complexes to release fewer than three CO's per molecule of CORM present. The percentage of CO released was calculated to be 72.3%.

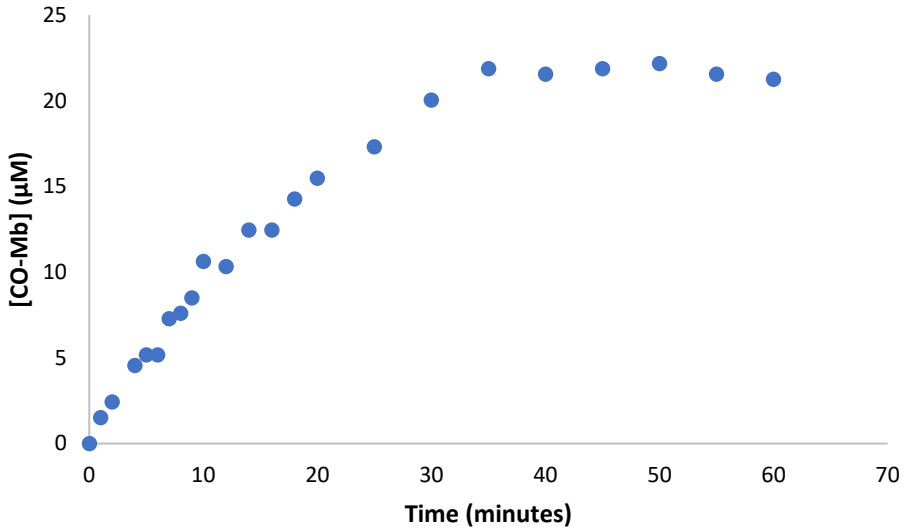

Figure 3.19. Plot of [COMb] (µM) formation with increasing irradiation time at 365 nm for a solution of complex **Mn-1** (10 µM)) in PBS (0.01 M, pH 7.4), myoglobin (60) and sodium dithionite (10 mM).

The rate of CO-release is determined using the half-life ($t_{1/2}$), defined as the time required for the complex to release half of the total CO-ligands present. The $t_{1/2}$ needs to be less than two hours to produce a high enough concentration of CO intracellularly.[18] CO-release is 1st order,[43] therefore, the half-life can be calculated by fitting a 1st order growth curve (**Figure 3.19**). The equation for 1st order exponential growth can be seen in **Equation 3.3**.

$$y = y_0 + A_1 e^{\frac{x}{t_1}} \qquad \ldots\ldots \text{Eqn } 3.3$$

$$[\text{COMb}] = y_0 + A_1 e^{\frac{t_{1/2}}{t_1}} \qquad \ldots\ldots \text{Eqn } 3.4$$

$$\frac{y_0}{2} = A_1 e^{\frac{t_{1/2}}{t_1}} + y_0 \qquad \ldots\ldots \text{Eqn } 3.5$$

$$t_{\frac{1}{2}} = t_1 \ln\left(\frac{-y_0}{2A_1}\right) \quad \ldots\ldots \text{Eqn 3.6}$$

The concentration of COMb is plotted on the *y-axis* of **Figure 3.19** and time on the *x-axis*, thus rearrangement of **Equation 3.3** and substitution of the relevant values gives **Equation 3.4.** y_0 is the point at which the concentration starts to plateau, therefore at $t_{1/2}$ the concentration of COMb equals half of y_0, resulting in **Equation 3.5**. Rearrangement of **Equation 3.5** to make $t_{1/2}$ the subject of the formula gives Equation 3.6, of which the values are obtained from the graph in **Figure 3.18**. The CO-release $t_{1/2}$ of complex **Mn-1** was therefore calculated to be 22.28 minutes, which is shorter than the threshold 2-hour period. This $t_{1/2}$ is comparable to *N*-*N*-Mn tricarbonyl complexes reported in literature.[42,44]

Berends *et al.* proposed the identity of the CORM photolyzed products,[44] as shown in **Scheme 3.7**. Upon photoexcitation, one Mn-CO bond is labilized (step 1) and a CO is released in step 2. These two steps result in the formation of a manganese dicarbonyl species, which is verified in the IR spectrum shown in **Figure 3.14**. This is followed by the photo-release of the remaining CO-molecules, resulting in an oxidized Mn(II) species. The oxidation state of the photolyzed product can however only be confirmed by EPR spectroscopy and is therefore only a speculation based on literature at this point.[42] The oxidizing agent is unknown and would need to be determined *via* further experiments. It can, however, be confirmed that O_2 is not the oxidizing agent, as during the O_2 free myoglobin assay CO is still released and COMb formed (step 5). Further studies into identifying the photolyzed products of this project will need to be conducted in the future.

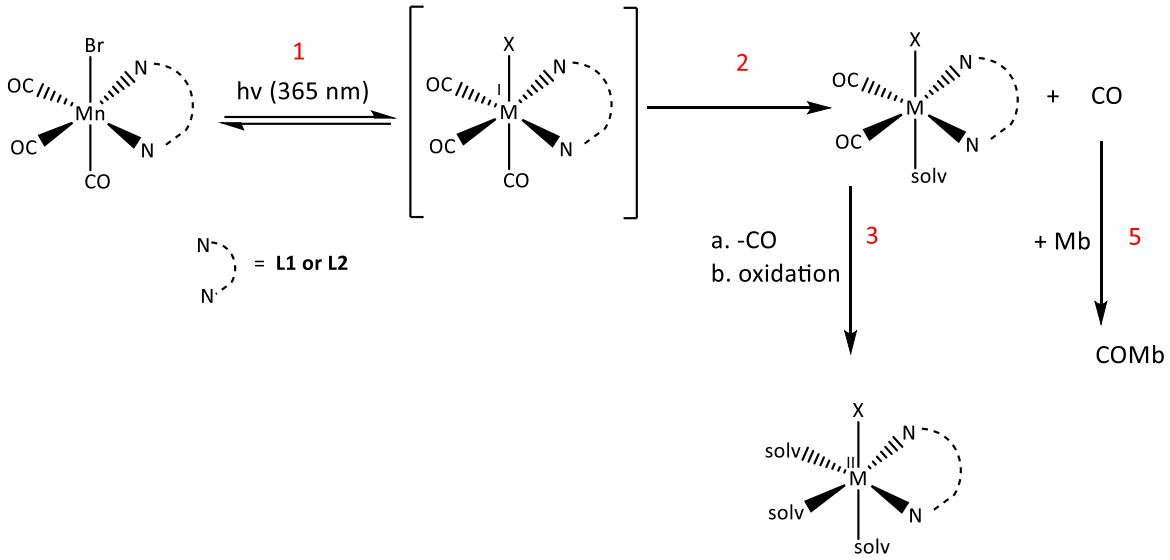

Scheme 3.7. Proposed CO-release mechanism and photolyzed products.[41]

3.9. Summary

Two new Mn(I) and Re(I) tricarbonyl complexes, based on a quinoline-1,2,3-triazole scaffold have been synthesised and characterised. Several attempts were made at salt metathesis using **Mn-1** to synthesise a cationic species. It can be concluded that using an *N*-donor with an electron-withdrawing group (isoniazid) hinders the reaction. A suitable coordinating counterion results in the formation of a more stable product than a non-coordinating counterion. The method using $AgCF_3SO_3$ as the metal salt and 4-picoline resulted in the most resolute ^1H NMR spectrum, but the isolation of **[Mn-1(4-picoline)](CF_3SO_3)** from unreacted **Mn-1** was unsuccessful.

Complexes **Mn-1** and **Mn-2** were further evaluated for their CO-releasing properties under various conditions and were found to be stable in both DMSO/PBS and DMSO/growth medium in the dark. Complexes **Mn-1** and **Mn-2** both release CO upon photo-excitation at 365 nm in DCM, DMSO/PBS and DMSO/growth medium solutions. The rate of CO-release is medium dependent and **Mn-1** releases CO faster than **Mn-2**. The standard Myoglobin assay was performed in the presence of complex **Mn-1** in DMSO and CO-release was confirmed due

to the successful conversion of deoxy-Mb to COMb. Complex **Mn-1** releases 2 equivalents of CO's per CORM present, with 72.3% of the CO's being released over the 1-hour period. The $t_{1/2}$ was found to be 22.28 minutes, which was far below the 2-hour threshold period of efficient CO-release. It should be noted that complex **Mn-2** produces an identified precipitate upon irradiation with a 32 W UV lamp. This precipitate was removed using a syringe filter before taking any spectroscopic readings. **Re-1** did not express any photosensitivity under the tested conditions.

The wavelength at which the manganese complexes release CO is not ideal for *in vivo biological studies*. Future work should involve red-shifting the CO-release to higher wavelengths around 700-800 nm. The higher wavelengths allow for the deeper skin penetration of the light and are also less damaging to DNA. It would be useful to perform kinetic studies to provide insight into the rates of CO-release so that if needed this could be improved on in the future. The identity of the photolyzed products is of great importance for biological use as well. Since the complexes are evaluated for their in vitro antiplasmodial activity in **Chapter 4**, it is essential to identify if the activity is solely due to the complex and CO-release or if the photolyzed products express any biological activity as well.

3.10. References

1 P. Govender, S. Pai, U. Schatzschneider and G. S. Smith, *Inorg. Chem.*, 2013, **52**, 5470–5478.

2 S. F. Medical and X. Francisco, *J. Biol. Chem.*, 1969, **244**, 6388–6394.

3 A. C. Kautz, P. C. Kunz and C. Janiak, *Dalton. Trans.*, 2016, **45**, 18045–18063.

4 L. E. Otterbein, F. H. Bach, J. Alam, M. Soares, H. T. Lu, M. Wysk, R. J. Davis, R. A. Flavell and A. M. K. Choi, *Nat. Med.*, 2000, **6**, 422–428.

5 L. Vítek, H. Gbelcová, L. Muchová, J. Zelenka, R. Koníˇ, J. Suk and M. Zadinova, *Dig. Liver Dis.*, 2014, **46**, 369–375.

6 B. S. Brouard, L. E. Otterbein, J. Anrather, E. Tobiasch, F. H. Bach, A. M. K. Choi and M. P. Soares, *J. Exp. Med.*, 2000, **192**, 1015–1025.

7 B. Chen, L. Guo, C. Fan, S. Bolisetty, R. Joseph, M. M. Wright, A. Agarwal and J. F. George, *Am. J. Pathol.*, 2009, **175**, 422–429.

8 J. Kohmoto, A. Nakao, R. Sugimoto, Y. Wang, J. Zhan, H. Ueda and K. R. Mccurry, *J. Thorac. Cardiovasc. Surg.*, 2008, **136**, 1067–1075.

9 G. Faleo, M. Ezzelarab, A. Nakao and B. Ekser, *Am. J. Transplant.*, 2011, **10**, 763–772.

10 M. D. Pizarro, J. V Rodriguez, M. E. Mamprin, B. J. Fuller, B. E. Mann, R. Motterlini and E. E. Guibert, *Cryobiology*, 2009, **58**, 248–255.

11 A. Nakao, H. Toyokawa and A. Tsung, *Am. J. Transplant.*, 2006, **6**, 2243–2255.

12 B. J. Aucott, J. S. Ward, S. G. Andrew, J. Milani, A. C. Whitwood, J. M. Lynam, A. Parkin and I. J. S. Fairlamb, *Inorg. Chem.*, 2017, **56**, 5431–5440.

13 R. Motterlini, J. E. Clark, R. Foresti, P. Sarathchandra, B. E. Mann and C. J. Green, *Circ. Res.*, 2002, **90**, e17–e24.

14 M. Faizan, N. Muhammad, K. U. K. Niazi, Y. Hu, Y. Wang, Y. Wu, H. Sun, R. Liu, W. Dong, W. Zhang and Z. Gao, *Materials (Basel).*, 2019, **12**, 1643–1683.

15 M. A. Gonzalez, N. L. Fry, R. Burt, R. Davda, A. Hobbs and K. Mascharak, *Inorg. Chem.*, 2011, **50**, 3127–3134.

16 U. Schatzschneider, *Br. J. Pharmacol.*, 2015, **172**, 1638–1650.

17 F. Zobi, A. Degonda, M. C. Schaub, A. Y. Bogdanova, Z. Ch-, Z. Ch- and Z. Ch-, *Inorg. Chem.*, 2010, 7313–7322.

18 U. Schatzschneider, *Inorg Chim. Acta Chim. Acta*, 2011, **374**, 19–23.

19 E. Kottelat and F. Zobi, *Inorganics*, 2017, **5**, 24–43.

20 J. Jimenez, I. Chakraborty, A. Dominguez, J. Martinez-Gonzalez, W. M. C. Sameera and P. K. Mascharak, *Inorg. Chem.*, 2018, **57**, 1766–1773.

21 L. S. Nobre, J. D. Seixas, C. C. Romão and L. M. Saraiva, *Antimicrob. Agents*

Chemother., 2007, **51**, 4303–4307.

22 D. Nguyen, T. Nguyen, S. A. Rice and C. Boyer, *Biomacromolecules*, 2015, **16**, 2776–2786.

23 E. Üstün, A. Özgür, K. A. Coşkun, S. Demir, İ. Özdemir and Y. Tutar, *J. Coord. Chem.*, 2016, **69**, 3384–3394.

24 A. Pamplona, A. Ferreira, J. Balla, V. Jeney, G. Balla, S. Epiphanio, Â. Chora, C. D. Rodrigues, I. P. Gregoire, M. Cunha-Rodrigues, S. Portugal, M. P. Soares and M. M. Mota, *Nat. Med.*, 2007, **13**, 703–710.

25 A. J. Atkin, J. M. Lynam, B. E. Moulton, P. Sawle, R. Motterlini, N. M. Boyle, T. Pryce and I. J. S. Fairlamb, *Dalton. Trans.*, 2011, **40**, 5755–5761.

26 J. B. Wittenberg and B. A. Wittenberg, *J. Exp. Biol.*, 2003, **206**, 2011–2020.

27 M. Waga, S. Takeda and A. Ax, *Anim. Sci. J.*, 2018, **89**, 467–473.

28 X. Fang, B. L. Scott, K. D. John and G. J. Kubas, *Organometallics*, 2000, **19**, 4141–4149.

29 T. A. Martin, C. E. Ellul, M. F. Mahon, M. E. Warren, D. Allan and M. K. Whittlesey, *Organometallics*, 2011, **3**, 2200–2211.

30 E. Hevia, J. Pe, S. Kassel and A. Rheingold, *Inorg. Chem.*, 2002, **41**, 3722–3728.

31 J. Jimenez, M. N. Pinto, J. Martinez-gonzalez and P. K. Mascharak, *Inorg Chim Acta*, 2019, **485**, 112–117.

32 F. Basolo, *Inorg Chim Acta*, 1985, **100**, 33–39.

33 J. D. Atwood and T. L. Brown, *J. Am. Chem. Soc*, 1976, **98:11**, 3160–3166.

34 R. K. Hocking and T. W. Hambley, *Organometallics*, 2007, **2**, 2939–2947.

35 I. C. and P. K. M. Samantha J. Carrington, *Chem. Commun*, 2013, **49**, 11254–11256.

36 D. J. Liston, C. A. Reed, Y. J. Lee and W. R. Scheidt, *J. Am. Chem. Soc.*, 1989, **111**, 6643–6648.

37 J. D. Jackson, J. Sharon, S. Bacon, R. D. Pike, C. William and G. B. Carpenter, *Organometallics*, 1994, **3980**, 3972–3980.

38 B. S. Uppal, R. K. Booth, N. Ali, C. Lockwood, C. R. Rice and P. I. P. Elliott, *Dalton. Trans.*, 2011, **40**, 7610–7616.

39 I. Chakraborty, S. J. Carrington and P. K. Mascharak, *Acc. Chem. Res.*, 2014, **47**, 2603–2611.

40 S. Pai, M. Hafftlang, G. Atongo, C. Nagel, J. Niesel, S. Botov, H. G. Schmalz, B. Yard and U. Schatzschneider, *Dalton. Trans.*, 2014, **43**, 8664–8678.

41 M. A. Wright and J. A. Wright, *Dalton. Trans.*, 2016, **45**, 6801–6811.

42 N. E. Brückmann, M. Wahl, G. J. Reiß, M. Kohns, W. Wätjen and P. C. Kunz, *Eur. J. Inorg. Chem.*, 2011, **2011**, 4571–4577.

43 L. Chen, X. Jiang, X. Wang, L. Long, J. Zhang and X. Liu, *New J. Chem.*, 2014, **38**, 5957–5963.

44 H. M. Berends and P. Kurz, *Inorg Chim Acta*, 2012, **380**, 141–147.

Chapter 4

Antiplasmodial evaluation

4.1. Introduction

During the blood stage of the malaria parasites life cycle, haemoglobin is ingested by the protozoan cytosome and transported into the parasite's acidic food vacuole.[1] The iron centre in haemoglobin undergoes oxidation,[2] and is broken down into free heme and amino acids.[3,4,5] When accumulated in high enough concentrations, heme is toxic and can cause early parasitic lysis.[6] At these high concentrations, reactive oxygen species (ROS) are produced. These ROS cause the parasite to undergo "lipid peroxidation", whereby the lipids in the membrane degrade resulting in parasitic death.[5] The parasite has therefore developed a detoxification method, in which it converts heme into inert biocrystals known as hemozoin as shown in **Figure 4.1**.[7] Hemozoin is a highly crystallized insoluble form of heme aggregates that is non-toxic to the parasite.

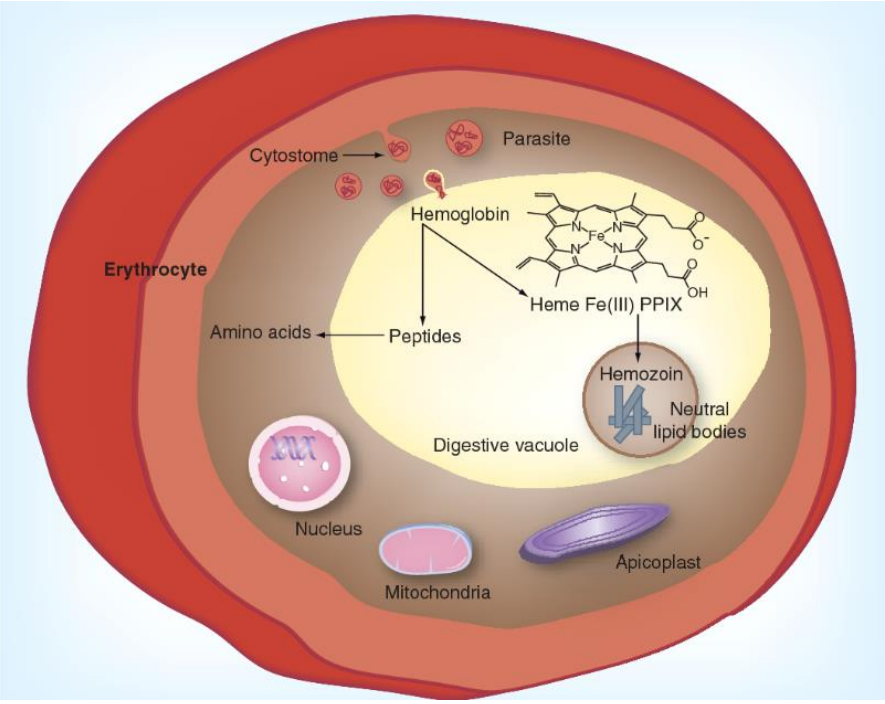

Figure 4.1. Proposed degradation of free heme to form non-toxic biocrystal hemozoin in acidic vacuole of the malaria paraste.[1]

As mentioned in **Chapter 2**, chloroquine (CQ) and quinoline-comprising drugs have been mainstays in antimalarial chemotherapy. CQ is a blood schizonticidal drug and therefore only acts during the blood stage of the parasitic life cycle.[8] CQ and its analogues work by preventing the formation of hemozoin, resulting in parasitic death. CQ is a weak base with pKa of 8.1 (quinoline nitrogen) and 10.2 (diethylamine side-chain nitrogen), it enters into the acidic parasitic digestive vacuole (pH of 5-5.2) in its unprotonated form.[8] Thus when entering into the DV, chloroquine becomes protonated, resulting in the accumulation of the drug in this form.[9] CQ is able to inhibit the polymerization of free heme into hemozoin, increasing intracellular heme,[10] as shown in **Figure 4.2**.[11] The exact mechanism by which chloroquine and its analogues work is unknown.[12] CQ-resistance in *P.falciparum* is conferred by the mutation in the *pfCRT* gene.[13] *PfCRT* is an acronym for "*Plasmodium falciparum* Chloroquine Resistance Transporter". Mutated *PfCRT* has the ability to transport protonated CQ out of the cell, preventing the accumulation of the drug and therefore resulting in CQ-resistance.[14]

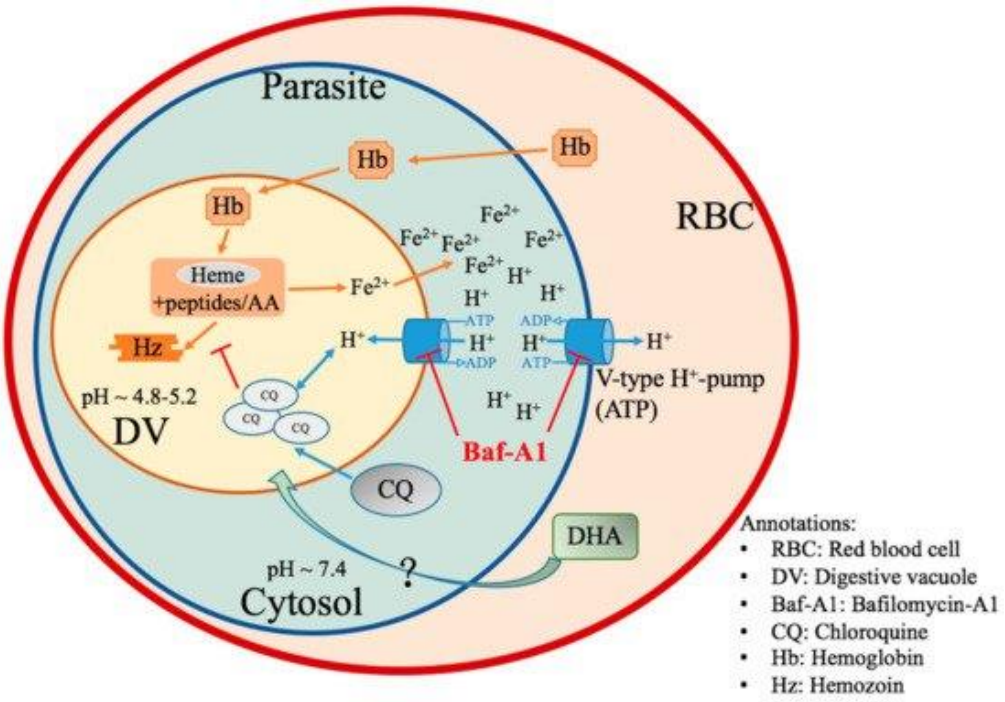

Figure 4.2. Mechanism of action of CQ.[11]

HO-1 is an enzyme encoded by the gene Hmxo1. It has several protective properties,[15] and is responsible for heme catabolism.[16] HO-1 is produced at low levels in all cells but production thereof can also be induced by various stimuli including the presence of heme (which is produced in the presence of malaria).[15] Pamplona and co-workers report that HO-1 inhibits the development of experimental cerebral malaria (ECM) in mice.[17] ECM is a severe neurological complication of *P.falciparum* malaria.[18] The prevention of pathogenesis expressed in the BALB/c mice was due to the higher expression of Hmox1. They then went onto to show that exposure to CO prevented ECM and death and therefore concluded that prevention is due to CO.[17] It was found that exposure to CO does not prevent or change the level of parasitaemia, but rather prevents the onset of ECM.[17] This serves as evidence that CORMs could be used to treat malaria, even though CO does not affect the level of parasitaemia in the conducted study. It is possible that treatment with a CORM which provides dual pharmacological effects, conferred by the pharmacological scaffold and CO-releasing properties may result in notable antimalarial properties.

In this chapter, we report the antiplasmodial activity of the synthesized quinoline-1,2,3-triazole ligands and their respective Mn(I) and Re(I) complexes. The antimalarial activity of the Mn(I) tricarbonyl complexes is evaluated in the dark and upon irradiation to determine the effects of CO on the antimalarial activity. Subsequently, the mode of action of the compounds is determined using a β-hematin inhibition assay.

4.2. Antiplasmodial evaluation using pLDH assay

4.2.1. *In vitro* antiplasmodial activity (dark)

Research on the antimalarial evaluation of manganese and rhenium tricarbonyl complexes is scarce. Therefore, it is worthwhile to investigate the antiplasmodial activity of the synthesized complexes. *In vitro* antiplasmodial activity is evaluated using a pLDH assay. Plasmodium lactate dehydrogenase (pLDH) is an enzyme secreted during the glycolytic pathway in the *Plasmodium* species, with species-specific isomers existing.[19] The enzyme converts pyruvate to lactate using the cofactor NADH.[20] The pLDH enzyme is representative of viable *Plasmodium* in the blood and disappears within 24 hours of effective treatment.[21] The assay is thus based on the detection of the pLDH enzyme.

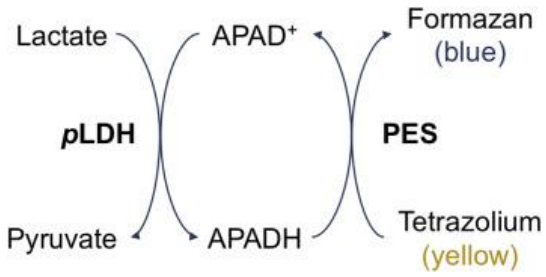

Scheme 4.1. Oxidation of lactate and reduction of nitroblue tetrazolium during pLDH assay.[22]

The assay replaces NADH with the structurally similar $APAD^+$, due to its ability to bind to pLDH more efficiently. During the assay, parasitic RBCs are present and pLDH oxidizes lactate to pyruvate and in turn, reducing the cofactor $APAD^+$ to APADH. APADH reduces tetrazolium dye (nitroblue tetrazolium) to formazan,[20] as shown in **Scheme 4.1**. The colour changes from yellow to blue and is indicative of cell viability.

The *in vitro* antiplasmodial activity of compounds **L1**, **L2**, **Mn-1, Re-1** and **Mn-2** (**Chapters 2 and 3**) were evaluated against the NF54-CQ-sensitive and K1-CQ-resistant strains of *plasmodium falciparum*. The IC_{50} values of each compound were obtained at a concentration of 10 000 ng/mL and were compared to that of chloroquine diphosphate (CQDP), as shown in **Table 4.1**.

Ligand **L1** was insoluble in DMSO at the tested concentration and therefore an IC_{50} value could not be obtained. However, complexation improves the solubility of the ligand. Complexes **Mn-1** and **Re-1** show good antiplasmodial activity in the low micromolar range in both strains of *P. falciparum*. The IC_{50} values of complexes **Mn-1** and **Re-1** in the NF54-CQ-sensitive are 3.81 μM and 4.61 μM respectively. In the K1-CQ-resistant strain, the IC_{50} values are 4.22 μM and 5.02 μM for complexes **Mn-1** and **Re-1** respectively. Complexes **Mn-1** and **Re-1** both retain their activity in the CQ-resistant strain, as they both have resistance indices of 1.1. CQ does not retain its activity in the CQ-resistant strain as indicated by the RI value of 7.2. The antiplasmodial activity of the manganese analog is relatively similar to that of the rhenium.

Ligand **L2** has IC_{50} values of 0.33 μM and 0.69 μM in the CQ-sensitive and CQ-resistant strains respectively. Complex **Mn-2** has an IC_{50} value of 0.54 μM in the CQ-sensitive strain and 1.16 μM in the CQ-resistant strain. The ligand **L2** expresses a 0.6- and 0.7-fold higher antiplasmodial activity than its manganese complex **Mn-1** in the CQ-sensitive and -resistant strains respectively. The RI values of compounds **L2** and **Mn-2** are greater than 1 (2.1) but are still lower than CQDP. Therefore, both compounds **L2** and **Mn-2** do partially retain their activities in the CQ-resistant strain.

Table 4.1. *In vitro* antiplasmodial activity (dark) and resistance indices of compounds **L1**, **Mn-1**, **Re-1**, **L2**, **Mn-2**and CQ against the NF54-CQ-sensitive and the K1-CQ-resistant strains of *P. falciparum.*

Compound	Structure	IC_{50} (µM) ±SE		
		Dark		
		NF54	K1	RI[a]
L1	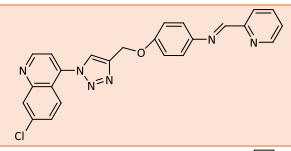	N/D[b]	N/D[b]	N/D[b]
Mn-1	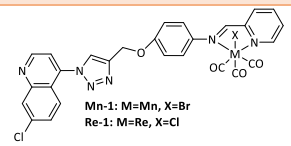 Mn-1: M=Mn, X=Br Re-1: M=Re, X=Cl	3.81 ± 0.13	4.22 ± 0.21	1.1
Re-1		4.61 ± 0.13	5.02 ± 0.14	1.1
L2	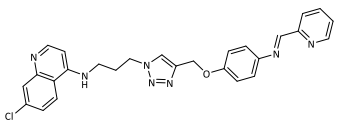	0.33 ± 0.12	0.69 ± 0.425	2.1
Mn-2	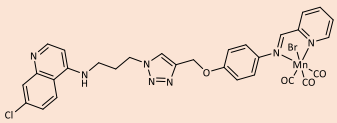	0.54 ± 0.051	1.16 ± 0.098	2.1
CQDP	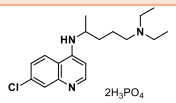	0.021 ± 0.00044	0.151 ± 0.00656	7.2

[a] Resistance index = $IC_{50}\ (CQ-resistant)/\ IC_{50}\ (CQ-sensitive)$

[b]Not determined

The IC_{50} values obtained for **Mn-2** are 7- and 4-fold lower than those obtained for **Mn-1** in the CQ-sensitive and -resistant strains respectively. The presence of a basic amino-propyl chain, therefore, improves the antimalarial activity, as seen in the literature.[22,23] Literature shows that including the 4-amino functionality improves the haematin binding ability of compounds and enhances the accumulation of the compound in the parasitic food vacuole.[23,24]

4.2.2. Antiplasmodial evaluation upon irradiation (using a 32W UV lamp)

The emergence of drug-resistant strains of *P. falciparum* poses the biggest malaria threat. It is thus essential to develop compounds that are active against the resistant strains of *P. falciparum*. The malaria parasite confers infection *via* the polymerisation of free heme into hemozoin and CO is known to prevent the oxidation of haemoglobin and formation of heme. Thus, CO presents a protective mechanism against malaria infection, as mentioned in **Section 4.1**. Considering this, the *in vitro* antiplasmodial activity of complexes **Mn-1** and **Mn-2** were evaluated in the K1-CQ-resistant strain upon photo-induced CO-release. Two 94-well plates were simultaneously set up, the first was a control plate kept in the dark throughout the assay. The second was an experimental plate that was irradiated using a 32 W UV lamp for 30 minutes. Complexes **Mn-1** and **Mn-2** were shown to release CO upon irradiation at 365 nm vide supra **Chapter 3**. The results of this experiment are shown in **Table 4.2**.

Table 4.2. IC_{50} values of complexes **Mn-1** and **Mn-2** against K1-CQ-resistant strain of *P. falciparum* in the dark and upon irradiation at 365 nm for 30 minutes.

Compound	Structure	IC_{50} (µM) ±SE in K1 strain		IC_{50} ratio[a]
		Dark	Light (365 nm)	
Mn-1	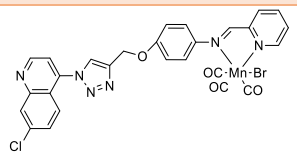	6.72 ± 0.55	0.994 ± 0.87	0.14
Mn-2	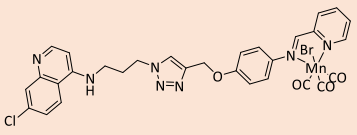	3.84 ± 3.03	1.41 ± 0.40	0.37
CQDP	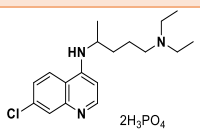	0.134± 0.04	0.141± 0.009	1.05

[a] $IC_{50}\ ratio\ IC_{50}\ light/IC_{50}\ dark$

The IC_{50} value of complex **Mn-1** decreases 7-fold from the dark (6.72 μM) to light irradiation (0.994 μM) as shown in **Table 4.2**. The IC_{50} value of complex **Mn-2** decreases 3-fold upon irradiation of 365 nm. The IC_{50} value of CQ remains constant as shown by the IC_{50} ratio of 1.05. This indicates that CQ and the parasitic viability is unaffected by the UV itself. As mentioned in **Section 4.1**, CO confers protection against malaria, therefore, it is expected that upon CO-release, the antiplasmodial activity of the compound should increase.[17] The IC_{50} ratios of complexes **Mn-1** and **Mn-2** are both below 1, attesting to the increased antiplasmodial activity induced upon CO-release. The IC_{50} values of complexes **Mn-1** and **Mn-2** in both the dark and light are not comparable to chloroquine. However, the increased efficacy of the drug induced upon CO-release suggests that the use of CORMs provides a promising method of combating drug-resistant *P. falciparum*. These antiplasmodial studies are preliminary and further studies are required. It is necessary to perform cytotoxic experiments to determine if the compounds affect healthy cells as well. CO is a toxic gaseous molecule; it is essential to determine the localization of the compounds and concentration of CO intracellularly.

4.3. Mechanistic studies: NP-40 Detergent-Mediated Assay for β-haematin inhibition

Literature reports that β-haematin resembles hemozoin chemically, spectroscopically and crystallographically and is thus considered a synthetic form of hemozoin.[5] Chloroquine is reported to inhibit β-haematin synthesis at physiological temperatures,[25,26] as discussed in **Section 4.1**. Since the synthesized compounds contain a quinoline scaffold, it is necessary to evaluate if their mode of action resembles that of chloroquine. An NP-40 detergent-mediated assay was used according to the method outlined by Sandlin *et al*.[27] in order to determine if the synthesized complexes are β-hematin inhibitors. Compounds **Mn-1**, **Re-1**, **L2** and **Mn-2** were evaluated for their β-haematin inhibition properties. The amount of synthetic heme was quantified using the colorimetric pyridine ferrochrome method developed by Egan and co-workers.[28] Pyridine does not complex to β-haematin, but does to free haem, allowing for the amount of synthetic hemozoin formed to be measured. This measurement was performed by recording the absorbance readings of each well in the 96-well plate.

The human body receives the majority of its iron (Fe) from the degradation of haemoglobin in the RBC.[29] RBCs are phagocytized by macrophages and degraded in phagolysosomes, liberating haemoglobin. Haemoglobin is comprised of a heme group (made up of a porphyrin ring and central iron)[30] and globins. The heme is oxidized by the enzyme heme oxygenase (heme-oxygenase-1 (HO-1) and heme oxygenase-2 (HO-2)) and biliverdin reductase. In the presence of high heme concentrations, HO-1 is upregulated catalysing the catabolism of heme into biliverdin, Fe^{2+} and carbon monoxide,[31] as shown in **Scheme 4.2**. Pamplona *et al*. reported that CO inhibits the degradation of haemoglobin into free heme.[17] This subsequently prevents the polymerization of heme into hemozoin (**Scheme 4.2**).

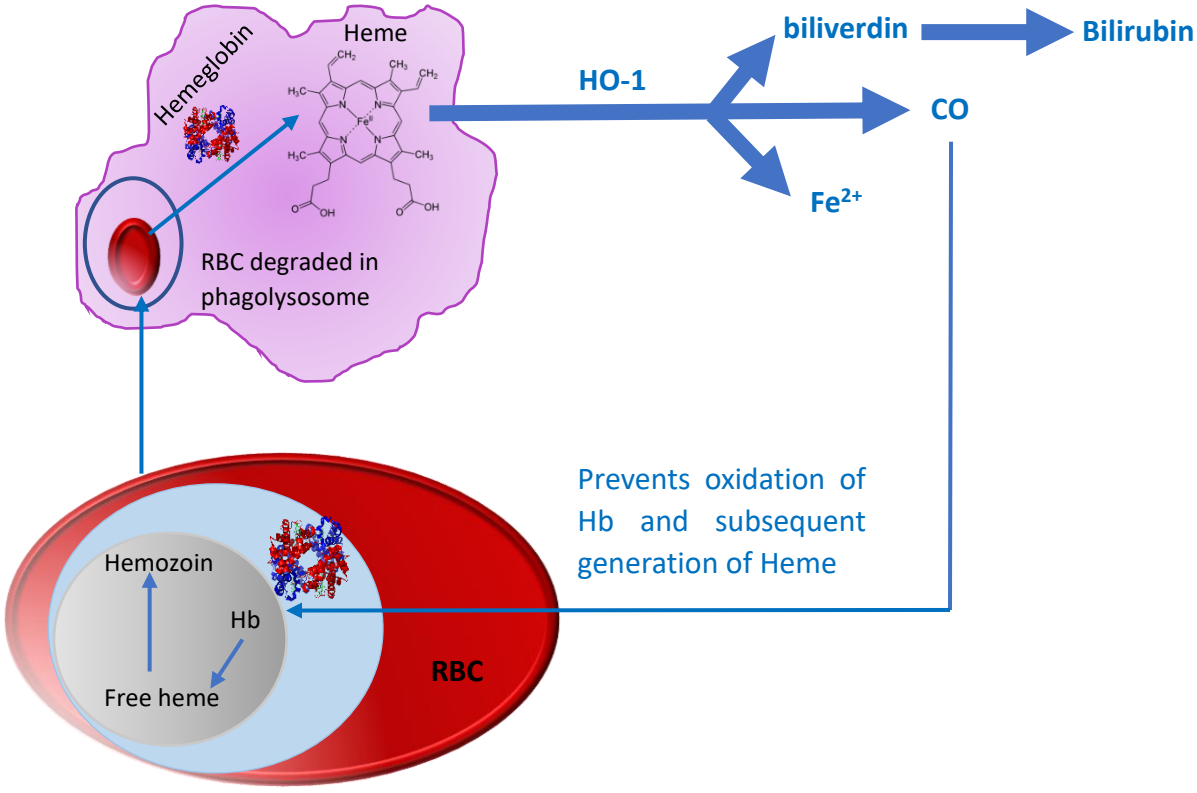

Scheme 4.2. Haemoglobin degradation pathway in macrophage and haemoglobin polymerisation to hemozoin in parasitic food vacuole.

It can, therefore, be assumed that upon photoexcitation and induction of CO-release, the β-hematin inhibition expressed by the complexes should increase. Thus, the β-hematin inhibition assay was performed simultaneously in both the dark and upon photoexcitation at 365 nm. **Figure 4.3** shows the dose-response curves obtained from the β-hematin inhibition assay in the dark and light. The curves of **Mn-1**, **Re-1**, **L2** and **Mn-2** in the dark indicate that the synthesized compounds mimic the expected sigmoidal shape seen for CQDP This shows that the ligand and complexes are all β-hematin inhibitors, with the synthesized complexes exhibiting a two-fold higher β-haematin inhibition compared to CQDP in the dark. **L2** inhibits β-hematin to a lesser extent than all the synthesized complexes and CQ. This can be seen in **Figure 4.3**, as the dose-response curve representative of ligand **L2** is shifted to the right of CQ and the complexes. The lower β-haematin inhibition displayed by **L2** does not coincide with the higher antiplasmodial activity exhibited by the compound. This indicates that **L2** may have a second mode of action that results in its higher antiplasmodial activity compared to the complexes. The β-haematin inhibition activity of compound **Re-1** is slightly greater than that of both manganese complexes, as seen by the IC_{50} values (**Table 4.3**) obtained from the log-based dose-response curves in **Figure 4.3.** Both manganese complexes exhibit relatively similar levels of β-haematin inhibition in the dark. Thus, the presence of the amine and 3-C spacer improves the antiplasmodial activity but not the ability of the complex to inhibit β-haematin formation.

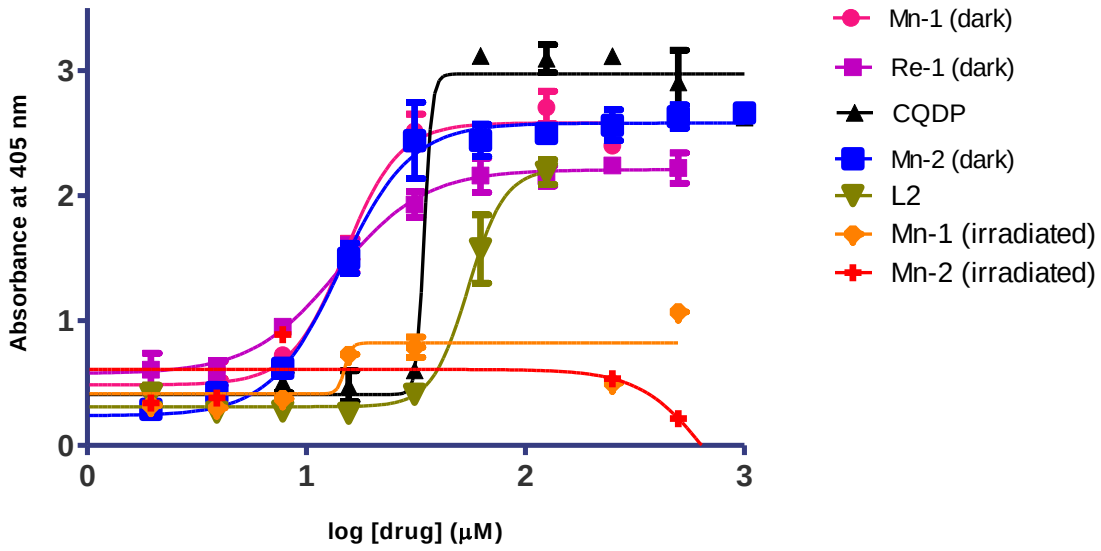

Figure 4.3. Log-based dose-response curves for the β-hematin inhibition of compounds **Mn-1, Re-1**, **Mn-2**, **L2** and **CQ** in the dark and light. Complexes **Mn-1** and **Mn-2** were irradiated at 365 nm with a 32 W UV lamp for 30 minutes prior to incubation.

Upon photoexcitation of complex **Mn-1** for 30 minutes, the β-hematin inhibition increases significantly as indicated by the shift to the left of the dose-response curve in **Figure 4.3** and the lower IC_{50} value in **Table 4.3.** It can be assumed that the increase in inhibition is due to CO-release. It would be useful to use gaseous CO as a control in the future. After irradiation of 30 minutes, complex **Mn-2** no longer takes on a sigmoidal shape. However, it should be noted that upon irradiation complex **Mn-2** forms an unidentified precipitate that may interfere with the absorbance. It can therefore not be confirmed whether the β-hematin inhibition ability of complex **Mn-2** is improved upon photoexcitation.

Table 4.3. IC_{50} values of compounds **Mn-1**, **Re-1**, **Mn-2**, **L2** and **CQ** obtained from β-hematin inhibition assay in the dark and light.

Compound	Structure	IC_{50} (µM) ± SE	
		Dark	**Light (365 nm)**
Mn-1	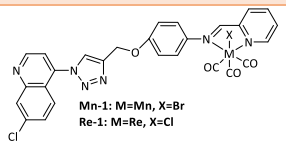	14.53 ± 0.75	11.37 ± 0.60
Re-1		13.48 ± 0.78	N/A[a]
L2	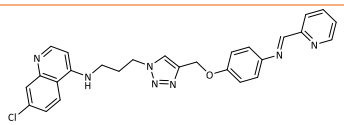	40.96 ± 1.05	N/A[a]
Mn-2	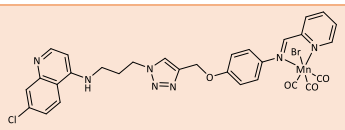	14.47 ± 0.53	N/D[b]
CQDP	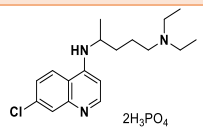	36.88 ± 0.79	31.53 ± 1.76

[a]Not applicable

[b]Not determined

The IC_{50} values of CQ in the dark and light are 36.88 µM and 31.53 µM respectively. This indicates that irradiation of 365 nm may influence one or more of the components used in the β-hematin assay. It should also be noted that the NP-40 Detergent-Mediated β-haematin inhibition assay is cell-free. While these synthesized compounds are β-hematin inhibitors under cell-free conditions, they may not exhibit the same mechanism of action intracellularly, as reported by Stringer *et al*.[32]

4.4. Summary

Two quinoline-1,2,3-triazole ligands and their respective manganese and rhenium tricarbonyl complexes were screened for their *in vitro* antiplasmodial activity against the NF54-CQ-sensitive and K1-CQ-resistant strains of *P. falciparum*. Ligand **L1** was not active at the tested concentration whereas its respective Mn (**Mn-1**) and Re (**Re-1**) complexes display good antiplasmodial activity, with IC_{50} values in the low μM range. The Mn(I) and Re(I) analogues display similar activity with the **Re-1** complex having a 0.2-fold higher IC_{50} value than **Mn-1** in both strains of *P. falciparum*. Complex **Mn-2** is 7- and 4-fold more active than **Mn-1** in the CQ-sensitive and -resistant strains respectively. The addition of an amino-propyl improves the antiplasmodial activity of the synthesized compounds, as it has shown to do in the literature as well.[22] The ligand **L2** exhibits the highest antiplasmodial activity in both the CQ-sensitive and -resistant strains respectively.

The antiplasmodial activity of complexes **Mn-1** and **Mn-2** increase 7- and 3-fold respectively in the K1-CQ-resistant strain upon photoexcitation at 365 nm. The increase in antiplasmodial activity exhibited upon light-induced CO-release presents a promising mechanism of combating drug-resistant *P. falciparum*. These *in vitro* CO-releasing studies of complexes **Mn-1** and **Mn-2** paves the way for future studies. Although these studies are preliminary, the outcome shows that CO CORMs could potentially be used to enhance the antimalarial activity of a given compound.

All compounds (**Mn-1**, **Mn-2**, **Re-1** and **L2**) showed β-hematin inhibition properties, with complexes **Mn-1**, **Mn-2** and **Re-1** being greater inhibitors than CQ. Ligand **L2** exhibited the greatest antiplasmodial activity between all tested compounds but showed the lowest β-hematin inhibition activity. Thus, further studies are required to determine the mechanism of action of ligand **L2**. Upon photo-induced CO-release, the β-hematin inhibition of complex **Mn-1** increases drastically, whereas the dose-response curve of complex **Mn-2** no longer takes the expected sigmoidal shape. Due to the unknown identity of the photolyzed products of either of the complexes, the reason for the loss of β-hematin inhibition upon photoexcitation of complex **Mn-2** cannot be predicted. The β-hematin inhibition assay is cell free and therefore

to confirm the proposed mechanism of action of the synthesized compounds, further studies are required.

The CO-release antiplasmodial studies are preliminary and further studies are required to conclude that the improved antiplasmodial activity is undoubtedly due to CO-release. It is essential to identify the photolyzed products and if these products display any biological properties of their own.

4.5. References

1 K. Y. Fong and D. W. Wright, *Future Med. Chem.*, 2013, **5**, 1437–1450.

2 R. G. Ridley, A. Dorn, S. R. Vippagunta and J. L. Vennerstrom, *Ann. Trop. Med. Parasitol.*, 1997, **91**, 559–566.

3 V. A. Nagaraj and G. Padmanaban, *Trends Parasitol.*, 2017, **33**, 583–586.

4 M. Navarro, W. Castro and C. Biot, *Organometallics*, 2012, **31**, 5715–5727.

5 C. Biot, W. Castro, C. Y. Botté and M. Navarro, *Dalton. Trans.*, 2012, **41**, 6335.

6 L. M. Coronado, C. T. Nadovich and C. Spadafora, *Biochim. Biophys. Acta - Gen. Subj.*, 2014, **1840**, 2032–2041.

7 J. M. Pisciotta, P. F. Scholl, J. L. Shuman, V. Shualev and D. J. Sullivan, *Int. J. Parasitol. Drugs Drug Resist.*, 2017, **7**, 110–119.

8 A. R. Parhizgar, *Iran. J. Med. Sci.*, 2017, **42**, 115–128.

9 R. E. Martin, R. V. Marchetti, A. I. Cowan, S. M. Howitt, S. Bröer and K. Kirk, *Science (80-.).*, 2009, **325**, 1680–1682.

10 R. E. Martin and K. Kirk, *Mol. Biol. Evol.*, 2004, **21**, 1938–1949.

11 T. Tang, W. Xu, J. Ma, H. Wang, Z. Cui, T. Jiang and C. Li, *Molecules*, 2019, **24**, 1–17.

12 R. Thomé, S. C. P. Lopes, F. T. M. Costa and L. Verinaud, *Immunol. Lett.*, 2013, **153**, 50–57.

13 R. L. Taylor, *J. Clin. Endocrinol. Metab.*, 1950, **10**, 1361–1362.

14 A. Ecker, A. M. Lehane, J. Clain, D. A. Fidock *Trends Parasitol.*, 2012, **4**, 504–514.

15 M. L. M. Pereira, C. R. F. Marinho and S. Epiphanio, *Front. Cell. Infect. Microbiol.*, 2018, **8**, 2235–2988.

16 A. Ferreira, I. Marguti, I. Bechmann, V. Jeney, Â. Chora, N. R. Palha, S. Rebelo, A. Henri, Y. Beuzard and M. P. Soares, *Cell*, 2011, **145**, 398–409.

17 A. Pamplona, A. Ferreira, J. Balla, V. Jeney, G. Balla, S. Epiphanio, Â. Chora, C. D. Rodrigues, I. P. Gregoire, M. Cunha-Rodrigues, S. Portugal, M. P. Soares and M. M. Mota, *Nat. Med.*, 2007, **13**, 703–710.

18 R. Idro, N. E. Jenkins and C. R. J. Newton, *Lancet Neurol.*, 2005, **4**, 827–840.

19 M. S. Harani, *J. Pakistan Med. Assoc.*, 2006, **56**, 167–171.

20 C. F. Markwalter, K. M. Davis and D. W. Wright, *Anal. Biochem.*, 2016, **493**, 30–34.

21 A. M. J. Oduola, G. O. Omitowoju, A. Sowunmi, M. T. Makler, C. O. Falade, D. E. Kyle, F. A. Fehintola, O. A. T. Ogundahunsi, R. C. Piper, B. G. Schuster and W. K. Milhous, 1997, **289**, 283–289.

22 S. Manohar, S. I. Khan and D. S. Rawat, *Chem. Biol. Drug Des.*, 2011, **78**, 124–136.

23 L. Taleli, C. De Kock, P. J. Smith, S. C. Pelly, M. A. L. Blackie and W. A. L. Van Otterlo, *Bioorg. Med. Chem.*, 2015, **23**, 4163–4171.

24 J. K. Natarajan, J. N. Alumasa, K. Yearick, K. A. Ekoue-kovi, L. B. Casabianca, A. C. De Dios, C. Wolf and P. D. Roepe, *J. Med. Chem.*, 2008, **51**, 3466–3479.

25 A. Dorn, S. R. Vippagunta, H. Matile, C. Jaquet, J. L. Vennerstrom and R. G. Ridley, *Biochem. Pharmacol.*, 1998, **55**, 727–736.

26 K. Kaur, M. Jain, R. P. Reddy and R. Jain, *Eur. J. Med. Chem.*, 2010, **45**, 3245–3264.

27 R. D. Sandlin, M. D. Carter, P. J. Lee, J. M. Auschwitz, S. E. Leed, J. D. Johnson and D. W. Wright, *Antimicrob. Agents Chemother.*, 2011, **55**, 3363–3369.

28 K. K. Ncokazi and T. J. Egan, *Anal. Biochem.*, 2005, **338**, 306–319.

29 C. L. Jones, *Immunity*, 2015, **33**, 395–401.

30 J. Chung, C. Chen and B. H. Paw, *Curr. Opin. Hematol.*, 2012, **19**, 156–162.

31 S. K. Chiang, S. E. Chen and L. C. Chang, *Int. J. Mol. Sci.*, 2019, **20**, 1–18.

32 T. Stringer, L. Wiesner and G. S. Smith, *Eur. J. Med. Chem.*, 2019, **179**, 78–83.

Chapter 5

Conclusion and Future outlook

5.1. Overall summary and conclusion

The main objective of this study was to synthesize two new Mn(I) and Re(I) PhotoCORMs based on a quinoline-1,2,3-triazole scaffold and characterize the parent ligands and their complexes using various spectroscopic analysis which included NMR, IR, and mass spectrometry. The ligands and their respective metal carbonyl complexes were evaluated for their antimalarial and CO-releasing properties. To the best of our knowledge, the antimalarial evaluation of Mn(I) PhotoCORMs has not been reported in the literature.

Two new quinoline-1,2,3,-tiazole compounds were synthesized using standard copper-catalysed azide/alkyne cycloadditions (CuAAC) and characterized using the aforementioned spectroscopic techniques. The reactions proceeded in DCM with reaction times of 4 h for ligand **L1** and 18 h for ligand **L2**. The yields of ligands **L1** and **L2** were only moderate but it was easy to purify and isolate these compounds once the reactions reached completion, in-line with the criteria defining “click” chemistry. Although DCM is not considered a “green” solvent, it is an easily removable solvent and therefore these reaction conditions partially follow the criteria of common “click” reactions.

Complexation of ligands **L1** and **L2** to the metal precursors $[MnBr(CO)_5]$/ $[ReCl(CO)_5]$ proceeded *via* a dissociative/ associative mechanism. This resulted in the synthesis of *fac*-Mn(I) and -Re(I) tricarbonyl complexes with the ligands chelating through the pyridyl and imine nitrogens *via* a cis-conformation. The reaction conditions for complexation of each ligand to Mn and Re centres were specific to the ligand and metal centre. **Re-2** was synthesized but attempts to separate the complex from unreacted ligand was unsuccessful.

The synthesis of a cationic **Mn-1** species was attempted using a salt metathesis method. Silver triflate was used in the halogen abstraction step with the addition of several metal salts for a

counterion exchange. A [2+1] approach was used in which the ligand representing the 1 was either isoniazid or 4-picoline. The most successful reaction conditions were the use of silver triflate and 4-picoline in MeCN, but purification of the desired product was unsuccessful.

The ligands and metal complexes were evaluated for their *in vitro* antiplasmodial activity against the NF54-chloroquine-sensitive and the K1-chloroquine-resistant strains of *Plasmodium falciparum* (*P. falciparum)*. All tested compounds show good antiplasmodial activity with IC_{50} values in the low micromolar range. The manganese and rhenium analogues exhibit similar antiplasmodial activities and retain their activity in the CQ-resistant. The ligand containing the amino-propyl chain (**L2**) exhibits the greatest antiplasmodial activity of all synthesized compounds. Mechanistic studies of the synthesized compounds indicate that they are potentially β-hematin inhibitors, with the metal complexes being greater inhibitors than CQ.

Manganese tricarbonyl complexes are known for their photochemical properties and the synthesized Mn(I) compounds were found to be photoactive as well. Complexes **Mn-1** and **Mn-2** release CO upon photoexcitation with UV light at 365 nm whereas the Re analogues do not upon long term exposure to UV. The rate of CO-release is medium-dependent and the **Mn-1** complex releases CO faster than the **Mn-2** complex. The antiplasmodial activity of complexes **Mn-1** and **Mn-2** increases 7- and 3-fold respectively upon photoexcitation at 365 nm in the K1-CQ-resistant strain. It was worthwhile to determine if the β-hematin inhibition of the complexes improved upon photo induced CO-release. This was indeed the case, the β-hematin inhibition of complex **Mn-1** increased drastically upon photoexcitation.

To the best of our knowledge, the synthesized complexes are the first Mn PhotoCORMs to be evaluated as antimalaria agents. These complexes exhibit good antimalarial activity and β-hematin inhibition with both activities increasing upon photo-induced CO-release. These results are promising and paves the way for future studies on the antimalarial evaluation of Mn PhotoCORMs.

5.2. Future Outlook

The results reported in this study show the potential of PhotoCORMs for the treatment of malaria. The study is preliminary and future work should include:

- The identification of the photolyzed products of complexes **Mn-1** and **Mn-2**
- Cytotoxicity of all the synthesized and tested compounds
- Synthesis of a fluorescent **Mn-1** and **Mn-2** complex

Synthesis of the fluorescent analogues of the Mn complex is essential to determine if the complexes are indeed taken up by the parasite and where they localize in the cell.

- Investigation of the concentration of Carboxy-haemoglobin (COHb) that forms in the presence of photo-dissociated complexes **Mn-1** and **Mn-2.**

The quantification of COHb that form upon treatment with complexes **Mn-1** and **Mn-2** upon photoexcitation is essential due to the known affinity of CO for haemoglobin and the toxicity associated with it.

Further photophysical studies should be explored such as kinetic and quantum yield studies to determine the exact rate of CO-release. DFT and TDDFT calculation can be performed to give insight into the electronic structure of the metal complexes and determine what optical transitions occur when CO is released

The antiplasmodial activity of the synthesized compounds could be improved by separating the compounds into two components as shown in **Figure 5.1**. The ligand **L2** exhibited greater antimalarial activity than its respective Mn complex and the antimalarial activity of the complex improved upon CO-release. It would be worthwhile to evaluate the antiplasmodial activity of the components of the hybrid molecule as shown in **Figure 5.1.** Doing so will help to determine if the components exhibit a synergistic or antagonistic effect.

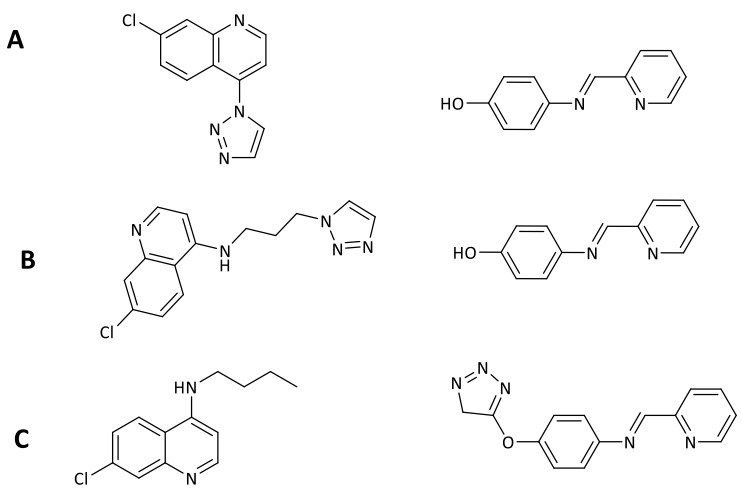

Figure 5.1. Combinations of components of the hybrid molecules that should be synthesized and evaluated for their antimalarial activity.

Future work should involve the synthesis of a prodrug that releases CO and can be administered in combination with a pharmacophore. This will help determine if having the CO-releasing scaffold attached to the pharmacophore is more advantageous. A Possible example of this is shown in **Figure 5.2** in which the compound could be considered a prodrug that acts as a transporter of CO.

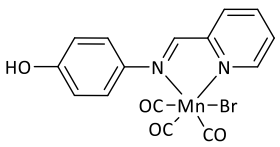

Figure 5.2. Possible prodrug that could be synthesized as a transporter of CO.

Chapter 6

Experimental procedures

6.1. Chemicals and General Methods

All reagents were purchased from Merck, KIMIX and Science World and were used without further purification. All solvents were of analytical grade and in the case of reactions done under Ar, the solvents were dried over molecular sieves. All reactions were monitored by TLC using aluminium-backed precoated silica-gel 60 F254 plates purchased from Merck. TLC plates were observed under ultraviolet light at 254 nm. All synthesised compounds were dried under high vacuum. All deuterated solvents that were used for NMR spectroscopy were purchased from Sigma-Aldrich. Purification using column chromatography was carried out using silica-gel (Fluka Silica Gel 60, 40-63 microns).

6.2. Spectroscopic and Analytical Methods

Nuclear magnetic resonance (NMR) spectra were either recorded on a Bruker Topsin GmbH 400 MHz spectrometer (^{1}H at 400.22 MHz; ^{13}C{^{1}H} at 100.65 MHz) or Varian Mercury 300 (^{1}H at 300.08 MHz at ^{13}C{^{1}H}: 75.46 MHz) which were equipped with a Bruker Biospin GmbH casing and sample injector at 30 °C. Chemical shifts for ^{1}H and ^{13}C{^{1}H} NMR are all reported using tetramethylsilane (TMS) as an internal standard. Chemical shifts and *J*-couplings are reported in ppm and Hz respectively. NMR spectra were recorded using either deuterated dimethylsulfoxide (DMSO-*d*6) or deuterated chloroform ($CDCl_3$). Infrared (IR) spectroscopy were recorded using a Perkin-Elmer Spectrum 100 FT-IR spectrometer and Attenuated Total Reflectance (ATR) or a NaCl solution cell for solution-state IR in which the vibrations were measured in cm^{-1}. Melting points were obtained using a Büchi Melting Point Apparatus B-540. High-resolution Mass spectrometry was recorded on a Waters Synapt G2, ESI probe, ESI Pos, Cone Voltage 15 V machine using the positive mode.

6.3. Synthesis of the terminal alkyne

6.3.1. Synthesis of 4-(pyridinylimine)phenol (1).[1]

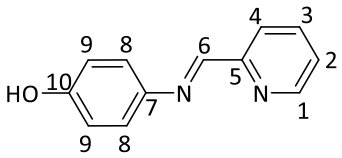

4-Aminophenol (972 mg, 8.91 mmol, 1 eq.) and 2-pyridinecarboxaldehyde (1.69 mL, 17.8 mmol, 2 eq.) were dissolved in methanol (100 mL). The reaction mixture was refluxed (65℃) for 21 hours and was monitored *via* Thin Layer Chromatography using a mobile phase of 20% petroleum ether/ethyl acetate. The excess solvent was removed *via* rotary evaporation and the residue was dissolved in minimal hot methanol. The round bottom flask containing the crude product in methanol was cooled on ice to form a beige precipitate. Compound **1** was collected *via* suction filtration and washed with ice-cold methanol.

Yield: 1.48 g, 84%. **Melting point:** 186.2-187.8 ℃ (lit.,[2] 186–187 ℃). **^{1}H NMR (300 MHz, $(CD_3)_2SO$): δ=** 9.61 (s, 1H, OH) 8.67 (d, $^3J_{HH}$=4.80 Hz, 1H, H-1), 8.58 (s, 1H, H-6), 8.10 (d, $^3J_{HH}$=7.90 Hz, 1H, H-4), 7.90 (td, $^4J_{HH}$=1.22 Hz, $^3J_{HH}$=7.90 Hz,1H, H-3), 7.41-7.58 (m, 1-H, H-2), 7.28 (d, $^3J_{HH}$=8.70, 2H, H-9), 6.82 (d, $^3J_{HH}$=8.70 Hz, 2H, H-8). **^{13}C {^{1}H} NMR (101 MHz, $(CD_3)_2SO$: δ** 156.99 (C-10), 156.88 (C-6), 154.52 (C-7),149.46 (C-1), 141.49 (C-5), 136.78 (C-3), 124.96 (C-2), 122.82 (C-9), 120.62(C-4), 115.77 (s, C-8). **IR (ATR, cm^{-1}):** 2465-2988 (broad, medium, aromatic CH's and OH), 1623 (sharp, medium, $C=N_{imine}$), 1581 (sharp, medium, $C=N_{pyridyl}$).

6.3.2. Synthesis of (E)-*N*-(4(prop-2-yn-1-yloxy)phenyl)-1-(pyridine-2-yl)methanimine (2).[2]

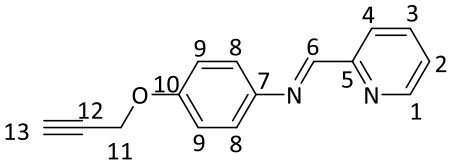

Compound **1** (526 mg, 2.65 mmol, 1 eq.), potassium carbonate (1.87 g, 13.6 mmol, eq.) and 18-crown-6 ether (361 mg, 1.37 mmol, 0.5 eq.) were mixed in acetone (20 mL). Propargyl bromide (0.2 mL, 2.65 mmol, 1 eq.) was diluted with acetone (10 mL) and added dropwise to the stirring reaction mixture. The solution was refluxed for 72 hours (56 ℃). The reaction was monitored using TLC. The solvent was removed *via* rotary evaporation and left in the fridge for 2 hours while still containing K_2CO_3. DCM (40 mL) was added to the residue and excess K_2CO_3 was filtered by gravity. The filtrate was washed with H_2O (3 × 30 mL). The combined organic extracts were washed with a saturated solution of ammonium chloride in H_2O (2 X 30 mL) and once more with H_2O (30 mL). The combined organic extracts were dried with anhydrous Na_2SO_4 which was subsequently filtered by gravity, resulting in a brown oil which underwent slow evaporation to form brown crystals (**2**).

Yield: 490 mg, 81%. **Melting point:** 104.4-106.2 ℃. **^{1}H NMR (300 MHz, $(CD_3)_2SO$) δ=** 8.69 (d, $^3J_{HH}$ = 4.8 Hz, 1H, H-1), 8.69 (s, 1H-6), 8.13 (d, $^3J_{HH}$ = 7.9 Hz, 1H, H-4), 7.93 (ddd, $^3J_{HH}$ = 7.9 Hz, $^4J_{HH}$= 1.7 Hz, 0.8 Hz, 1H, H-3), 7.49 (ddd, $^3J_{HH}$ = 7.5 Hz, $^3J_{HH}$=4.8 Hz, $^4J_{HH}$=1.7 Hz, 1H, H-2), 7.41 – 7.36 (m, 2H, H-9), 7.08 – 7.03 (m, 2H, H-8), 4.83 (d, $^4J_{HH}$ = 2.4 Hz, 2H, H-11), 3.56 (t, $^4J_{HH}$ = 2.4 Hz, 1H, H-13). **^{13}C {^{1}H} NMR (101 MHz, $(CD_3)_2SO$: δ** 158.64 (C-6), 156.39 (C-10), 154.37 (C-7), 149.52 (C-1), 143.98 (C-5), 132.89 (C-3), 125.23 (C-2), 122.57 (C-9), 121.03 (C-8), 79.27 (C-12), 78.17 (C-13), 55.77 (C-11). **IR (ATR, cm^{-1}):** 3171 (sharp, medium, ≡C-H), 2964 (Sharp, weak, C≡C), 1623 (sharp,weak,C=N_{imine}), 1600 (sharp, weak, C=$N_{pyridyl}$), 1579 (sharp, strong, C=C), 1239 (sharp, strong, C-O-C).

6.4. Synthesis of 4-azido-7-chloroquinoline (3).[3]

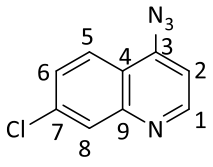

4,7-Dichloroquinoline (561 mg, 2.83 mmol, 1 eq.) was dissolved in anhydrous DMF (5 mL). NaN_3 (361 mg, 5.55 mmol, 2 eq.) was added and the resulting mixture was stirred at 65 ℃ for 6 hours while being monitored *via* TLC in a 30% ethyl acetate/hexane. After completion, the mixture was cooled to room temperature. Ethyl acetate (20 mL) was added to the reaction mixture and excess NaN_3 was filtered by gravity. The filtrate was washed with H_2O (3 × 30 mL), brine (2 × 30 mL) and then H_2O (2 × 30 mL). The combined organic extracts were dried over anhydrous Na_2SO_4. The Na_2SO_4 was removed *via* gravity filtration and the solvent removed from the filtrate *via* rotary evaporation. The crude product was recrystallised from hot DCM/ cold hexane to yield compound **3** as yellow needle crystals.

Yield: 359 mg, 62%. **Melting point:** 116.3-118.5 ℃ (lit.,[3] 115 ℃). **^{1}H NMR (300 MHz, $CDCl_3$): δ=** 8.83 (d, $^3J_{HH}$=4.94 Hz, 1H, H-1), 8.07 (d, $^5J_{HH}$=2.07 Hz, 1H, H-8), 8 (d, $^3J_{HH}$= 8.94 Hz, 1H, H-6), 7.49 (dd, $^5J_{HH}$= 2.07 Hz, $^3J_{HH}$=8.94 Hz, 1H, H-5), 7.13 (d, $^3J_{HH}$=4.94 Hz, 1H, H-2). **^{13}C {^{1}H} NMR (101 MHz, ($CDCl_3$) : δ** 151.37 (C-1), 149.65 (C-9), 146.77 (C-7), 136.97 (C-3), 128.23 (C-8), 127.81 (C-5), 123.93 (C-6), 120.03 (C-4), 108.66 (C-2). **IR (ATR, cm^{-1}):** 2117 (sharp, strong, N_3), 1608 (sharp, medium, C=N), 766 (sharp, strong, C-Cl).

6.5. Synthesis of (7-chloroquinolin-4-yl)-amino]propane derivatives.

6.5.1. Synthesis of 3-[(7-Chloroquinolin-4-yl)amino]propan-1-ol (4).[4]

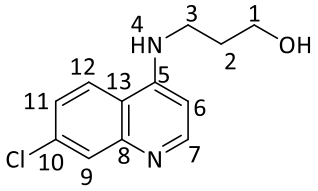

4,7-Dichloroquinoline (1.44 g, 7.25 mmol, 1 eq.) and 3-aminopropan-1-ol (5.5 mL, 72.5 mmol, 10 eq.) were heated to 80 ℃ for 1 hour without stirring. The temperature was then increased to 130 ℃ and the solution was stirred under reflux conditions for 16 hours. The reaction was allowed to cool to room temperature. H_2O (10 mL) was added, resulting in the immediate formation of a white precipitate. The desired product (**4**) was collected *via* suction filtration and washed with H_2O, yielding a white solid that was dried in vacuum.

Yield: 904 mg, 62%. **Melting point:** 142.2-143.4 ℃ (lit.,[4] 142-143). **^{1}H NMR (300 MHz, DMSO) δ** 8.39 (d, $^3J_{HH}$ = 5.4 Hz, 1H, H-7), 8.24 (d, $^3J_{HH}$ = 9.0 Hz, 1H, H-11), 7.77 (d, $^5J_{HH}$ = 1.6 Hz, 1H, H-9), 7.43 (dd, $^3J_{HH}$ = 9.0, $^3J_{HH}$= 1.6 Hz, 1H, H-12), 7.27 (brs, 1H, H-4), 6.47 (d, $^3J_{HH}$ = 5.4 Hz, 1H, H-6), 4.56 (brs, 1H, OH), 3.55 (t, $^3J_{HH}$ = 5.9 Hz, 2H, H-1), 3.33 (q, $^3J_{HH}$= 6.4 Hz, 2H, H-3), 1.82 (p, 2H, H-2). **^{13}C {^{1}H} NMR (101 MHz, $(CD_3)_2SO$) δ** 151.91 (C-5), 150.49 (s,C-11), 148.99 (C-8), 133.45 (C-12), 127.63 (C-7), 124.09 (C-9), 124.13 (C-10), 117.74 (C-3), 98.56 (C-6), 48.46 (C-1), 40.94 (C-3), 31.23 (C-2). **IR (ATR, cm^{-1}):** 3312 (broad, weak, OH), 3058 (sharp, weak, NH), 1609 (strong, sharp, C=N)**.**

6.5.2. Synthesis of 3-((7-chloroquinolin-4-yl)amino)chloropropane (5a).[4]

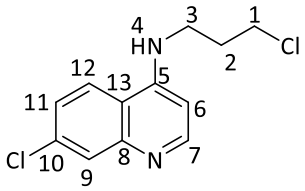

Compound **4** (513 mg, 2.55 mmol, 1 eq.) was dissolved in excess thionyl chloride (3.70 mL, 51.1 mmol, 20 eq.). Catalytic amounts of DMF (50 µL) was added and the reaction was set to stir under argon at ambient temperature for 16 hours. The excess thionyl chloride was quenched using a saturated solution of sodium bicarbonate in H_2O. Compound **5a** was collected *via* suction filtration and washed with ice-cold ethyl acetate. The beige solid was dried in vacuum.

Yield: 447 mg, 67 %. **Melting point:** 127.9-128.2 ℃. **^{1}H NMR (300 MHz, DMSO) δ** 9.50 (br s, 1H, H-4), 8.71 (d, $^3J_{HH}$= 7 Hz, 1H, H-7), 8.52 (d, $^3J_{HH}$= 9.1 Hz, 1H, H-11), 8.09 (d, $^5J_{HH}$ = 2.1 Hz, 1H, H-9), 7.75 (dd, $^3J_{HH}$ = 9.1, $^3J_{HH}$= 2.1 Hz, 1H, H-12), 6.85 (d, $^3J_{HH}$ = 7 Hz, 1H, H-6), 3.80 (t, $^3J_{HH}$= 6.4 Hz, 2H, H-1), 3.63 (q$^3J_{HH}$= 6.4 Hz, 2H, H-3), 2.16 (p, $^3J_{HH}$ = 6.4 Hz, 2H, H-2).). **^{13}C {^{1}H} NMR (101 MHz, $(CD_3)_2SO$) δ** 155. 11 (C-5), 143.12 (C-11), 139.39 (C-8), 126.63 (C-12), 126.11 (C-7), 122.92 (C-9), 119.54 (C-10), 115.83 (C-3) 98.95 (C-6), 44.19 (C-1), 39.88 (C-3), 30.96 (C-2). **IR (ATR, cm^{-1}):** 3219 (sharp, weak, N-H), 1614 (strong, sharp, C=N), 734, (sharp, medium CCl).

6.5.3. Synthesis of 3-[(7-chloroquinolin-4-yl)amino]propylmethanesulfonate (5b).[5]

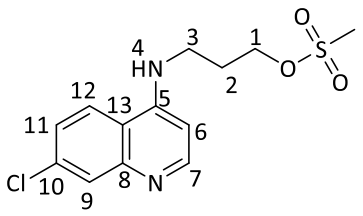

Methansulfonyl chloride (501 mg, 2.49 mmol, 1 equiv) was added to a solution of compound **4** (288 μL, 3.73 mmol, 1.5 equiv) and Et_3N in THF (10 mL) at 0 ℃. The mixture was stirred for 3 hours after which a saturated solution of $NaHCO_3$ (20 mL) was added. Compound **5b** was extracted with chloroform (3 × 20 mL). The combined organic extracts were dried over anhydrous Na_2SO_4, which was subsequently filtered *via* gravity filtration. The solvent was removed from the filtrate using rotary evaporation to yield crude compound **11** as an off-white powder. The crude product was purified via column chromatography using MeOH: DCM in increasing ratios up to 10:9.

Yield: 447 mg, 67 %. **^{1}H NMR (300 MHz, DMSO) δ** 8.40 (d, $^3J_{HH}$ = 5.3 Hz, 1H, H-7), 8.25 (d, $^3J_{HH}$ = 9.0 Hz, 1H, H-11), 7.78 (d, $^5J_{HH}$ = 2.2 Hz, 1H, H-9), 7.45 (dd, $^3J_{HH}$ = 9.0 Hz, $^5J_{HH}$= 2.2 Hz, 1H, H-12), 7.31 (t, $^4J_{HH}$ = 5.3 Hz, 1H, H-4), 6.50 (d, $^3J_{HH}$ = 5.3 Hz, 1H, H-6), 4.33 (t, $^3J_{HH}$ = 6.4 Hz, 2H, H-1), 3.37 (q, $^3J_{HH}$= 6.4 Hz, 2H, H-3), 3.19 (s, 3H, C$\underline{H_3}$), 2.07 (q, *J* = 13.1, $^3J_{HH}$= 6.4 Hz, 3H, H-2). **^{13}C {^{1}H} NMR (101 MHz, $(CD_3)_2SO$) δ** 155.48 (C-5), 150.32 (C-11), 148.34 (C-8), 133.35 (C-12), 126.95 (C-7), 124.01 (C-9), 124.10 (C-10), 117.34(C-3) 98.80 (C-6), 58.30 (C-1), 39.21 (C-3), 31.25 (C-2), 27.45 (CH_3). **IR (ATR, cm^{-1}):** 3065 (sharp, weak, N-H), 1609 (strong, sharp, C=N).

6.5.4. Synthesis of 3-[(7-chloroquinolin-4-yl)amino]azidopropane (6).

*6.5.4.1. Synthesis of compound **6** using compound **5a** as a reactant*

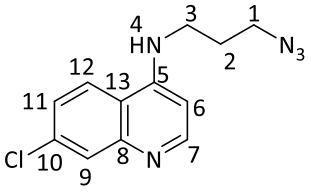

Compound **5a** (292 mg, 1.14 mmol, 1 eq.) was dissolved in DMF (4 mL). NaN_3 (128 mg, 1.97 mmol, 2 eq.) was added and the reaction was heated to 80 ℃ under reflux and argon for 16 hours. Ethyl acetate (30 mL) was added and the organic layer washed with H_2O (1 × 30 ml), brine (2 × 30 mL) and H_2O (2 × 30 mL). The organic extracts were collected and dried over anhydrous $MgSO_4$. The $MgSO_4$ was removed *via* gravity filtration and the solvent was removed from the filtrate *via* rotary evaporation resulting in a pale-yellow product (**6**) that was dried in vacuum.

Yield: 80.8 mg, 23 %. **Melting point:** 149-150.7 ℃ (lit.,[4] 149-150 ℃). **^{1}H NMR (300 MHz, DMSO) δ** 8.41 (d, $^3J_{HH}$ = 5.4 Hz, 1H, H-7), 8.27 (d, $^3J_{HH}$ = 9.0 Hz, 1H, H-11), 7.79 (d, $^5J_{HH}$ = 2.2 Hz, 1H, H-9), 7.46 (dd, $^3J_{HH}$ = 9.0 Hz, $^3J_{HH}$= 2.2 Hz, 1H, H-12), 7.30 (t, $^4J_{HH}$ = 5.4 Hz, 1H, H-4), 6.50 (d, $^3J_{HH}$ = 5.4 Hz, 1H, H-6), 3.50 (t, $^3J_{HH}$ = 6.7 Hz, 2H, H-1), 3.63 (q, $^3J_{HH}$ =6.7 Hz, 2H, H-3), 1.93 (q, $^3J_{HH}$ = 6.7 Hz, 2H, H-2). **^{13}C {^{1}H} NMR (101 MHz, $(CD_3)_2SO$): δ** 151.86 (C-5), 149.83 (C-11), 149.02 (C-8), 133.31 (C-12), 127.49 (C-7), 124.01 (C-9), 122.11 (C-10), 117.44 (C-3) 98.62 (C-6), 48.53 (C-1), 40.10 (C-3), 27.09 (C-2). **IR (ATR, cm^{-1})** 2111 (sharp, strong, N_3), 3191 (sharp, strong, NH), 1609 (sharp, strong, C=N).

*6.5.4.2. Synthesis of compound **6** using **5b** as a reactant.*[5]

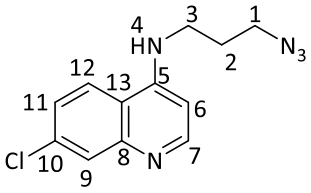

To a solution of compound **11** (450 mg, 0.151 mmol, 1 eq.) in anhydrous DMF, NaN_3 (196 mg, 0,301 mmol, 2 eq.) was added and the mixture heated at 55 ℃ for 20 hours. H_2O (30 mL) was added and the product was extracted with toluene (3 X 50 mL). The organic extracts were washed with a saturated brine solution (2X 50 mL) and then with H_2O (2 X 50 mL). The organic extracts were then dried over Na_2SO_4, which was subsequently filtered using gravity filtration. The solvent was removed from the filtrate *via* rotary evaporation. The crude product was purified *via* column chromatography using increasing rations of MeOH: DCM (9:1) to yield the product (**6**) as a pale-yellow solid.

Yield: 207 mg, 52%. **^{1}H NMR (300 MHz, DMSO) δ** 8.41 (d, $^3J_{HH}$ = 5.4 Hz, 1H, H-7), 8.27 (d, $^3J_{HH}$ = 9.0 Hz, 1H, H-11), 7.79 (d, $^5J_{HH}$ = 2.2 Hz, 1H, H-9), 7.46 (dd, $^3J_{HH}$ = 9.0, $^5J_{HH}$= 2.2 Hz, 1H, H-12), 7.30 (t, $^4J_{HH}$ = 5.4 Hz, 1H, H-4), 6.50 (d, $^3J_{HH}$ = 5.4 Hz, 1H, H-6), 3.50 (t, *J* = 6.7 Hz, 2H, H-1), 3.38 – 3.33 (m, 2H, H-3), 1.93 (q, *J* = 6.8 Hz, 2H, H-2).

6.6. The general method for the synthesis of 7-chloroquinoline-1,2,3-triazole ligands

A Schlenk tube covered in aluminium foil was evacuated and filled with argon after which CuI (10 mol %) and DIPEA (1 mL) were added and allowed to stir for 10 minutes. Compound **2** (1 eq.) in dry DCM (1 mL) was added to the stirring solution of CuI and allowed to stir for a further 5 minutes. Compound **3** (1 eq.) in DCM (1 mL) was added and the reaction mixture was

refluxed under argon for 4 or 18 hours. The completion of the reaction was determined by TLC in ethyl acetate: petroleum either mixture in ration 8:2. DCM (50 mL) was added and the precipitate was filtered *via* gravity filtration. The filtrate was washed with a saturated solution of NH_4Cl (2 X 50 mL) and H_2O (2 X 50 mL). The combined organic extracts were dried over anhydrous Na_2SO_4 which was subsequently filtered by gravity. The solvent was removed from the filtrate *via* rotary evaporation. The crude product was recrystallized from either acetone or diethyl ether and collected using suction filtration to produce the ligands as beige powders which were dried *in vacuo*.

6.6.1. Synthesis of quinoline-triazole ligand (L1)

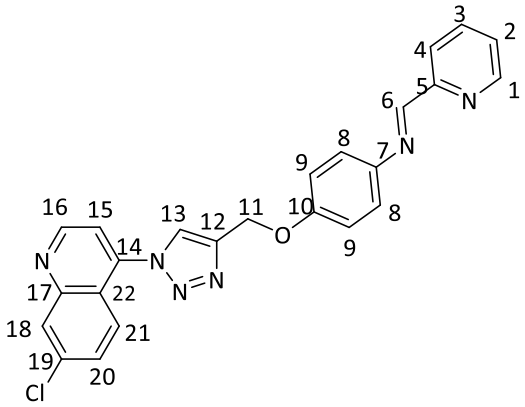

CuI (12.0 mg, 0.063 mmol, 10 mol %), DIPEA (1 mL), compound **2** (255 mg, 1.08 mmol,0.83 mmol,1.3 eq.) and compound **3** (170 mg, 1 eq.) were reacted in DCM for 4 hours. Ligand **L1** was purified *via* a water wash and recrystallization from acetone. The product (**L1**) was isolated as a beige powder.

Yield: 200 mg, 56%. **Melting point:** 207.5-209.2 ℃ (decomp). **^{1}H NMR (300 MHz, $(CD_3)_2SO$) δ=** 9.23 (d, $^3J_{HH}$ = 4.7 Hz, 1H,H-16), 9.05 (s, 1H, H-13), 8.77 (d, $^3J_{HH}$ = 4.8 Hz, 1H, H-1), 8.70 (s, 1H, H-6), 8.36 (d, $^5J_{HH}$ = 2.1 Hz, 1H, H-18), 8.21 (d, $^3J_{HH}$ = 7.9 Hz, 1H, H-3), 8.07 (d, $^3J_{HH}$ = 9.1 Hz, 1H, H-20), 8.00 (td, $^3J_{HH}$ = 7.9 Hz, $^4J_{HH}$= 1.4 Hz, 1H, H-4), 7.95 (d, $^3J_{HH}$ = 4.7 Hz, 1H, H-15), 7.86 (dd, $^3J_{HH}$ = 9.1 Hz, $^5J_{HH}$ 2.1 Hz, 1H, H-21), 7.57 (ddd, $^3J_{HH}$ = 7.9 Hz, $^3J_{HH=}$ 4.8 Hz, $^4J_{HH}$= 1.4 Hz, 1H, H-2), 7.49 (d, 2H, $^3J_{HH}$=9.0 Hz H-9), 7.26 (d, $^3J_{HH}$ = 9.0 Hz, 2H, H-8), 5.38 (s, 2H, H-11). **^{13}C {^{1}H}**

NMR (101 MHz, ($CDCl_3$): δ IR (ATR, cm^{-1}): 168.66 (C-10), 168.04 (C-6), 158.43 (C-5), 154.85 (C-1), 152.71 (C-16), 150.57 (C-17), 143.11(C-7) , 141.84(C-4) , 140.11 (C-19), 133.74 (C-14) , 124.48 (C-21), 124.23 (C-2), 123.96 (C-3), 123.42 (C-21), 122.07 (C-13), 115.42 (C-20), 114.95 (C-9), 114.57 (C-22), 98.52 (C-8), 61.10 (C-11). **IR (ATR, cm^{-1})** 1623 (sharp, weak, imine- C=N), 1595 (sharp, medium, C=C), 1579 (sharp, strong, pyridyl-C=N) 1562 (sharp, strong, quinoline-C=N).

6.6.2. Synthesis of aminoquinoline-triazole ligand (L2).

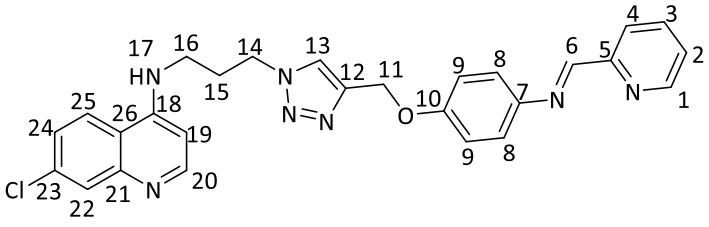

CuI (11.0 mg, 10 mol %), DIPEA (1 mL), compound **2** (137 mg, 0.582 mg ,1.3 eq.) and compound **6** (117 mg, 0.447 mmol, 1 eq.) were reacted in DCM for 18 hours. Ligand **L2** was purified *via* a water wash and recrystallization from diethyl ether. The product (**L2**) was isolated as a beige powder. The crude product was crystallised *via* slow crystallisation in diethyl ether to yield compound **13** as a beige powder.

Yield: 92.9 mg, 42%. **Melting point:** 153.2-154.8 °C. **^{1}H NMR (300 MHz, DMSO) δ** 8.71 (d, $^3J_{HH}$ = 4.4 Hz, 1H, H-1), 8.62 (s, 1H, H-6), 8.40 (d, $^3J_{HH}$ = 5.4 Hz, 1H, H-20), 8.30 (s, 1H, H-13), 8.27 (d, $^3J_{HH}$ = 9.1 Hz, 1H, H-24), 8.14 (d, $^3J_{HH}$ = 7.8 Hz, 1H, H-4), 7.95 (t, $^3J_{HH}$ = 7.8 Hz, 1H, H-3), 7.79 (d, $^3J_{HH}$ = 2.3 Hz, 1H, H-22), 7.54 – 7.50 (dd, $^3J_{HH}$ = 7.8 Hz, $^3J_{HH=}$ 4.4 Hz, 1H, H-2), 7.47 (dd, $^3J_{HHH}$ = 9.1 Hz, $^5J_{HH}$= 2.3 Hz, 1H, H-25), 7.39 (d, $^3J_{HH}$ = 8.9 Hz, 2H, H-9), 7.34 (brs,1H, H-17),7.12 (d, $^3J_{HH}$ = 8.9 Hz, 2H, H-8), 6.44 (d, $^3J_{HH}$ = 5.4 Hz, 1H, H-19), 5.19 (s, 2H, H-11), 4.55 (t, $^3J_{HH}$ = 6.9 Hz, 2H, H-14), 3.39 (d, $^3J_{HH}$ = 6.9 Hz, 2H, H-16), 2.25 (q, 2H, H-15). **^{13}C {^{1}H} NMR (101 MHz, (CD_3)$_2$SO: δ** 158.85 (C-6), 157.76 (C-10), 154.75 (C-18), 152.32 (C-20), 150.01 (C-1), 149.41 (C-5), 143.64 (C-7), 143.063 (C-12), 137.36 (C-3),133.84 (C-23) 127.88 (C-22), 125.71 (C-2),

125.077 (C-13), 124.62 (C-25), 124.54 (C-24), 123.17 (C-9), 121.32 (C-4), 117.89 (C-26), 115.44 (C-8), 99.05 (C-19), 61.76 (C-11), 47.48 (C-14), 39.98 (C-16), 28.84 (C-15). **IR (ATR, cm^{-1}):** 1612 (sharp, weak, $C=N_{imine,quinoline}$), 1592 (sharp, strong, $C=N_{pyridine}$).

6.7. The general method for the synthesis of metal tricarbonyl complexes

Either $[MnBr(CO)_5]$ or $[ReCl(CO)_5]$ in DCM (10 mL) was added dropwise to a stirring solution of either ligand **L1** or **L2**) in DCM (20 mL). The reaction mixture was allowed to stir at room temperature or under reflux conditions while being wrapped in aluminium foil for protection against light. The solvent was removed *via* rotary evaporation and the product recrystallized from DCM/pentane in the dark. The desired complex was collected *via* suction filtration and dried *in vacuo*.

6.7.1. Synthesis of Mn-1

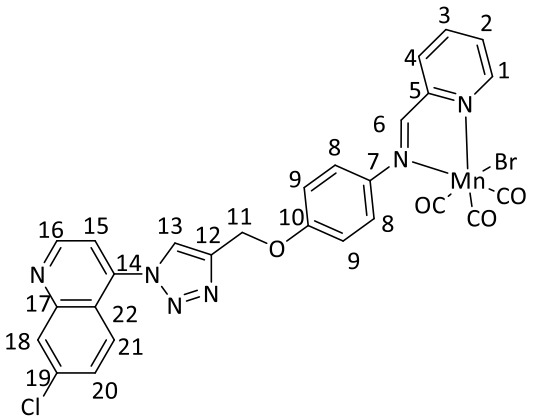

$[MnBr(CO)_5]$ (51.6 mg, 0.188 mmol, 1.3 eq.) and ligand **L1** (64.0 mg, 0.145 mmol, 1 eq.) were reacted in DCM at room temperature for 72 hours. The solvent was removed *via* rotary evaporation and the residue was dissolved in ethyl acetate. The impurities were filtered off

using gravity filtraction and the solvent was removed from the filtrate *via* rotary evaporation. The product **Mn-1** was recrystallized from DCM/pentane to produce an orange powder

Yield: 104 mg, 93%. **Melting point:** 145.2-147.8 ℃ (decomp). **^{1}H NMR (300 MHz, DMSO): δ** 9.22 (d, $^{3}J_{HH}$ = 5.2 Hz, 1H, H-1), 9.17 (d, $^{3}J_{HH}$ = 4.6 Hz, 1H, H-16), 9.02 (s, 1H,H-13), 8.87 (s, 1H, H-6), 8.30 (d, $^{5}J_{HH}$ = 2.0 Hz, 1H, H-18), 8.25 (d, *J* = 4.2 Hz, 2H, H-3, H-4), 8.02 (d, *J* = 9.1 Hz, 1H, H-20), 7.89 (d, *J* = 4.6 Hz, 1H, H-15), 7.82 (d, $^{5}J_{HH}$ = 2.0 Hz, 1H, H-21), 7.80 – 7.77 (m, 1H, H-2), 7.60 (d, $^{3}J_{HH}$ = 8.8 Hz, 2H, 9), 7.32 (d, $^{3}J_{HH}$ = 8.8 Hz, 2H, H-8), 5.42 (s, 2H, H-11). **^{13}C {^{1}H} NMR (101 MHz, $(CD_3)_2SO$: δ** 222.22 (C≡O), 221.18 (C≡O), 218.83 (C≡O), 167.18 (C-6), 157.90 (C-10), 154.96 (C-5), 153.59 (C-1), 152.36 (C-16), 149.31 (C-17), 145.53 (C-12), 143.27 (C-7), 140.43 (C-3), 139.16 (C-19), 135.35 (C-14), 129.14 (C-20), 128.78 (C-4), 128.06 (C-21), 126.99 (C-13), 125.29 (C-18), 123.15 (C-9), 120.19 (C-22), 117.09 (C-15), 115.14 (C-8), 61.53 (C-11). **IR (ATR, cm^{-1}):** 2024 (sharp, strong C≡O), 1914 (broad, strong, C≡O), 1610 (sharp, weak, C=$N_{imine,quinoline}$), 1598 (sharp, strong, pyridyl-C=N), 1564 (sharp, medium, C=C). **MS (HR-ESI, m/z):** 660.9620 (100% [M+H^{+}]), 660.7680 (calc.).

6.7.2. Synthesis of Re-1.

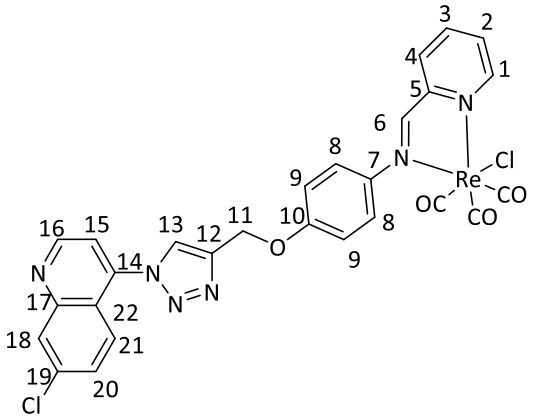

$[ReCl(CO)_5]$ (59.1 mg, 0.163 mmol, 1 equiv) and ligand **L1** (70.5 mg, 0.156 mmol, 1 equiv) were reacted in DCM (20 mL) at 40 ℃ for 4 days. The product was recrystallized from DCM/pentane to produce **Re-1** as a yellow powder.

Yield: 99.7 mg, 84%. **Melting point:** 197.7-199.5 ℃ (decomp). **^{1}H NMR (300 MHz, DMSO) δ** 9.31 (s, 1H, H-6), 9.18 (d, $^3J_{HH}$ = 4.7 Hz, 1H, H-16), 9.07 (d, $^3J_{HH}$ = 6.2 Hz, 1H, H-1), 9.03 (s, 1H, H-13), 8.37 (td, $^4J_{HH}$=1.2 Hz, $^3J_{HH}$=*5.4 Hz,* 1H, H-4), 8.35 (d, $^3J_{HH}$=*5.4 Hz* 1H, H-3), 8.31 (d, $^5J_{HH}$ = 2.1 Hz, 1H, H-18), 8.03 (d, $^3J_{HH}$ = 9.0 Hz, 1H, H-20), 7.90 (d, $^3J_{HH}$ = 4.7 Hz, 1H, H-15), 7.84 (ddd, $^3J_{HH}$ = 6.2 Hz, $^3J_{HH}$ = 5.4 Hz, $^4J_{HH}$ = 1.2 Hz, 1H, H-2) 7.81 (dd, $^5J_{HH}$=2.1 Hz, $^3J_{HH}$=9.0 Hz, 1H H-21), 7.62 (d, $^3J_{HH}$ = 8.9 Hz, 2H, H-9), 7.34 (d, $^3J_{HH}$ = 8.9 Hz, 2H, H-8), 5.44 (s, 2H, H-11). **^{13}C {^{1}H} NMR (101 MHz, $(CD_3)_2SO$) δ** 197.73 (C≡O), 197.19 (C≡O), 187.81 (C≡O), 168.63 (C-6), 158.73 (C-10), 155.43 (C-5), 153.30 (C-16), 152.90 (C-1), 149.45 (C-17), 144.17 (C-12), 143.36 (C-7), 140.23 (C-4),140.48 (C-19) 135.53 (C-19), 130.24 (C-3), 129.71 (C-2), 129.17 (C-21), 128.28 (C-18), 127.22 (C-13), 125.90 (C-20), 123.93 (C-9), 120. 45 (C-14), 117.31 (C-15), 115.54 (C-8), 61.32 (C-11). **IR (ATR, cm^{-1}):** 2019 (sharp, strong, C≡O), 1886 (broad, strong, C≡O), 1614 (broad, weak, $C=N_{imine,\ quinoline}$), 1595 (broad, weak, $C=N_{pyridine}$). **MS (HR-ESI, m/z):** 747.0309 (100% [$M+H^+$]),747.5880 (calc.).

6.7.3. Synthesis of Mn-2.

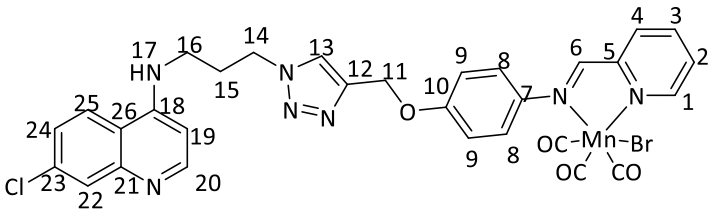

$[MnBr(CO)_5]$ (48.8 mg, 0.177 mmol, 1.3 equiv) and **L1** (67.1 mg,0.135 mmol, 1 equiv) were reacted at 25℃ in DCM for 24 hours. The product (**Mn-2**) was recrystallized from DCM/pentane to yield an orange powder.

Yield: 67.5 mg, 70%. **Melting point:** 108.4-110 ℃. **^{1}H NMR (300 MHz, DMSO) δ** 9.23 (d, $^3J_{HH}$ = 5.2 Hz, 1H, H-1), 8.86 (s, 1H, H-6), 8.41 (d, $^3J_{HH}$ = 5.5 Hz, 1H, H-20), 8.34 (s, 1H, H-13), 8.29 – 8.24 (m, 1H,H-3, H-4, H-24), 8.26, 7.83 – 7.77 (m, 2H, H-2,22), 7.58 (d, $^3J_{HH}$ = 8.9 Hz, 2H, H-9), 7.47 (dd, $^3J_{HH}$ = 8.9 Hz, $^5J_{HH}$= 1.9 Hz, 1H, H-25), 7.34 (brs, 1H, H-17), 7.24 (d, $^3J_{HH}$ = 8.9 Hz, 2H,

H-8), 6.46 (d, $^3J_{HH}$ = 5.5 Hz, 1H, H-19), 5.24 (s, 2H, H-11), 4.56 (t, $^3J_{HH}$ = 6.9 Hz, 2H, H-14), 3.33 (d, $^3J_{HH}$ = 6.9 Hz, 2H, H-16), 2.26 (q, 2H, H-15). **^{13}C {^{1}H} NMR (101 MHz, $(CD_3)_2SO$: δ** 222.33 (C≡O), 221.22 (C≡O), 219.25 (C≡O), 167.85 (C-6), 158.42 (C-10), 154.99 (C-18), 153.69 (C-1) 151.78 (C-20), 149.92 (C-5), 149.00 (C-7), 145.25 (C-12), 139.17 (C-3),133.37 (C-23) 129.13 (C-22), 128.03 (C-2), 124.718 (C-13), 124.05 (C-25, 24), 123.05 (C-9), 122.43 (C-4), 117.76 (C-26), 115.04 (C-8), 98.700 (C-19), 61.4 (C-11), 47.41 (C-14), 40.00 (C-16), 28.39 (C-15). **IR (ATR, cm^{-1}):** 2024 (sharp, strong, C≡O), 1914 (C≡O), 1603 (sharp, strong, C=$N_{imine,\ quinoline}$), 1592 (sharp, weak, C=$N_{pyridine}$). **MS (HR-ESI, m/z):** 736.4257 (100% $[M+MeCN+Na]^+$), 736.4400 (calc).

6.7.4. Synthesis of Re-2.

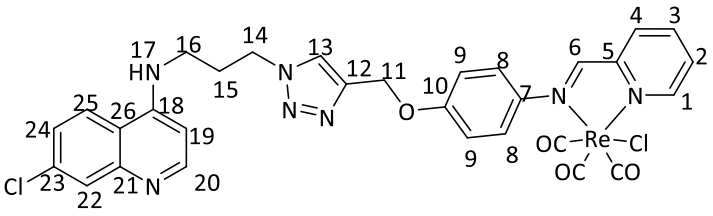

$[ReCl(CO)_5]$ (43.0 mg, 0.012 mmol, 1 eq.) and **L2** (60.6 mg, 0.012 mmol, 1 equiv) were reacted in DCM at 30 ℃ for 24 hours. A crude product of **Re-2** was obtained via recrystallization in DCM and pentane to yield a bright yellow powder.

Yield: 71.3 mg, 73%. **^{1}H NMR (300 MHz, DMSO): δ** 9.29 (s, 1H, H-6), 9.06 (d, $^3J_{HH}$ = 5.4 Hz, 1H, H-1), 8.41 (d, $^3J_{HH}$ = 5.5 Hz, 2H, H-20), 8.36 (dd, $^3J_{HH}$ = 7.0 Hz, 2H, H-24), 8.33 (s, 1H, H-13), 8.30 (d, $^4J_{HH}$ = 1.4 Hz, 1H, H-4), 8.26 (br s, 1H, H-3), 7.87 – 7.81 (m, 1H, H-2), 7.80 (d, $^5J_{HH}$ = 2.1 Hz, 1H, H-25), 7.58 (d, $^3J_{HH}$ = 9.0 Hz, 2H, H-9), 7.50 – 7.45 (m, 2H, H-25), 7.39 (d, $^3J_{HH}$ = 8.8 Hz, 2H, H-17), 7.25 (d, $^3J_{HH}$ = 9.0 Hz, 2H, H-8), 6.47 (d, $^3J_{HH}$ = 5.5 Hz, 1H, H-19), 5.25 (s, 2H, H-11), 4.55 (t, $^3J_{HH}$ = 6.9 Hz, 4H, H-14), 3.39 (dd, *J* = 14.0 Hz, $^3J_{HH}$= 6.9 Hz, 3H, H-16), 2.34 – 2.20 (m, 4H, H-15).). **IR (ATR, cm^{-1}):** 2019 (sharp, strong, C≡O), 1889 (C≡O), 1603 (sharp, weak, C=$N_{imine,\ quinoline}$), 1592 (sharp, weak, C=$N_{pyridine}$)

6.8. Reactivity studies: [2+1] approach

6.8.1. Attempted synthesis of 4-picoline containing cationic complex ([Mn-1(4-picoline)](CF_3SO_3)).

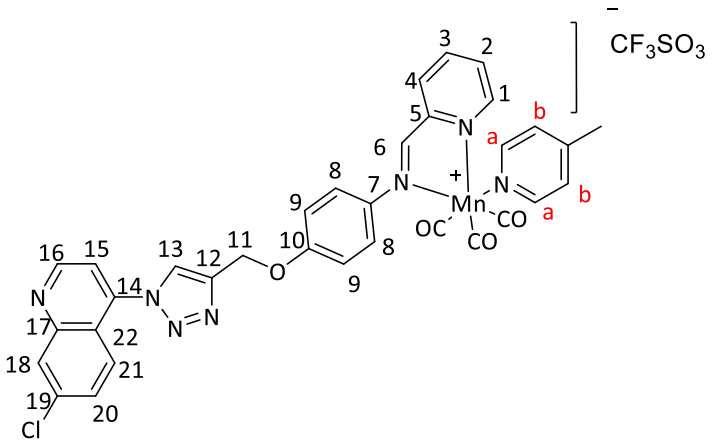

A Schlenk flask was evacuated and purged with argon, after which complex **Mn-1** (40.9 mg, 0.062 mmol, 1 eq.) and MeCN (30 mL) was added. Silver trifluoromethanesulfonate (31.2 mg, 0.124 mmol, 2 eq.) in acetonitrile (5 mL) was added to the stirring solution. The mixture was stirred under argon conditions for 2.5 hours. Isoniazid or 4-picoline (12 μL, 0.124 mmol, 2 eq.) in MeCN (5 mL) was added and the reaction mixture stirred for 20 hours. The solvent was removed *via* rotary evaporation. DCM (~20 mL) was added and the resulting precipitate filtered through celite. The solvent was reduced from the filtrate and the product was attempted to be purified *via* recrystallisation in DCM/hexane afforded a bright yellow powder.

^{1}H NMR (300 MHz, DMSO) δ 9.31 (d, *J* = 5.3 Hz, 1H, H-1), 9.19 (d, *J* = 4.7 Hz, 1H, H-16), 9.04 (s, 1H, H-13), 9.00 (s, 1H, H-6), 8.39 (d, *J* = 7.7 Hz, 2H, H-a), 8.35 (br s, 1H, H-21), 8.33 (d, *J* = 2.0 Hz, 2H, H-4,3), 8.30 (d, *J* = 7.4 Hz, 1H, H-18), 8.03 (d, *J* = 9.1 Hz, 2H, H-18), 7.94 (br s, 1H, H-2), 7.90 (d, *J* = 4.7 Hz, 2H, 15), 7.82 (dd, *J* = 9.1, 2.2 Hz, 2H, H-20), 7.60 (t, *J* = 8.6 Hz, 3H, H-9), 7.38 (d, *J* = 8.9 Hz, 2H, H-9), 7.35 (d, J=7.7 Hz, 2H, H-b) 5.45 (s, 2H, H-11), 2.08 (s, 3H, CH_3).

6.8.2. Synthesis of 4-(pyridinylimine)phenol Mn complex (Mn-4)

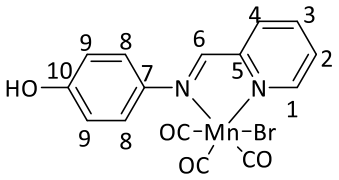

To a solution of **4-(pyridinylimine)phenol** (**1**) (105 mg, 0.530 mmol, 1 eq.) in MeOH (20 mL), $[MnBr(CO)_5]$ (173 mg, 0.635 mmol, 1.2 eq.) in MeOH (10 mL) was added to a flask covered in aluminium foil. The reaction mixture was heated to 40°C and allowed to stir under reflux conditions for 18 hours. The solvent was removed *via* rotary evaporation and the residue recrystallized by layering pentane over DCM. Complex **Mn-4** was isolated as a dark orange powder.

Yield: 96 mg, 43%. **^{1}H NMR (300 MHz, DMSO) δ** 9.88 (s, 1H, OH), 9.88 (brs, 1H,H-1), 8.79 (s, 1H, H-6), 8.22 (brs, 2H, H-4,3), 7.76 (brs, 1H, H-2), 7.44 (d, $^3J_{HH}$ = 7.3 Hz, 2H, H-9), 6.91 (d, $^3J_{HH}$ = 7.3 Hz, 2H, H-9). **IR (ATR, cm^{-1}):** 2027 cm^{-1} (sharp, strong, C=O), 1918 cm^{-1} (sharp, strong, C=O), 1604 (sharp, weak, C=N_{imine}), 1591 (sharp weak, C=$N_{pyridine}$).

6.8.3. Synthesis of [Mn-4(4-picoline)](PF_6)

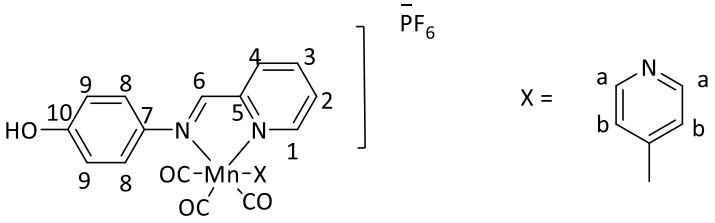

To a stirring solution of complex **Mn-4** (78.5 mg, 0.188 mmol, 1 eq.) in DCM (20 mL), $AgPF_6$ (56.9 mg, 0.225 mmol, 1.2 eq.) was added. The reaction mixture was stirred at room

temperature under an inert atmosphere for 18 hours in the dark. 4-picoline (21.9 µL, 2.25 mmol, 1.2 eq.) was added to the solution was stirred at room temperature for 48 hours. The mixture was filtered through Celite to remove AgBr and the solvent was removed from the filtrate *via* rotary evaporation. The resulting residue was recrystallised from DCM/pentane to yield a yellow solid.

Yield: 36 mg, 45%. **^{1}H NMR (300 MHz, DMSO) δ** 10.18 (s, 1H, brs, OH), 9.29 (d, $^3J_{HH}$ = 5.0 Hz, 1H, H-1), 8.89 (s, 1H, H-6), 8.42 (d, 1H, $^3J_{HH}$ = 6.6 H-4), 8.33 (dd, $^3J_{HH}$ = 7.4 Hz, $^3J_{HH}$= 6.6 Hz, 1H, H-3), 8.18 (d, $^3J_{HH}$ = 7.4 Hz, 1H, H-2), 7.99 (d, $^3J_{HH}$ = 6.4 Hz, 2H, H-a), 7.41 (d, $^3J_{HH}$ = 8.8 Hz, 2H, H-9), 7.33 (d, $^3J_{HH}$ = 6.4 Hz, 2H, H-b), 6.99 (d, $^3J_{HH}$ = 8.8 Hz, 2H, H-8), 2.30 (s, 1H, CH_3). **IR (ATR, cm^{-1}):** 2031 cm^{-1}, 1932 cm^{-1} and 1902 cm^{-1} (sharp, strong, C≡O), 1928 cm^{-1} (sharp, broad, C≡O).

6.9. Photochemical Studies

6.9.1. CO-release using spectroscopic techniques

Photochemical studies were recorded using IR and UV/vis spectroscopy. Infrared (IR) spectroscopy were recorded in DCM on a Perkin-Elmer Spectrum 100 FT-IR spectrometer and a NaCl plate. An initial solution state IR spectrum was recorded after which the sample was irradiated at 365 nm for 30 minutes using a 32 W UV lamp. Irradiation was repeated until a CO absorption band was no-longer observed. Electronic absorption spectra were recorded in a mixture of DMSO and either 0.01 M PBS (pH 7.4) or growth medium solution (5:95 % *v/v*). Electronic absorption spectra were recorded using a Cary 60 UV/Vis spectrometer with a fibre optic dip probe attachment. Growth medium contains RPMI with glutamine and $NaHCO_3$, glucose, Hepes buffer, Hypoxanthine, albumax and gentamycin**.** Dark stability was determined in DMSO/PBS and DMSO/growth medium solutions were determined by taking a reading every 1 hour for 5 hours and a final reading was taken after 24 hours. The solutions of complexes were then irradiated at 365 nm in 1-minute increments for 10 minutes, 2-minute increments for 2-minutes and 5-minute increments for 40 minutes. The electronic absorption spectrum was recorded after each irradiation period.

6.9.2. CO-release using the Myoglobin assay

The myoglobin solution was prepared by dissolving *ca*. 30 mg of equine skeletal muscle myoglobin (purchased from Sigma Aldrich) in 10.0 mL of PBS solution (0.01 M). The concentration of each myoglobin solution was determined by reducing myoglobin to deoxy-myoglobin (using sodium dithionite in PBS (0.01 M)) and using the Beer-Lambert law with the known extinction coefficient of deoxy-myoglobin (13.8 $mM^{-1}cm^{-1}$ at 557 nm). A stock solution of the complex in DMSO was prepared. The myoglobin in PBS solution (890 µL) was degassed with argon and reduced with a solution of sodium dithionite (100 µL, 0.01 M). To this mixture, the stock complex solution (10 µL) was added to give a final volume of 1000 µL, which was added to a quartz cuvette. The concentrations of the stock solutions were prepared to give a final mixture with 10 µM metal complex, 60 µM deoxy-myoglobin and 10 mM of sodium dithionite. A t = 0 spectrum was recorded, after which the cuvette was irradiated at 365 nm with a 32 W UV lamp. The cuvette was irradiated in 1-minute increments for 10 minutes, 2-minute increments for 10 minutes and 5-minute increments for 40 minutes. An electronic absorption was recorded after each irradiation period.

6.10. Antiplasmodial Studies

The samples were evaluated in triplicate against both the NF54-CQ-sensitive and the K1-CQ-resistant) strains of *Plasmodium falciparum*. A modified literature method was adapted for the *in vitro* cultures of asexual erythrocyte stages of the parasite.[6] The *in vitro* antiplasmodial activity of the compounds was evaluated using the well-known parasitic lactate dehydrogenase (pLDH) assay. The method used in the assay was adapted from Makler *et al.*[7] The compounds were sonicated in DMSO to make stock solutions of 20 mg/mL and were stored at -20 °C until the day of the experiment. Relevant dilutions were made on the day of the assay. Chloroquine diphosphate was used as the reference drug for all experiments. A starting concentration of 10 000 ng/mL was used after which the solutions were serially diluted 2-fold in growth medium to give 10 different concentrations (the lowest being 20 ng/ml). The IC_{50} values of all the compounds were obtained from a non-linear dose-response curve which was generated using GraphPad Prism v.5.0 software.[8] Antiplasmodial activity

with CO-release was determined by irradiating the 96-well plate for 30 minutes with a 32 W UV lamp before incubation with the potential drug.

6.11. NP-40 Detergent-Mediated β-hematin inhibition assay

The β-hematin inhibition assay was followed according to the method outlined by Carter *et al*.[9] A 305.5 µM stock solution of NP-40 detergent was prepared. The respective samples were dissolved in the relevant volumes of DMSO to give a stock solution of 20 mM. Each sample (20 µL), mili-q water (140 µL) and NP-40 detergent (40 µL, 305.5 µM) was added to column 12 of a 96 well plate. A solution of water NP-40 (305.5 µM)/DMSO (100µL) in a v/v ratio of 7/2/1 was added to wells 1-11. A serial dilution from column 12-2 was performed, discarding a 100 µL from column 1. Thus column 1 serves as a blank without any sample present. A pre-read of the plate was taken at 405 nm on a plate reader. A 25 mM stock solution of hematin was prepared by sonicating 16.3 mg of hematin in 1 mL of DMSO. 178 µL of this stock solution was then added to 20 mL of acetate buffer (1 M, pH 4.8). The hematin suspension (100 µL) was added to each well. The plates were covered with the plate cover and foil in the case of plates kept in the dark. For the CO-release study, the plate was irradiated with a 32 W UV lamp for 30 minutes. The plates were incubated at 37 ℃ for 16 hours in a water bath. The analysis was carried out using the pyridine-ferrichrome method developed by Ncokazi and Egan.[10] A solution of pyridine/H_2O/acetone/ HEPES buffer (2 M, pH 7.4) in a v/v ratio of 5/2/2/1 was prepared and added to each well (32 µL). Acetone (60 µL) was added to each well. The UV/vis absorbance was recorded on a SpectraMax P340 plate reader at 405 nm. Sigmoidal dose-response curves were obtained using the absorbance values on using GraphPad Prism v.5.0 software.

6.12. References

1 T. Ahamad and S. M. Alshehri, *Polym. Int.*, 2012, **61**, 1640–1647.

2 Q. Zhang, H. Su, J. Luo and Y. Wei, *Catal. Sci. Technol.*, 2013, **3**, 235–243.

3 G. C. Brandão, F. C. Rocha Missias, L. M. Arantes, L. F. Soares, K. K. Roy, R. J. Doerksen, A. Braga de Oliveira and G. R. Pereira, *Eur. J. Med. Chem.*, 2018, **145**, 191–205.

4 P. M. Njogu, J. Gut, P. J. Rosenthal and K. Chibale, *ACS Med. Chem. Lett.*, 2013, **4**, 637–41.

5 M. P. Kristina Starcevic, Dijana Pesic, Ana Toplak, Goran Landek, Sulejman Alihodzic, Esperanza Herreros, Santiago Ferrer, Radan Spaventi, *Eur. J. Med. Chem.*, 2012, **49**, 365–378.

6 R. L. Taylor, *J. Clin. Endocrinol. Metab.*, 1950, **10**, 1361–1362.

7 M. T. M. An and D. J. Hinrichs, *Am. J. Trop. Med. Hyg.*, 1993, **48**, 205–210.

8 T. Stringer, R. Seldon, N. Liu, D. F. Warner, C. Tam, L. W. Cheng, K. M. Land, P. J. Smith, K. Chibale and G. S. Smith, *Dalton. Trans.*, 2017, **46**, 9875–9885.

9 M. Carter, V. Phelan, R. Sandlin, B. Bachmann and D. Wright, *Comb. Chem. High Throughput Screen.*, 2010, **13**, 285–292.

10 K. K. Ncokazi and T. J. Egan, *Anal. Biochem.*, 2005, **338**, 306–319.